Development and validation of an expanded antibody toolset that captures alpha-synuclein pathological diversity in Lewy body diseases

Melek Firat Altay[1], Senthil T. Kumar[1], Johannes Burtscher[1], Somanath Jagannath[1], Catherine Strand[2], Yasuo Miki[2,5], Laura Parkkinen[3,4], Janice L. Holton[2], Hilal A. Lashuel*[1]

[1] Laboratory of Molecular and Chemical Biology of Neurodegeneration, Brain Mind Institute, EPFL, Switzerland

[2] Queen Square Brain Bank for Neurological Disorders, University College London Queen Square Institute of Neurology, London, England

[3] Oxford Parkinson's Disease Centre, University of Oxford, Oxford, UK

[4] Nuffield Department of Clinical Neurosciences, University of Oxford, Oxford, UK

[5] Department of Neuropathology, Institute of Brain Science, Hirosaki University Graduate School of Medicine, Hirosaki 036-8562, Japan

Running title: unmasking alpha-synuclein pathologies in Lewy body diseases

*To whom correspondence should be addressed: Laboratory of Molecular and Chemical Biology of Neurodegeneration, Brain Mind Institute, Ecole Polytechnique Fédérale de Lausanne, 1015 Lausanne. Tel: +41216939691, Fax: +41216939665.
e-mail: hilal.lashuel@epfl.ch

Keywords: alpha-synuclein, Parkinson's disease, Parkinson's disease with dementia, dementia with Lewy bodies, Lewy body disorders, post-translational modification, phosphorylation, nitration, truncation, antibody, neuropathology, aggregation, human post-mortem tissue, *SNCA* mutation, *SNCA* duplication

ABSTRACT

The abnormal aggregation and accumulation of alpha-synuclein (aSyn) in the brain is a defining hallmark of synucleinopathies. An increasing number of studies show that aSyn in pathological aggregates exists as a complex mixture of various post-translationally modified forms and conformations. The distribution of these different species changes during disease progression and varies among the different synucleinopathies. Current approaches for detecting aSyn in human tissues and disease models rely on a limited set of antibodies that have not been thoroughly assessed for their ability to capture the diversity of aSyn proteoforms and aggregation states, and thus are unlikely to provide a complete estimation of aSyn pathology in the brain. To address these challenges, we developed, validated, and characterized an expanded set of antibodies that target different sequences and post-translational modifications (PTMs) along the entire length of aSyn, and recognize all conformations of the protein (monomers, oligomers and fibrils). We demonstrate that the use of multiple antibodies targeting different regions on aSyn is necessary to reveal the heterogeneity of aSyn pathology in human Lewy body disease (LBD) brains, and in neuronal and animal models of aSyn aggregation and inclusion formation. We also present, for the first time, the profiling of aSyn pathology using antibodies against all its key post-translationally modified forms across sporadic and familial LBDs. The antibody validation pipeline we describe here paves the way for a more systematic investigation of the diversity of aSyn pathology in the human brain and peripheral tissues, and in cellular and animal models of synucleinopathies.

INTRODUCTION

Synucleinopathies are a subgroup of neurodegenerative diseases primarily including Parkinson's disease (PD), dementia with Lewy bodies (DLB) and multiple system atrophy (MSA) (Baba et al., 1998; Spillantini et al., 1998a, 1998b). Mounting evidence points to the aggregation and accumulation of the presynaptic protein alpha-synuclein (aSyn) as critical processes in the pathophysiology of synucleinopathies: 1) Fibrillar and aggregated forms of aSyn are enriched in inclusions that are the defining pathological features of PD, DLB and MSA, including Lewy bodies (LBs), Lewy neurites (LNs), glial cytoplasmic inclusions (GCIs) and neuronal cytoplasmic inclusions (NCIs) (Baba et al., 1998; Spillantini et al., 1998b, 1998a); 2) mutations and duplications of the aSyn-encoding gene *SNCA* have been shown to cause familial forms of PD (Appel-Cresswell et al., 2013; Chartier-Harlin et al., 2004; Kapasi et al., 2020; Kiely et al., 2013; Krueger et al., 1998; Lesage et al., 2013; Pasanen et al., 2014; Polymeropoulos et al., 1997, 1996; Proukakis et al., 2013; Singleton et al., 2003; Spira et al., 2001; Zarranz et al., 2004); and 3) inoculation of recombinant aSyn fibrils or PD and MSA brain-derived aSyn aggregates is sufficient to induce LB-like inclusion formation in cellular and animal models (Kumar et al., 2021; Luk et al., 2012, 2009; Mahul-Mellier et al., 2020, 2018; Tarutani et al., 2016; Volpicelli-Daley et al., 2014), and to induce the spreading of LB-like intracellular pathology in brain regions and along the gut-brain axis (Arotcarena et al., 2020; Dehay and Bezard, 2019; Recasens et al., 2014; Rey et al., 2016, 2013).

Despite aSyn being the common denominator of synucleinopathy brain pathologies, increasing evidence suggests that aSyn within these inclusions exists as a mixture of different post-translationally modified and aggregated forms or strains of the protein (Anderson et al., 2006; Schweighauser et al., 2020; Shahmoradian et al., 2019). The morphology (Kuusisto et al., 2003), composition (Leverenz et al., 2007; Wakabayashi et al., 2013; Xia et al., 2008), structure (Shahmoradian et al., 2019; Strohaeker et al., 2019) and distribution (Alafuzoff et al., 2009) of the aSyn inclusions show considerable diversity (Figure 1A) depending not only on the type of synucleinopathy but also on the cell type, the brain region and the individual patient concerned. At the fibril level, the recent cryogenic electron microscopy (cryo-EM) studies of fibrils generated from full-length, truncated and modified recombinant and semisynthetic aSyn monomers *in vitro* revealed that aSyn is capable of forming fibrils of variable morphologies and conformations (Guerrero-Ferreira et al., 2019; Li et al., 2018) (Figure 1B). Likewise, recent cryo-EM studies of fibrils isolated from MSA and DLB brains (Schweighauser et al., 2020) show polymorphism and suggest the presence of significant biochemical and structural heterogeneity in aSyn-related pathologies.

In the field of aSyn research, the detection, quantification and monitoring of aSyn pathology in LBs, LNs, GCIs and NCIs have largely depended on the use of antibodies targeting different sequences, modifications or conformations of aSyn (Covell et al., 2017; Dhillon et al., 2017; Duda et al., 2002; Fayyad et al., 2020; Giasson et al., 2000b; Henderson et al., 2020; Kovacs et al., 2012; Vaikath et al., 2015; Waxman et al., 2008). aSyn accumulating within the neuronal and glial inclusions is subjected to different types of post-translational modifications (PTMs) at multiple residues (Figure 1C), including

phosphorylation, ubiquitination, nitration, acetylation and N- and C-terminal truncations. Of these modifications, aSyn phosphorylated at Serine 129 (aSyn pS129) has been described as the most common aSyn PTM in pathological aSyn aggregates, and aSyn pS129 levels have been reported to increase by multiple folds in PD, DLB and MSA brains (Anderson et al., 2006; Fujiwara et al., 2002). These observations have led to the emergence of aSyn pS129 as a key marker of aSyn pathology. Several antibodies against aSyn pS129 have been developed as the primary tools for assessing aSyn pathology formation and spreading in the central nervous system and peripheral tissues. However, the extent to which these antibodies capture the full spectrum of aSyn pathology has not been systematically investigated. Furthermore, recent findings support a potentially protective effect of aSyn pS129 (Ghanem et al., 2022), and therefore the absence of this modification does not necessarily indicate the absence of aSyn pathology.

Several immunohistochemical and mass spectrometry studies on the distribution of aSyn species in LBs and GCIs revealed the presence of various aSyn proteoforms that are cleaved at different residues within the C-terminal region of the protein (e.g. 1-115, 1-119, 1-122, 1-133, 1-135) (Anderson et al., 2006; Baba et al., 1998; Campbell et al., 2001; Dickson et al., 1999; Gai et al., 1999; Kellie et al., 2015; Lewis et al., 2010; Moors et al., 2019; Ohrfelt et al., 2011; Tofaris et al., 2003; Tong et al., 2010), and of other aSyn C-terminal modifications, including phosphorylation and/or nitration at tyrosine residues 125 (Y125), 133 (Y133) and 136 (Y136) (Chen et al., 2009; John E. Duda et al., 2000; Giasson et al., 2000a; Mahul-Mellier et al., 2014) (Figure 1C). Interestingly, the most abundant C-terminally truncated species, i.e. aSyn 1-119 and 1-122 (Anderson et al., 2006; Bhattacharjee et al., 2019; Kellie et al., 2015; Killinger et al., 2018; Ohrfelt et al., 2011), lack the epitope for aSyn pS129 antibodies. Furthermore, the occurrence of several modifications in close proximity to S129 suggests that they may interfere with the immunoreactivity of several aSyn C-terminal or pS129 antibodies (Lashuel et al., 2022; Mahul-Mellier et al., 2018).

Interestingly, a large part of the immunohistochemistry and biochemistry studies on human brain samples, including the PD staging work by Braak and colleagues (Braak et al., 2001, 2003, 2002), has relied primarily on the use of antibodies with epitopes against the C-terminal region of aSyn. Yet, these most commonly used antibodies are less likely to capture truncated forms of aSyn, aggregated but not yet phosphorylated aSyn, or aggregated aSyn bearing multiple C-terminal modifications (Anderson et al., 2006; Chen et al., 2009; Giasson et al., 2000a; Kiely et al., 2013; Mahul-Mellier et al., 2014). Reliance on a single or a restricted number of antibodies in human post-mortem, cellular and *in vivo* studies thus may significantly underestimate the amount, and under-represent the diversity, of aSyn pathology. Furthermore, the cellular environment dramatically influences the kinetics of aSyn aggregation, fibril polymorphism and PTMs (Peng et al., 2018). It is likely that the aSyn aggregates formed in the different types of synucleinopathies, regions or stages of disease progression, possess distinct biochemical and structural signatures that expose amino acid sequences and antibody epitopes differentially. Therefore, it is crucial to use multiple, well-characterized and validated antibodies to elucidate the biochemical and structural features underlying the pathological heterogeneity of aSyn in different synucleinopathies

(Baba et al., 1998; Covell et al., 2017; Dhillon et al., 2017; Duda et al., 2000b; Giasson et al., 2000b). If successfully deciphered, these differences could be exploited to develop novel approaches to identify disease-specific biomarkers for PD and other synucleinopathies. They will also improve our currently insufficient understanding of the association of aSyn pathology and disease progression (Jellinger, 2009; Milber et al., 2012; Parkkinen et al., 2011, 2008; Steiner et al., 2018).

Towards this goal, we sought to develop an antibody toolbox that would enable capturing the diversity of soluble, aggregated and post-translationally modified forms of aSyn, thus making it possible to profile the full heterogeneity of aSyn pathology in post-mortem LB disease (LBD) brains. First, a combination of peptides and wild-type (WT) or site-specifically modified aSyn proteins were designed and used as immunogens to identify antibodies targeting different epitopes and modifications along the sequence of aSyn. The newly generated antibodies were complemented with a selection of pre-existing antibodies, and these were then systematically characterised with regards to their a) epitopes and species reactivity; b) sensitivities to aSyn PTMs neighbouring their epitopes; and c) conformational selectivity, using a library of recombinant aSyn monomers, oligomers and fibrils (Figure 1D). We validated their specificity to aSyn by employing aSyn knockout (KO) mouse neurons and brain tissues. The antibodies were then titrated for use on post-mortem synucleinopathy tissues. We selected a subset of antibodies that would allow the full coverage of the N-terminus, non-amyloid component (NAC) and C-terminus regions of aSyn as well as the post-translationally modified aSyn forms. The antibodies were next used to profile the pathological diversity of lesions in sporadic and familial LBDs. The use of this expanded toolbox revealed distinct and heterogeneously modified aSyn pathologies rich in pS129, but also in N-terminal nitration at Tyrosine 39 (Y39) and in N- and C-terminal tyrosine phosphorylations, scattered both to neurons and glial cells. To the best of our knowledge, this is the first study to employ antibodies targeting all disease-associated PTMs to profile aSyn brain pathology in the same set of LBD cases. Finally, we used these validated antibodies to assess the dispersion of differentially modified aSyn aggregates in seeding-based cellular and animal models. Altogether, our results highlight the critical importance of re-visiting human tissues and cellular/tissue samples from model organisms using toolsets that capture the full diversity of aSyn species. This is a necessary first step towards understanding the relationship between aSyn pathology formation, neurodegeneration, disease symptomatology and disease progression.

RESULTS

Design, development and generation of aSyn mouse monoclonal antibodies

To generate antibodies that capture the biochemical and structural diversity of aSyn, we employed a collection of human aSyn proteoforms as antigens. These included large peptide fragments and proteins spanning the N-terminal, NAC and C-terminal regions and pathology-associated PTMs of aSyn (Supplementary Table 1). The C-terminal region of aSyn was extensively covered by using antigen sequences encompassing aSyn residues 108-120, 113-127 and 108-140, to ensure that all the disease-associated C-terminal truncations are targeted. To increase the likelihood of generating antibodies with epitopes in the N-terminal and/or the NAC region of the protein, human aSyn full-length (1-140) and

aSyn 1-119 recombinant proteins and aSyn 1-20 peptide were employed as immunogens. For the generation of aSyn pS129 antibodies, we initiated two programmes – one with human aSyn 124-135 peptide phosphorylated at S129 (aSyn 124-135 pS129), and another one with human aSyn 120-135 peptide doubly phosphorylated at Y125 and S129 (aSyn 120-135 pY125/pS129). This way, we sought to develop phospho-specific antibodies that would detect aSyn pS129 even in the presence of neighbouring PTMs. Lastly, the mice were immunised with aSyn 34-45 peptide nitrated at Y39 (aSyn 34-45 nY39) to produce monoclonal antibodies against this N-terminal PTM, for which there are no validated antibodies currently available. Following the immunisation of the BALB/c mice, test bleeds, hybridoma supernatants and subclones were analysed via enzyme-linked immunosorbent assay (ELISA), Western blot (WB) and slot/dot blot (DB) against a selected library of aSyn proteins (Supplementary Table 2) to determine the strongest and the most specific antibody response. Details of the monoclonal antibody generation process are provided in the Materials and Methods section. A total of 12 aSyn mouse monoclonal antibodies were obtained (Supplementary Table 3), the purity of which was validated by SDS-PAGE/Coomassie staining and WB.

Characterisation of aSyn antibodies using recombinant synuclein proteins and peptides

Epitope mapping and sequential specificity

Using aSyn and beta-synuclein (bSyn) recombinant protein standards (Supplementary Table 2), we first sought to assess the sequential specificity of our novel monoclonal aSyn antibodies and narrow down their epitopes by DB (Figure 2A) and WB (Supplementary Figure 1). The two antibodies, LASH-EGT403 and 5B10-A12, targeted the N-terminus of aSyn, i.e. residues 1-5 and 1-10, respectively. All the other novel monoclonal antibodies were mapped to the C-terminal region spanning residues 110-132, and showed staggered coverage of this region of the protein (Figure 2B; Supplementary Table 3). The epitopes of these seven antibodies were mapped to residues 110-115 (2F10-E12), 115-125 (7H10-E12), 120-125 (4E9-G10), 121-125 (1F10-B12), 121-132 (4E9-C12), 123-125 (2C4-B12) and 126-132 (6B2-D12). The results of the epitope mapping of all the novel monoclonal antibodies are summarised in Figure 2B (antibodies marked with *).

The newly produced monoclonal antibodies alone were not sufficient to achieve full coverage of the aSyn sequence. Therefore, we expanded the antibody set to include in-house polyclonal aSyn antibodies (Figure 2B, antibodies marked with **), as well as a number of commercially available and frequently used aSyn antibodies (Figure 2B, antibodies marked with ***). It is worth noting that, of these commercial antibodies, LASH-BL 34-45, LASH-BL 80-96, LASH-BL 117-122, LASH-BL A15127A (120-122) as well as LASH-BL pY39 were developed jointly with Biolegend (Figure 2B, antibodies marked with *°*). The epitopes and sequential specificities of all these antibodies were validated by DB (Figure 2A) and WB (Supplementary Figure 1). We mapped the epitope of the homemade polyclonal LASH-EGTNter antibody to aSyn residues 1-20. For all the commercial antibodies, the epitopes we identified were similar to those reported in the literature (Figure 2A-B; Supplementary Figure 1).

In addition to the antibodies against non-modified aSyn, we also generated novel monoclonal antibodies that target specific aSyn PTMs. Three aSyn PTM antibodies were developed, two of which were mapped to aSyn nY39 (5E9-G8 and 5E9-C10), and one to aSyn truncated at residue 120 (6A3-E9) by DB and WB (Figure 2B-C; Supplementary Figure 2A). Amongst the monoclonal antibodies against aSyn nY39, we observed that 5E1-G8 was weakly positive to aSyn WT and aSyn nY39 by WB (Supplementary Figure 2A, red arrow) but not by DB (Figure 2C). On the other hand, the other monoclonal antibody 5E1-C10 was positive only for aSyn nY39 both by DB and WB (Figure 2C; Supplementary Figure 2A). The specificity of 6A3-E9 was further validated via supplementary DB, WB and surface plasmon resonance (SPR) analyses (Supplementary Figure 2B-D), all of which showed that it only detects human aSyn cleaved at residue 120. We complemented our battery of antibodies against the aSyn PTMs with the previously generated in-house polyclonal antibodies against aSyn nY39 (LASH-EGT nY39), aSyn pY39 (LASH-EGT pY39), aSyn pS87 (LASH pS87), aSyn pY125 (LASH-EGT pY125), aSyn pS129 (LASH-EGT pS129), with the monoclonal aSyn pY39 antibody generated in collaboration with Biolegend (LASH-BL pY39) and with the commercially available aSyn pS129 antibody AB EP1536Y, which were also screened and validated in parallel to the novel monoclonal aSyn PTM antibodies. These antibodies were found to be specific to their targeted modifications by DB and WB (Figure 2B-C; Supplementary Figure 2A). Altogether, this selection provided us with 18 aSyn non-modified and 10 aSyn PTM antibodies to work with.

Sensitivity to neighbouring aSyn PTMs

We have recently shown that the aSyn pS129 antibody binding could be affected by the presence of aSyn PTMs neighbouring S129 (Lashuel et al., 2022), and hypothesised that sensitivity to neighbouring PTMs could also be applicable to other C-terminal as well as N-terminal or NAC region antibodies. Therefore, we investigated the reactivity of the non-modified aSyn antibodies in the presence of PTMs nearby their epitopes by DB and WB, and the results are summarised in Table 1. We note that a large number of the aSyn C-terminal antibodies (i.e. 8 out of 12) showed sensitivity to the presence of aSyn pY125 and/or truncations across residues ~119-125 (Table 1). In the presence of aSyn pY125, for instance, antibody 4E9-G10 (120-125) failed to produce a positive result both by DB and WB (Figure 2A; Supplementary Figure 1, red arrow). This finding is in line with the mapped epitope of this antibody (Figure 2B), which covers Y125. Therefore, phosphorylation of this residue may hinder the antibody recognition. Similarly, the antibody 4E9-C12 (121-132) generated a weaker signal by DB and WB when aSyn pY125 was present or if residues 120-125 were absent (Figure 2A; Supplementary Figure 1, red arrows). Interestingly, the antibodies 1F10-B12 (121-125) and 2C4-B12 (123-125) were sensitive to this modification only by DB (Figure 2A, red arrows), but were not noticeably affected by the presence of aSyn pY125 under the denaturing conditions of WB (Supplementary Figure 1). The 6B2-D12 (126-132) positive signal was weakened in the presence of aSyn pS129, especially by DB (Figure 2A, red arrow). The positive signals revealed by AB LB509 (115-122), 7H10-E12 (115-125) and LASH-BL 117-122 were all affected by C-terminal truncations roughly between residues 119-125 (Figure 2A; Supplementary Figure 1, red arrows), but less so by the presence of aSyn pY125. We expanded the same analysis to the NAC region and N-terminal antibodies. Of the two antibodies with epitopes in the NAC region, the

BD SYN-1 (91-99) signal appeared to be weaker when aSyn is phosphorylated at Serine 87 (Supplementary Figure 1, red arrow), whereas this modification did not have an impact on the positivity of LASH-BL 80-96. The LASH-BL 34-45 antibody showed no sensitivity to the presence of nY39 or pY39, but lost all positive signal with the N-terminal truncation at residue 39 (Figure 2A; Supplementary Figure 1, red arrows). Collectively, our results highlight that the antibody sensitivities to the presence of PTMs should always be considered before aSyn antibodies are selected for prospective experimental studies.

Species reactivity

Next, we assessed the reactivity of the full antibody panel to human and mouse aSyn. All N-terminal and NAC-region antibodies, including LASH-EGT403 (1-5), 5B10-A12 (1-10), LASH-EGTNter (1-20), LASH-BL (34-45), LASH-BL (80-96) and BD SYN-1 (91-99) were identified as both human- and mouse-reactive (Figure 2A). The large majority of the C-terminal antibodies, on the other hand, detected only human aSyn proteins, with the exception of 2F10-E12 (110-115), 6B2-D12 (126-132) and Abcam (134-138) antibodies that were reactive to both human and mouse aSyn (Figure 2A). These findings are consistent with the sequence differences between human and mouse aSyn in the C-terminus, particularly across the region covering residues 115-125 (Supplementary Figure 3A). Interestingly, the N-terminal antibodies LASH-EGT403 (1-5), LASH-EGTNter (1-20), LASH-BL (34-45) and the extreme C-terminal antibody AB (134-138) showed reactivity also to bSyn, whereas the N-terminal antibody 5B10-A12 (1-10), the NAC-region antibodies and the rest of the C-terminal antibodies were negative to bSyn (Figure 2A; Supplementary Figure 1). These results are consistent with the sequence similarities and differences between aSyn and bSyn (Supplementary Figure 3B). All antibodies used in this study are listed in Supplementary Table 4.

Conformational selectivity

aSyn exists in different conformations in healthy and diseased human tissues (Covell et al., 2017; Gai et al., 2003; Kovacs et al., 2012; Roberts et al., 2015; Spillantini et al., 1998a, 1998b). Therefore, we sought to determine the selectivity of the antibodies against non-modified aSyn towards the different aSyn conformations. To this end, DB and WB analyses were run on purified recombinant aSyn WT monomers, oligomers and fibrils (Figure 3A-B; Table 1), which were prepared and characterized as described previously (Kumar et al., 2020b). Electron microscopy (EM) analysis revealed that monomers, oligomers and fibrils of aSyn exhibit morphological differences (Figure 3A). Interestingly, all antibodies were strongly positive for all conformations of aSyn both by DB and WB except for LASH-BL 34-45, which was positive for aSyn monomers, oligomers and fibrils by DB, but lost its positivity to high-molecular weight (HMW) aSyn oligomers under denatured conditions (Figure 3B, red arrow). These results suggest that the vast majority of the selected antibodies are capable of recognizing all conformations and aggregation states of aSyn.

Validation of antibodies using aSyn KO mouse primary neurons and brain tissues

aSyn KO mouse primary neurons

To validate the specificity of the antibodies to aSyn species, we assessed their immunoreactivity using primary neurons derived from C57BL/6J-OlaHsd mice (SNCA−/−) lacking expression of mouse aSyn. We first determined the minimal working concentration for each of the mouse-reactive antibodies on WT naïve and mouse aSyn pre-formed fibril(PFF)-seeded hippocampal neurons by immunocytochemistry (ICC). This approach allowed us to work on aSyn KO neurons with appropriate antibody concentrations that otherwise permit the detection of endogenous aSyn, exogenously added aSyn fibrils and the newly formed aSyn aggregates in WT neurons, based on a well-characterised neuronal seeding model (Mahul-Mellier et al., 2020, 2018; Volpicelli-Daley et al., 2014). For the antibodies that are human-reactive only, we opted for the recommended dilutions by the suppliers when such information was available, and if not, we aimed at a final antibody concentration of 2-5µg/mL for ICC. We then screened the antibodies using aSyn KO hippocampal and cortical neurons.

By ICC, we observed that LASH-EGT403 (1-5), 5B10-A12 (1-10), BD SYN-1 (91-99), 2F10-E12 (110-115), AB LB509 (115-122), 4E9-G10 (120-125), 4E9-C12 (121-132) and 6B2-D12 (126-132) antibodies showed no non-specific background in hippocampal (Supplementary Figure 4A) and cortical Supplementary Figure 4B) aSyn KO neurons. The LASH-EGTNter (1-20), LASH-BL (34-45) and AB (134-138) antibodies showed positivity, possibly for bSyn protein, both in hippocampal and cortical aSyn KO neurons (Supplementary Figure 4A-B, blue arrows), an observation consistent with DB and WB results on recombinant bSyn reactivity using these antibodies (Table 1; Figure 2A, Supplementary Figure 1). Collectively, all of these antibodies showed specificity by ICC on aSyn KO hippocampal and cortical neurons. The cytoplasmic and/or nuclear signals detected in hippocampal and cortical aSyn KO neurons with BL 4B12 (103-108), 7H10-E12 (115-125), LASH-BL (117-122), LASH-BL A15127A (120-122), 1F10-B12 (121-125) and 2C4-B12 (123-125), on the other hand, were deemed to be non-specific background (Supplementary Figure 4A-B, red arrows). Interestingly, the LASH-BL 80-96 antibody revealed a weak, non-specific cytoplasmic signal in the hippocampal (Supplementary Figure 4A, red arrow) but not in cortical aSyn KO neurons (Supplementary Figure 4B). The specificity of the aSyn PTM antibodies was screened also by ICC. The LASH-BL pY39, LASH-EGT pY39, LASH-EGT pY125, AB EP1536Y pS129, LASH-EGT pS129, LASH-EGT nY39 and 6A3-E9 antibodies were negative by ICC (Supplementary Figure 5A-B), suggesting that these antibodies are specific and show no cross-reactivity. In contrast, the monoclonal aSyn nY39 antibodies 5E1-G8 and 5E1-C10 showed strong positivity both in the hippocampal and cortical aSyn KO neurons, and mild nuclear positivity was observed with LASH pS87 (Supplementary Figure 5A-B, red arrows).

We used a similar approach to investigate the specificity of the aSyn antibodies in neuronal lysates by WB. For the WB, sequential extraction was run on aSyn KO hippocampal and cortical neurons, and then the soluble and insoluble fractions were profiled using the battery of aSyn antibodies. aSyn mouse or human recombinant standards were used as positive controls. Of the human-reactive non-modified aSyn antibodies, faint non-specific bands were present mainly in the high molecular weight (HMW) regions of the soluble and/or insoluble fractions of BL 4B12 (103-108), AB LB509 (115-122), LASH-BL A15127A (120-122), 4E9-G10 (120-125) (Supplementary Figure 6A, red arrows), but not in the region

to which monomeric aSyn migrates, at 15kDa. Non-specific bands were not observed with the human-reactive 7H10-E12 (115-125), LASH-BL (117-122), 1F10-B12 (121-125), 4E9-C12 (121-132) and 2C4-B12 (123-125) antibodies (Supplementary Figure 6A). The human- and mouse-reactive non-modified aSyn antibodies i.e. LASH-EGT403 (1-5), 5B10-A12 (1-10), LASH-EGTNter (1-20), LASH-BL (34-45), LASH-BL (80-96), BD SYN-1 (91-99), 2F10-E12 (110-115), 6B2-D12 (126-132) and AB (134-138), did not detect any non-specific bands at 15kDa in the phosphate buffered saline(PBS)-treated soluble or insoluble fractions (Supplementary Figure 6A), with AB (134-138) possibly detecting bSyn in the PBS-treated soluble neuronal fractions (Supplementary Figure 6A, blue arrows). On the other hand, LASH-EGT403, 5B10-A12, LASH-EGTNter, LASH-BL 34-45, LASH-BL 80-96, 2F10-E12, 6B2-D12 and AB 134-138 showed non-specific bands in the HMW regions in the soluble and/or insoluble fractions (Supplementary Figure 6A, red arrows). The aSyn PTM antibodies did not reveal any non-specificity, except for LASH-BL pY39, LASH-EGT pY39, 5E1-G8 nY39 and 5E1-C10 nY39 that detected a few non-specific bands between 35-180kDa, and LASH-EGT pS129 which detected both HMW bands and bands around 15kDa in the insoluble fractions (Supplementary Figure 6B, red arrows).

aSyn KO mouse brain tissues

Next, we validated the specificity of the non-modified and PTM aSyn antibodies on aSyn KO mouse amygdala tissue, a brain region previously shown to be particularly affected by aSyn pathology (Burtscher et al., 2019). By immunofluorescence (IF), we observed no background with any of the antibodies against non-modified aSyn (Supplementary Figure 7A). With the aSyn PTM antibodies, on the other hand, we observed non-specific punctate cytoplasmic positivity with LASH pS87, LASH-EGT pY125, LASH-EGT pS129 and mild diffuse background with 5E1-G8 and 5E9-C10 nY39 antibodies (Supplementary Figure 7B, red arrows). A summary of the findings on aSyn KO neurons and mouse tissue for each antibody is presented in Table 2.

Antibody validation and application in human post-mortem brain tissues

Following the characterisation and validation of the antibodies using recombinant aSyn proteins, aSyn KO mouse primary neurons and brain tissues, we sought to apply these tools on human post-mortem formalin-fixed paraffin-embedded (FFPE) brain tissues. The antibodies were first titrated for immunohistochemistry (IHC) by comparing different pre-treatment (i.e. epitope retrieval) conditions and antibody dilutions. All of the non-modified aSyn antibodies (18) revealed moderate to extensive staining of aSyn pathology in the PD cingulate cortex (Figure 4A) except for the LASH-EGT403 (1-5) and 6B2-D12 (126-132) antibodies, which were rarely immunoreactive to LBs and did not detect LNs. Amongst the three PTM antibodies against aSyn nY39, we observed positivity only with the LASH-EGT nY39 polyclonal antibody, which detected cortical LBs and LNs. The 5E1-G8 and 5E1-C10 nY39 monoclonal antibodies, on the other hand, were negative on PD tissue by IHC. With regards to aSyn phosphorylation, some LBs but also thin neurites were positive for aSyn pY39, detected both by the monoclonal LASH-BL pY39 and by the polyclonal LASH-EGT pY39 antibodies. Likewise, extensive LB and LN pathology was revealed both by the commercial AB EP1536Y and the homemade LASH-EGT pS129 antibodies. On the contrary, the LASH pS87 and LASH-EGT pY125 antibodies showed little to

no reactivity in the PD cingulate cortex. The truncation-specific antibody 6A3-E9 (aSyn-120) detected exclusively the LBs without producing signal in the neurites (Figure 4A).

Interestingly, triple immunolabelling using aSyn N-terminal, C-terminal and PTM antibodies revealed that the cortical LBs were equally detected by all antibodies (Figure 4B, Supplementary Figure 8). Yet, some of the LNs and neuropil dots were selectively revealed by the LASH-BL 34-45 antibody, and not by the AB 134-138 or the 81A pS129 antibodies (Figure 4B, arrows), suggesting that a portion of neuritic pathology is non-phosphorylated and may be cleaved in the extreme C-terminus. Overall, these results support our hypothesis that capturing the diversity of aSyn species in pathological aggregates requires the use of multiple antibodies targeting different domains and disease-relevant PTMs.

A selected panel of aSyn antibodies reveal the biochemical and morphological diversity of human aSyn pathology

aSyn exists in heterogeneous conformations and proteoforms in human tissues (Anderson et al., 2006; John E Duda et al., 2000; John E. Duda et al., 2000; Fujiwara et al., 2002; Giasson et al., 2000b; Kuusisto et al., 2003); yet, profiling of the same set of synucleinopathy tissues systematically for a full range of aSyn PTMs to capture pathological diversity, has not been performed previously. Therefore, we sought to characterize aSyn pathology across different types of LBDs using our battery of antibodies. For this, we selected the best performing aSyn antibody subset that would allow for the maximal coverage of the aSyn sequence and PTMs. This subset included two antibodies against the N-terminus (LASH-EGTNter 1-20 and LASH-BL 34-45), two antibodies against the NAC region (LASH-BL 80-96 and BD SYN-1 91-99), and two antibodies against the C-terminus (i.e. 2F10-E12 110-115 and AB 134-138) of aSyn. Two additional antibodies were incorporated to cover the aSyn serine phosphorylations: AB EP1536Y pS129, as this antibody has been the most specific to aSyn pS129 species in our hands and in the literature (Delic et al., 2018; Lashuel et al., 2022), and LASH pS87, which was recently shown to detect LBs in PD and GCIs in MSA (Sonustun et al., 2022). For the N-terminal tyrosine phosphorylation modification, we opted for the monoclonal LASH-BL pY39 antibody. For the C-terminal phosphorylation at Y125, we switched to the polyclonal aSyn pY125 antibody from Abcam as our homemade LASH-EGT pY125 antibody revealed no positivity in the PD cingulate cortex (Figure 4A) and showed high background when applied to aSyn KO mouse brain tissues (Supplementary Figure 7B). To cover all possible C-terminal tyrosine phosphorylation modifications, we also included the polyclonal aSyn pY133 and pY136 antibodies from Abcam. To the best of our knowledge, these two C-terminal tyrosine phosphorylations have not been explored in post-mortem tissues, with the exception of one recent study (Sano et al., 2021). The specificities of these three Abcam antibodies were validated in hippocampal and cortical aSyn KO neurons by ICC and WB (Supplementary Figure 9A-C; Table 2). Finally, we added 6A3-E9 against aSyn 1-120 and LASH-EGT nY39 to our selection. The final antibody subset (14) chosen for further human tissue screening is presented in Figure 5A.

The specificity of these antibodies to aSyn species in human brain tissue was validated directly using post-mortem materials of cases with neurodegenerative diseases that are not classified as

synucleinopathies. The frontal cortices of progressive supranuclear palsy (PSP) and corticobasal degeneration (CBD), and the hippocampi of Alzheimer's disease (AD), Pick's disease (PiD) and frontotemporal lobar degeneration of TAR DNA-binding protein 43 type C (FTLD-TDP/C) cases were immunostained. None of the non-modified aSyn antibodies showed any immunoreactivity (Supplementary Figure 10). With regards to the aSyn PTM antibodies, LASH-EGT nY39 and 6A3-E9 aSyn-120 were negative in all cases stained (Supplementary Figure 10). AB EP1536Y (pS129) detected neuritic aSyn and AB pY133 extracellular aSyn structures in AD hippocampi (Supplementary Figure 10, arrows). AB pY136 showed rare neuronal cytoplasmic positivity in the FTLD-TDP/C hippocampus, and LASH-BL pY39 scarce diffuse cytoplasmic positivity in PSP and extracellular aSyn in CBD frontal cortices (Supplementary Figure 10, arrows). Interestingly, both the LASH pS87 and AB pY125 antibodies revealed sparse granular cytoplasmic structures in the FTLD-TDP/C, AD and PiD hippocampi (Supplementary Figure 10, arrows). These results suggest that the positive structures are genuine aSyn species that are found co-existing in brain tissues of patients with neuropathologies not classified as synucleinopathies.

The selected aSyn antibodies were then used to immunohistochemically analyse the substantia nigra of sporadic (PD n=5, PDD n=2, DLB n=1) and familial (*SNCA* G51D n=3, *SNCA* H50Q n=1, *SNCA* duplication n=1) LBDs, and the results summarised in Table 3. The LBs and LNs were uniformly detected by all aSyn non-modified and PTM antibodies except for AB pY125 and 6A3-E9 (aSyn-120) (Figure 5B; Table 3). The neuronal diffuse cytoplasmic aSyn with or without an aggregate were likewise revealed by all antibodies with the exception of LASH-BL pY39 and AB pY136. The neuronal punctate cytoplasmic aSyn species were revealed only by a subset of the non-modified aSyn antibodies, namely LASH-BL 34-45, LASH-BL 80-96 and BD SYN-1 (91-99). Similarly, the astroglial accumulations were exclusively revealed by these three non-modified aSyn antibodies and the LASH-BL pY39 and the LASH-EGT nY39 antibodies, and not by any other antibodies included in the study (Figure 5B; Table 3). Interestingly, in the cingulate cortex of these LBDs, we observed a similar phenomenon where LASH-BL pY39 and LASH-EGT nY39 antibodies picked up star-shaped glial structures (Figure 5C). The presence of coiled body-like oligodendroglial accumulations of aSyn in the substantia nigra has been reported previously (Wakabayashi et al., 2000). These oligodendroglial species were revealed best by 2F10-E12 (110-115) (Table 3). The extracellular aSyn species were detected by all aSyn non-modified and PTM antibodies except for AB pY125, and were particularly enhanced with truncation at residue 120 as well as nitration at Y39 (Figure 5B; Table 3).

Both in the substantia nigra and the cingulate cortex, the most abundant aSyn PTM we observed was aSyn pS129, and the AB EP1536Y antibody against this modification labelled LBs, diffuse neuronal cytoplasmic aSyn, neurites and neuropil dots extensively (Figure 5B-C). In contrast, LASH pS87 together with AB pY125 revealed only sparse structures across the LBDs. LASH pS87 antibody unveiled very rare puncta in the neuronal cytoplasm, dystrophic neurites and diffuse neuronal cytoplasmic accumulations in the substantia nigra (Figure 5B) but no glial accumulations or thin threads (Figure 5B-C). Similarly, AB pY125 labelled only very rare punctate cytoplasmic aSyn structures and rare diffuse

cytoplasmic inclusions in the substantia nigra, without staining any neurites or LBs in either of the two regions examined (Figure 5B-C). The other C-terminal tyrosine phosphorylation antibody AB pY133 detected some neurons containing multiple LBs, diffuse neuronal cytoplasmic inclusions and rare thin threads, whereas AB pY136 moderately picked up LBs, dystrophic neurites, neuropil dots and thin threads. The truncation-specific 6A3-E9 antibody (aSyn-120), on the contrary, stained diffuse neuronal cytoplasmic and extracellular aSyn structures, but no neurites. Altogether, our set of antibodies was able to uncover large heterogeneity of aSyn pathology in LBDs in neuronal and glial cells that cannot be discerned in its entirety when only individual antibodies are used. We further observed the cell-specific occurrence of different aSyn modifications, and report co-existence of differentially modified aSyn species, including several combinations that have not been previously described systematically, such as aSyn nY39, pY133 and pY136.

Biochemical and morphological diversity of aSyn aggregates in cellular and animal seeding models

aSyn antibodies are essential for the characterisation of preclinical models. Seeding-based cellular and animal models using aSyn PFFs have emerged as the most common tools to investigate mechanisms and pathways of aSyn pathology formation (Kumar et al., 2021; Luk et al., 2012, 2009; Mahul-Mellier et al., 2020, 2018; Volpicelli-Daley et al., 2014, 2011). In the majority of the studies using these models, monitoring, quantification and characterisation of aSyn are based on the detection of aSyn pS129 species. However, no study has systematically assessed the occurrence of other disease-associated PTMs in these models, with the exception of some C-terminal cleaved aSyn species (Elfarrash et al., 2019; Luk et al., 2012, 2009; Mahul-Mellier et al., 2020, 2018; Volpicelli-Daley et al., 2011). Therefore, our knowledge about the role of PTMs in regulating aSyn seeding and LB formation in these models remains incomplete.

To address this knowledge gap and characterize the diversity of aSyn species in these PFF models, we first investigated the ability of our antibodies to detect exogenously added PFFs in aSyn KO hippocampal and cortical neurons by ICC and WB (Supplementary Figure 4-6) 14 hours after treatment. Our findings are summarised in Table 4. All of the 9 non-modified and mouse aSyn-reactive antibodies i.e. the N-terminal LASH-EGT403 (1-5), 5B10-A12 (1-10), LASH-EGTNter (1-20) and LASH-BL 34-45; the NAC-region LASH-BL 80-96, BD SYN-1 (91-99); and the C-terminal 2F10-E12 (110-115), 6B2-D12 (126-132) and AB 134-138 antibodies detected exogenous fibrils in the PFF-treated hippocampal (Supplementary Figure 4A) and cortical (Supplementary Figure 4B) aSyn KO neurons by ICC. By WB, bands specific to exogenously added fibrils were revealed between 10kDa-35kDa by these antibodies (Supplementary Figure 6A, green arrows) except for the 6B2-D12 (126-132) antibody, which failed to detect any bands in the PFF-added neuronal fractions. With the aSyn PTM antibodies, no positivity was detected in the PFF-treated hippocampal or cortical aSyn KO neurons using the aSyn pY39, pS129, pY133 or pY136 antibodies by ICC (Supplementary Figure 5A-B; Supplementary Figure 9A-B) or by WB (Supplementary Figure 6A; Supplementary Figure 9C). Similarly, no positivity was revealed with the LASH-EGT nY39 antibody in the hippocampal or cortical aSyn KO neurons by ICC (Supplementary

Figure 5A-B) or WB (Supplementary Figure 6B). On the contrary, the monoclonal nY39 antibodies 5E1-G8 and 5E1-C10 were positive both in the PFF-treated and control (PBS-treated) aSyn KO neurons, signals which we presumed to be non-specific by ICC (Supplementary Figure 5A-B, red arrows). Intriguingly, 6A3-E9 antibody against aSyn-120 showed no background in PBS-treated control neurons (Supplementary Figure 5A-B) but showed positivity to PFF-treated hippocampal and cortical aSyn KO neurons by ICC (Supplementary Figure 5A-B, green arrows), and so we cannot rule out the possibility that this antibody may be reactive to aSyn full-length mouse fibrils. By WB, on the other hand, no bands were revealed in the PFF-treated aSyn KO hippocampal and cortical soluble and insoluble fractions (Supplementary Figure 6B). Collectively, these results confirm the specificity of our antibodies, and suggest that the internalised PFFs do not undergo any type of PTMs, except for N- and C-terminal cleavages, in the absence of seeding.

Finally, the mouse aSyn-reactive antibodies (Table 4; Supplementary Table 4) were used to characterize the PTM profile of newly formed aSyn aggregates in the neuronal seeding model (Mahul-Mellier et al., 2020, 2020; Volpicelli-Daley et al., 2014, 2011), and in the PFF-injected *in vivo* model (Burtscher et al., 2019; Luk et al., 2012; Masuda-Suzukake et al., 2013) of aSyn. Whilst all the non-modified aSyn antibodies detected the endogenous aSyn in PFF-treated or control (PBS-treated) WT hippocampal neurons by ICC, the 5B10-A12 (1-10), LASH-EGTNter (1-20), LASH-BL 34-45 and AB 134-138 antibodies showed almost complete overlap with the aSyn pS129-positive inclusions in the PFF-treated neurons (Table 4; Figure 6A, arrows), suggesting that these could be useful and alternative tools to aSyn pS129 for monitoring the aSyn aggregation in cell culture, especially if the cross-reactivity of the pS129 antibodies may confound the results. A similar pattern of overlap with the aSyn-positive inclusions, specifically for 5B10-A12 (1-10), LASH-EGTNter (1-20), 2F10-E12 (110-115) and AB 134-138 antibodies (Table 4; Figure 6C, arrows), was also observed in the amygdala of WT mice that had been injected with PFFs in the striatum. The amygdala has previously been reported to be particularly prone to develop early and substantial aSyn pathology in this model (Burtscher et al., 2019). We speculate that this staining pattern may be due to the preferential exposure of epitopes in the extreme N- and C-terminal aSyn, whereas the hydrophobic NAC region is less accessible and buried in the core of the newly formed aggregates.

With the aSyn nY39 antibodies, we did not see any positivity in the neurons or in mouse tissue (Table 4; Figure 6B-C), except for diffuse cytoplasmic staining with the 5E1-G8 and 5E1-C10, which we also observed in aSyn KO neurons and therefore deemed non-specific (Supplementary Figure 5A-B). With the N-terminal tyrosine phosphorylation at Y39, on the other hand, both in the PFF-treated neurons and in the PFF-injected mouse amygdala, we detected punctate structures in close proximity to, and partially overlapping with, the aSyn pS129-positive inclusions (Table 4; Figure 6B-C, arrowheads). We noted similar punctate positivity also with aSyn pY133 and pY136 antibodies in the neuronal seeding model (Table 4; Figure 6B, arrowheads), which again partially overlapped with the aSyn pS129-positive accumulations. Altogether, these data suggest that aSyn may become hyperphosphorylated during the aggregation and inclusion maturation processes. Further research is needed to decipher the mechanism

of formation and fate of these puncta structures, which are not detectable by the aSyn pS129 antibodies. To the best of our knowledge, this work the first and most comprehensive profiling of aSyn aggregation and PTM patterns of the PFF neuronal seeding model. Our results illustrate the power of the antibodies we have presented in this study to investigate the role of PTMs in regulating aSyn seeding and inclusion formation, and to capture the morphological and biochemical diversity of aSyn aggregates in the cellular and *in vivo* models of aSyn seeding.

DISCUSSION

Previous studies focusing on the development and application of multiple antibodies have been instrumental in the understanding of pathological heterogeneity of aSyn in LBDs and MSA (Almandoz-Gil et al., 2017; Covell et al., 2017; Croisier et al., 2006; Dhillon et al., 2017; Duda et al., 2002, 2000b; Fagerqvist et al., 2013; Galvin et al., 2000; Giasson et al., 2000a, 2000b; Henderson et al., 2020; Vaikath et al., 2015; Waxman et al., 2008). On the other hand, no reports are yet available that characterise and validate aSyn antibodies targeting the entire sequence of aSyn and all key aSyn PTMs in a single study, followed by pathology profiling on the same set of LBD cases. In this study, we presented the development, validation and characterization of 12 novel monoclonal antibodies against different regions and PTMs of aSyn. These were complemented with pre-existing in-house and commercial antibodies to guarantee a more comprehensive coverage of the aSyn biochemical and structural diversity. In total, 31 antibodies were thoroughly characterised using a stringent validation pipeline (Figure 1D), leading to the selection of 14 of them for profiling the diversity of aSyn pathology in LBDs (Table 3). Although all of the antibodies targeting non-modified aSyn sequences efficiently detected LBs, considerable differences particularly in the revelation of astroglial aSyn accumulations, punctate neuronal cytoplasmic inclusions and a subset of LNs and neuropil dots were observed in the substantia nigra and cingulate cortex of LBDs. This finding suggests differential capacities of the individual antibodies to uncover specific aspects of aSyn pathology with important implications for disease staging and characterisation of disease subtypes. Specifically, our results indicate that the use of single antibodies or inappropriate antibody combinations may result in profound underrating of the aSyn pathological load and diversity.

LBs are mature inclusions composed of a mixture of full-length, N- and C-terminally truncated and other modified aSyn species of different conformational properties (Bhattacharjee et al., 2019; Moors et al., 2021; Prasad et al., 2012). This makes LBs more likely to be detected by aSyn antibodies regardless of their sequential epitopes. Yet, other types of aSyn accumulations, which are dominated by specific forms or conformations of aSyn, may be difficult to detect using single antibodies. These may include less mature and poorly characterised manifestations of aSyn pathology, such as punctate neuronal inclusions, astroglial aSyn accumulations, and a subset of LNs, which could be composed of homogenous aSyn proteoforms. The availability of the expanded toolbox presented herein enables us to perform systematic profiling of aSyn species and pathology at a single cell level by ICC/IHC, which is not possible by biochemical methods such as WB. With this work, we identified antibodies that were able to detect specific aSyn species and inclusions in distinct cell types. This paves the way for future

elucidation of the sequence, cell type or cell environment determinants of aSyn pathology formation and multiple cellular and molecular processes linked to neurodegeneration.

Our pioneering study allowed for the investigation of the most prominent disease-associated phosphorylation, nitration and truncation PTMs of aSyn on the same set of LBD cases. This was enabled by the combined use of a total of 6 non-modified aSyn antibodies against all three regions of the protein and 8 different aSyn PTM antibodies that were used to screen a subset of LB disorders. Our results revealed a wide range of aSyn inclusion types at differing densities. We confirm that aSyn pS129 is the most abundant disease-related modification of aSyn in the substantia nigra, an observation consistent with previous publications reporting similar results on aSyn pS129 enrichment in diseased brains by mass spectrometry analyses (Anderson et al., 2006; Fujiwara et al., 2002). Uniquely, we report here that LB disorders are also rich in N-terminal nitration at Y39. Nitrated aSyn in post-mortem human studies has been previously reported (Duda et al., 2000) but the site-specific N-terminal nitration at Y39 was not investigated due to the lack of an antibody targeting this modification specifically. Similarly, only a handful of studies so far have investigated the N-terminal (Chen et al., 2009; Mahul-Mellier et al., 2014) and C-terminal (Sano et al., 2021) tyrosine phosphorylations. Here we describe the widespread co-presence of these modifications across LB disorders scattered to neurons and glia. One limitation of our study is that it did not investigate the distribution of ubiquitinated, acetylated or N- and C-terminally truncated aSyn species other than aSyn-120. This is due to the lack of antibodies against this particular modification of the protein, and future efforts to develop appropriate tools to fill this gap will provide an even more complete picture of aSyn pathology heterogeneity. Although the scope of this work primarily covered sporadic and familial LBDs, studies are underway to characterise aSyn pathology in MSA using this toolset.

The neuronal seeding model of aSyn aggregation and LB-like inclusion formation has been well characterised, and the occurrences of the phosphorylation at Serine 129 and C-terminal truncations have been described by several groups (Mahul-Mellier et al., 2020, 2018; Volpicelli-Daley et al., 2014, 2011). Here, we present the most comprehensive profiling of the post-translationally modified aSyn species in this model. We show that the neuronal aSyn inclusions are hyperphosphorylated, and report for the first time the formation of punctate intracellular structures that are positive for N- or C-terminal tyrosine phosphorylations (pY39, pY133, pY136), which are not revealed by the aSyn pS129 antibodies. These findings illustrate the power of using multiple antibodies to gain insight into the role of PTMs in regulating the formation of different types of aSyn aggregates. Prospective studies to decipher the cellular mechanisms modulating these modifications, and the role of these PTMs in aSyn aggregation, aggregate maturation and aSyn-mediated toxicity may be of crucial translational value.

In summary, our work highlights the limitations of relying on individual antibodies for aSyn pathology characterisation, and provide a selected, well-characterised toolset of antibodies for an extensive evaluation of aSyn pathology diversity. Clearly, not every study design will justify the use of the complete set used here. However, the provided characterizations of the individual antibodies, including their

capacities to uncover specific features of aSyn pathology, will enable the choice of appropriate antibodies for specific studies based on solid rationales, a possibility that did not exist before. On the other hand, re-visiting the staging studies of PD and other LBDs based on aSyn pathology would greatly benefit from using a good selection of several well-suited antibodies described here to possibly resolve inconsistencies observed when correlating pathology with symptomatology (Jellinger, 2009; Milber et al., 2012; Parkkinen et al., 2008, 2007; Steiner et al., 2018).

Our finding that capturing the diversity of aSyn pathology requires the use of a combination of carefully selected antibodies provides a unique opportunity to investigate the relationship between aSyn aggregation, neuronal dysfunction and neurodegeneration in PD and other synucleinopathies more systematically. For instance, several studies have reported the absence of LBs in a subset of PD patients with *LRRK2* mutations (Agin-Liebes et al., 2020; Funayama et al., 2005; Gaig et al., 2007; Giasson et al., 2006; Henderson et al., 2019; Kalia et al., 2015; Marti-Masso et al., 2009; Takanashi et al., 2018; Vilas et al., 2019; Wszolek et al., 2004). Many of these studies relied on the use of a single antibody or a small number of antibodies targeting the C-terminus of aSyn, leaving the possibility that other forms of aSyn may still be present. Re-examining aSyn pathology using our antibody toolbox offers a new window to determine conclusively whether LB or other aSyn pathology is truly absent in these cases.

Finally, we believe that future research aimed at re-visiting 1) PD and other LBD staging in the central nervous system using large cohorts, and 2) aSyn aggregation in the periphery using this validated antibody toolset would open new avenues in our comprehension of spreading of aSyn pathology, and help identify novel therapeutic targets to interfere with these mechanisms.

MATERIALS AND METHODS

Generation of aSyn monoclonal antibodies

A combination of aSyn human recombinant proteins and peptides against different forms and modifications of aSyn was used for the immunisation of BALB/c mice (Supplementary Table 1). These were solubilised in PBS and, where appropriate, conjugated to the carrier protein keyhole limpet hemocyanin (KLH). Following pre-immune serum collection, BALB/c mice were subcutaneously injected with the immunogen-complete Freund's adjuvant (CFA) mixture on Day 0, and with immunogen-incomplete Freund's adjuvant (IFA) on Day 21 and Day 42. Test bleeds were run on Days 35 and 56, and antibody response was evaluated by ELISA, WB and DB. Animals with strong immunoreactivities were euthanised and their splenocytes surgically harvested.

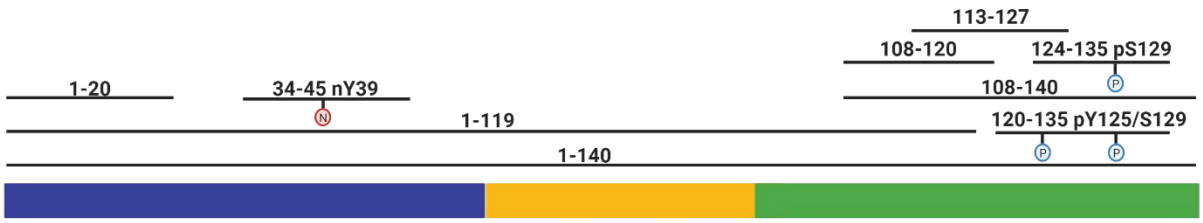

A schematic of the aSyn human proteins and peptides used for BALB/c mouse immunisation. Created with Biorender.com (agreement no: *NS23V1NZV8).*

Hybridoma technology was used for the production of monoclonal antibodies, where the antibody-producing lymphocytes were fused with Sp2/0-Ag14 (ATCC #CRL-8287) mouse myeloma cells using polyethylene glycol (PEG) at a 5:1 ratio. The hybridomas were grown in hypoxanthine-aminopterin-thymidine (HAT) selective media to eliminate unfused myeloma cells. Supernatants of 6 to 44 clones per programme were tested by ELISA, DB and WB against a selected library of aSyn proteins (Supplementary Table 2) to determine the clones with the strongest and the most specific results. Selected clones were further sub-cultured for several rounds to maintain stability, subjected to serial dilution to ensure monoclonality, and screened by ELISA, DB and WB for the identification of positive and specific clones. Isotyping and *in vitro* production of antibodies were carried out with the selected subclones, on an Akta 25 FPLC system using a 25mL protein G sepharose column (Cytiva) according to the instructions of the manufacturer. Briefly, the resin was equilibrated using 10 column volumes (CV) of buffer A (20mM phosphate buffer pH7.2) before loading the filtrated sample on the column. Following a wash step of 10 CV with buffer A, antibodies were eluted using an isocratic elution with buffer B (100mM glycine pH2.7), and were immediately pH-neutralised with 1M Tris buffer pH8.0 upon their harvest in fractionation tubes. Buffer exchange was performed against 10mM PBS using a 30kDa dialysis membrane, and the harvested antibodies were stored at -70 °C. Antibody concentrations were determined using absorbance reading at 280nm, and purity was determined by size exclusion chromatography. An average of 45mg from each of the 12 antibodies were obtained.

Expression and purification of aSyn monomers

The expression and purification of human and mouse aSyn were carried out as described (Fauvet et al., 2012). Briefly, pT7-7 plasmids encoding variants of mouse and human aSyn were used to transform BL21(DE3) chemically competent *E. coli* and let to grow on an agar dish with ampicillin. One colony was transferred to 400mL of Luria broth (LB) media with ampicillin at 100µg/mL and left to grow at 37 °C on shaker (at 180RPM) for 16h. The small culture was then used to inoculate a large culture of 6L LB media with ampicillin at 100µg/mL. At an optic density (OD_{600}) of 0.5-0.6, isopropyl β-D-1-thiogalactopyranoside was added at a final concentration of 1mM to induce aSyn expression. The large culture was left to grow further for 4h on shaker, centrifuged at 4,000*g* for 15min at 4 °C. The pellet was re-suspended on ice in lysis buffer (10mL p/L of culture) containing 20mM Tris pH8.0, 0.3mM phenylmethylsulfonyl fluoride (PMSF) protease inhibitor and cOmplete, mini, EDTA-free protease inhibitor cocktail tablet (Roche #4693159001; one tablet per 10mL lysis buffer). Cells were lysed by sonication (59s-pulse and 59s-no pulse over 5min at 60% amplitude). The lysate was centrifuged at 4 °C for 30min at 20,000*g*, the supernatant boiled for 5-15min at 100 °C, and the centrifugation step repeated. Supernatant was filtered using a 0.22µm syringe filter, and purified via anion exchange chromatography and reverse-phase high performance liquid chromatography (HPLC). The quality control of the proteins was run via analysis by liquid chromatography-mass spectrometry (LC-MS), ultra-performance liquid chromatography (UPLC) and SDS-PAGE separation and Coomassie staining. aSyn nY39, pY39, pS87, pY125 and pS129 protein standards were prepared using semi-synthesis as previously described (Hejjaoui et al., 2012).

aSyn oligomer generation

Generation of aSyn oligomers was carried out as previously described (Kumar et al., 2020b). Briefly, aSyn human WT monomers were dissolved in PBS for a final concentration of 12mg/mL, and was supplemented with benzonase at 1uL/mL. The solution was incubated in low-protein binding tubes at 37 °C for 5h at 900rpm, centrifuged for 10min at 12,000*g* at 4 °C, and 5mL of supernatant was run through a PBS-equilibrated Hiload 26/600 Superdex 200pg column. Eluted fractions were screened via SDS-PAGE. Oligomeric fractions were characterised by EM, circular dichroism (CD) before being collected, snap frozen and stored at -20 °C.

Generation of aSyn pre-formed fibrils *in vitro*

Lyophilised human or mouse aSyn WT monomers were re-suspended in PBS, and the pH was adjusted to 7.5. The protein solution was passed through filters with 100kDa cut-off to remove any spontaneously formed aggregates. Protein concentration was measured via ultraviolet (UV) absorption at 280nm and/or by bicinchoninic acid (BCA) assay. Monomers in solution were left on an orbital shaker (at 1000RPM) for 5 days at 37 °C. For application to cellular seeding models, the fibrils were sonicated to achieve a median fibril length of 50-100nm. The final fibril prep was characterised for the monomer-to-fibril ratio by sedimentation and filtration assays as described in (Kumar et al., 2020a), for amyloid formation by ThT assay, and for fibril length quantification by electron microscopy analysis.

Dot blot/slot blot and Western blot analyses using aSyn recombinant proteins

For the dot blot/slot blot analysis, aSyn proteins were diluted in PBS and blotted on a nitrocellulose membrane of 0.22µm in 50µL volume corresponding to 250ng of protein loading. For the WB analysis, aSyn proteins were diluted in PBS and Laemmli buffer 4X (50% glycerol, 1M Tris at pH 6.8, 20% β-mercaptoethanol, 10% SDS and 0.1% bromophenol blue), loaded onto a 4-16% Tricine gel in 10µL volume corresponding to 100ng of protein loading and transferred onto a nitrocellulose membrane of pore size 0.22µm using a semi-dry transfer system (BioRad) for 45min at 0.5A and 25V. Where appropriate, Ponceau S staining (2% Ponceau S in 5% acetic acid) was applied as protein loading control. The membranes were blocked overnight at 4 °C in Odyssey blocking buffer (Li-Cor). They were incubated with primary antibodies diluted in PBS for 2h at RT, washed three times for 10min in PBS with 0.01% Tween-20 (PBS-T), incubated in dark with secondary antibodies diluted in PBS and washed three times for 10min in PBS-T. For the primary and secondary antibody details, see Supplementary Table 4. The membranes were imaged at 700nm and/or 800nm using the Li-Cor Odyssey CLx imaging system, and the images were processed using Image Studio 5.2.

Surface plasmon resonance (Biacore)

SPR data were collected on a Biacore 8 K device (GE Healthcare). Antibody (6A3) was immobilized on a CM5 biosensor chip (GE Healthcare) at 10–20 µg/mL concentration in 10 mM acetate solution (GE Healthcare) at pH 4.5 to reach a final surface ligand density of around 2000–4000 response units (RUs). In short, the whole immobilization procedure using solutions of 1-ethyl-3-(3-dimethyl aminopropyl)

carbodiimide (EDC) and N-hydroxy succinimide (NHS) mixture, antibody sample and ethanolamine, was carried out at a flow rate of 10 µL/min into the flow cells of the Biacore chip. Firstly, the carboxyl groups on the sensorchip surface were activated by injecting 200 µL of 1:1 (v/v) mixture of EDC/NHS (included in the amine coupling kit, Cytiva Life Sciences) into both flow cells 1 and 2 and followed by the injection of antibodies overflow cell 2 for 180 s. The remaining activated groups in both the flow cells were blocked by injecting 129 µL of 1 M ethanolamine-HCl pH 8.5. The sensor chip coated with antibodies were equilibrated with PBS buffer before the initiation of the binding assays. Serial dilutions of analytes such as α-syn monomers (human WT 1-20 or human WT 1-140) at a concentration ranging between 2.5 µM to 0.1 µM in PBS buffer were injected into both flow cells at a flow rate of 30 µL/min at 25 °C. Each sample cycle has the contact time (association phase) of 120 s and is followed by a dissociation time of 600 s. After every injection cycle, surface regeneration of the Biacore chips was performed using 10 mM glycine (pH 3.0).

Mouse primary neuronal culture and seeding assay

Primary hippocampal and cortical neurons were collected from P0 pups of WT (C57BL/6J-RccHsd, Harlan) or aSyn KO (C57BL/6J-OlaHsd, Harlan) mice, according to the dissection procedure described elsewhere (Steiner et al., 2002). Following the plating in poly-L-lysine-coated plates (300,000 cells/mL), the neurons were left to mature at 37 °C with 5% CO_2. WT neurons were treated with 70nM aSyn mouse WT PFFs on day *in vitro* (DIV)7 and left to incubate for 14 days; and aSyn KO neurons on DIV20 and left to incubate for 24h, as described (Mahul-Mellier et al., 2020, 2018; Volpicelli-Daley et al., 2014, 2011).

Immunocytochemistry and confocal imaging

Mouse primary neurons were washed twice in PBS, fixed with 4% PFA for 20min at RT and stained as described elsewhere (Mahul-Mellier et al., 2015). The antibodies used for ICC are detailed in Supplementary Table 4. Imaging was carried out on a confocal laser-scanning microscope (LSM 700, Carl Zeiss, Germany) and image analysis on Zen Digital Imaging software (RRID: SCR_013672).

Cell lysis, sequential extraction and Western blotting

Mouse primary neurons were washed in PBS twice on ice and extracted in Tris-buffered saline (TBS; 50mM Tris and 150mM NaCl at pH7.5) with 1% Triton X-100 and with protease inhibitor (PI) cocktail (1:100), 1mM phenylmethane sulfonyl fluoride (PMSF), phosphatase inhibitor cocktails 2 and 3 (1:100), as described previously (Mahul-Mellier et al., 2020, 2018; Volpicelli-Daley et al., 2014, 2011). The cells were lysed via sonication (1s intermittent pulse 10 times at 20% amplitude) using a small probe (Sonic Vibra Cell, Blanc Labo, Switzerland). The lysate was incubated for 30min on ice and centrifuged at 100,000*g* for 30min at 4 °C. The supernatant i.e. the 'soluble' fraction, was collected and diluted in 4X Laemmli buffer (50% glycerol, 1M Tris at pH 6.8, 20% β-mercaptoethanol, 10% SDS and 0.1% bromophenol blue). As the wash step, the pellet was re-suspended in lysis buffer, sonicated and centrifuged as described above. Supernatant was discarded and the pellet re-suspended in TBS with 2% sodium dodecyl sulphate supplemented with protease and phosphatase inhibitors as described

above. The re-suspension, i.e. the 'insoluble fraction', was sonicated (1s intermittent pulse 15 times at 20% amplitude) and diluted in 4X Laemmli buffer. Protein concentration was determined by BCA assay separately for the soluble and the insoluble fractions.

The soluble and insoluble fractions were separated on a 16% Tricine gel (ThermoFisher), transferred onto a nitrocellulose membrane of pore size 0.22µm using a semi-dry transfer system (BioRad) for 45min at 0.5A and 25V. The membranes were blocked overnight at 4 °C in Odyssey blocking buffer (Li-Cor), and washed three times for 10min in PBS with 0.01% Tween-20 (PBS-T). Membranes were incubated with primary antibodies diluted in PBS for 2h at RT, washed three times for 10min in PBS-T, incubated in dark with secondary antibodies diluted in PBS and washed three times for 10min in PBS-T. For the antibody details, see Supplementary Table 4. The membranes were imaged at 700nm and/or 800nm using the Li-Cor Odyssey CLx imaging system, and the images processed using Image Studio 5.2.

Animals and intra-striatal stereotaxic injection procedure

All animal experimentation was performed in compliance with the European Communities Council Directive of 24 November 1986 (86/609EEC) and with approval of the Cantonal Veterinary Authorities (Vaud, Switzerland) and the Swiss Federal Veterinary Office (authorisation number VD2067.2). C57BL/6JRj male mice (Janvier Labs) at 3 months of age were stereotaxically injected with aSyn mouse WT PFFs (5mg in 2mL PBS) in the right dorsal striatum. 6 months post-injection, the animals were sacrificed by intracardiac perfusion with heparinized sodium chloride (NaCl; 0.9%), and fixed with 4% paraformaldehyde (PFA) in PBS overnight, and paraffin-embedded for immunohistochemical studies. For the antibody validation studies, naïve adult aSyn KO mice (C57BL/6J OlaHsd, Harlan) were sacrificed and brain sections were prepared in the same way as for PFF-injected WT animals.

Immunofluorescent double-labelling of mouse tissue and imaging

WT and aSyn KO mouse paraffin-embedded brain sections were cut coronally to 4µm and dewaxed. Epitope retrieval was carried out in 10mM trisodium citrate buffer at pH6.0 for 20min at 95 °C. Tissue blocking was run by incubation in 3% bovine serum albumin (BSA) and 0.1% Triton X-100 in PBS for 1h at RT. Sections were then incubated with the primary antibody solution overnight at 4 °C, and with the secondary antibody solution for 60min at RT (Supplementary Table 4). Slides were mounted using an aqueous mounting medium, and tiled imaging was carried out on the Olympus VS120 microscope.

Human brain tissue samples

The cases selected from the Queen Square Brain Bank (QSBB), UCL Institute of Neurology in London, UK, were collected in accordance with the London Multicentre Research Ethics Committee-approved protocol. All donors had given written informed consent prior to the brain collection. The samples were stored under the licence (no: 12198) approved by the Human Tissue Authority. The ethical approval for research was given by the National Research Ethics Service (NRES) Committee London Central.

Immunohistochemistry of human brain samples and imaging

5 PD, 2 PDD, 1 DLB, 1 *SNCA* H50Q, 3 *SNCA* G51D mutation and 1 *SNCA* duplication brain were used for the immunohistochemical studies. FFPE sections were cut sequentially to 8µm of thickness and de-paraffinised. For epitope retrieval, the sections were treated with 80-100% formic acid for 10min at room temperature (RT) and/or with citrate buffer (pH6.0) for 10min at 121°C under pressure. Sections were treated with 3% hydrogen peroxide in PBS for 30min to quench the endogenous peroxidase. After the blocking in 10% foetal bovine serum (FBS) for 30min, sections were incubated in primary antibody solution overnight at 4°C. For the primary antibody details, see Supplementary Table 4. After being rinsed in PBS-Tween 0.1% (PBS-T), sections were incubated in the secondary antibody-horseradish peroxidase (HRP) complex from the REAL EnVision detection kit (Dako #K5007) for 1h at RT. Sections were rinsed in PBS-T before visualisation with 3,3'-diaminobenzidine (DAB). They were counterstained with haematoxylin, cleared in xylene and mounted using distyrene plasticiser xylene (DPX).

FIGURE LEGENDS

Figure 1: (A) Diversity of aSyn pathology in synucleinopathies with **(Ai)** granular/ punctate cytoplasmic inclusions in the neurons; **(Aii)** classical LBs in the neuronal soma; **(Aiii)** LNs in the neuronal processes; **(Aiv)** astrocytic aSyn accumulations; **(Av)** oligodendroglial cytoplasmic inclusions. These pathological structures show differences in their positivity to aggregation markers, including ubiquitin (Ub) and p62. Schematic created with BioRender.com (agreement no: *QW23G6FJ76*). **(B)** Cryo-EM three-dimensional reconstructions of the recombinant full-length aSyn PFFs to show the polymorphism of aSyn fibrils generated *in vitro* (Guerrero-Ferreira et al., 2019; Li et al., 2018). Four distinct polymorphs were identified based on the protofilament fold and inter-protofilament interfaces: Polymorph 1a 'rod' (PDB-6CU7, EMD-7618); polymorph 1b 'twister' (PDB-6CU8, EMD-7619); polymorph 2a (PDB-6SSX, EMD-10307); and polymorph 2b (PDB-6SST, EMD-10305). **(C)** aSyn PTMs identified in synucleinopathy brain tissues, which include acetylation, ubiquitination, phosphorylation, nitration and truncation across the whole sequence of the protein. **(D)** A schematic representation of the steps followed for the generation, characterisation, validation and application of the novel aSyn monoclonal mouse antibodies. These involved (**Di**) antibody design via the selection of immunogens comprising of aSyn recombinant proteins and peptides; (**Dii**) immunisation of the mice followed by lymphocyte-myeloma fusion; (**Diii**) screening of the hybridomas via ELISA, DB and WB, isotyping and subcloning, and (**Div**) acquisition of purified antibodies. These antibodies were then (**Dv**) characterised using a library of aSyn and bSyn recombinant proteins for their epitopes, conformational selectivity, sensitivity, specificity and reactivity via DB and WB. The antibody specificity was then further validated on (**Dvi**) aSyn KO mouse primary hippocampal and cortical neurons, and in aSyn KO mouse tissue of amygdala. (**Dvii**) The antibodies were validated on human brain tissues of different LB disorders. (**Dviii**) The mouse aSyn-reactive antibodies were applied to neuronal seeding model and PFF-injected mouse brain tissues to profile the newly formed aggregates. Schematic created with BioRender.com (agreement no: *FN23G6E1SR*). aSyn = alpha-synuclein; bSyn = beta-synuclein; DB = dot blot; cryo-EM = cryogenic electron microscopy; ELISA = enzyme-linked immunoassay; KO = knockout; LB = Lewy body; LN = Lewy neurite; PFFs = pre-formed fibrils; PTM = post-translational modification; Ub = ubiquitin; WB = Western blot

Figure 2: Validation and epitope mapping of aSyn antibodies. **(A)** DB validation of the novel monoclonal, in-house polyclonal and commercially available aSyn antibodies against the N-terminal, non-amyloid component (NAC) and the C-terminal regions of aSyn for epitope mapping, specificity and species reactivity using a selected library of aSyn and bSyn recombinant proteins under native conditions. Protein loading control was run via Ponceau S staining. All loaded proteins represent human aSyn forms except for human bSyn and mouse aSyn full-length (m FL) proteins. Red arrows highlight the sensitivities of the antibodies to the presence of neighbouring aSyn PTMs. **(B)** A schematic to represent the novel monoclonal (marked with *), in-house polyclonal (marked with **) and pre-existing commercial aSyn antibodies (marked with ***) included in this study. The commercial antibodies developed jointly with Biolegend are marked with *°*. The epitope information of each antibody is indicated in blue. Schematic created with BioRender.com (agreement no: *JR23G6G5LA*). **(C)** Validation of the aSyn PTM antibodies via DB screening. aSyn = alpha-synuclein; bSyn = beta-synuclein; DB = dot blot; FL = full-length; m = mouse; PTM = post-translational modification

Figure 3: Selectivity of aSyn antibodies over aSyn conformations. **(A)** Representative EM images of aSyn human WT monomers, oligomers and fibrils. **(B)** DB and WB characterisation of the novel monoclonal, in-house polyclonal and commercially available aSyn antibodies to determine their conformational selectivity using aSyn human WT recombinant monomers, oligomers and pre-formed fibrils. aSyn = alpha-synuclein; DB = dot blot; EM = electron microscopy; f = fibrils; m = monomers; o = oligomers; WB = Western blot; WT = wild-type

Figure 4: Application and validation of the aSyn antibodies on PD tissue. **(A)** The in-house monoclonal, polyclonal and commercial aSyn antibodies were optimised for IHC on the PD cingulate cortex. **(B)** Triple labelling of PD cingulate cortex by IF using an aSyn N-terminal (LASH-BL 34-45), a C-terminal (AB 134-138) and a pS129 (BL 81A-biotin) antibody. aSyn = alpha-synuclein; IF = immunofluorescence; IHC = immunohistochemistry; PD = Parkinson's disease

Figure 5: A selected panel of aSyn antibodies reveal the broad diversity of human pathology in the substantia nigra of LBDs. **(A)** An outline to show the epitopes of the aSyn antibody selection used for IHC studies on LBD tissues. Schematic created with BioRender.com (agreement no: *NU23G6E7KK*). **(B)** Representative images from the substantia nigra of sporadic (PD, DLB) and familial (*SNCA* H50Q) LBDs screened with the selection of aSyn non-modified and aSyn PTM antibodies. **(C)** Representative images from the cingulate cortex of sporadic (DLB) and familial (*SNCA* G51D) LBDs screened with the selected aSyn PTM antibodies. aSyn = alpha-synuclein; DLB = dementia with Lewy bodies; IHC = immunohistochemistry; LBD = Lewy body disorder; PD = Parkinson's disease; PTM = post-translational modification

Figure 6: Application of the aSyn antibodies to the cellular and animal seeding models to profile the newly formed aSyn aggregates. WT hippocampal neurons were seeded with PFFs for 14 days, and the

newly formed aggregates monitored by ICC using the mouse-reactive **(A)** non-modified aSyn and **(B)** aSyn PTM antibodies in parallel to aSyn pS129 antibodies BL 81A or AB MJF-R13. **(C)** The same type of screening was run in PFF-injected mouse amygdala tissues by IHC. The non-modified aSyn antibody signals overlapping with the aSyn pS129-positive aggregates are marked with an arrow. The punctate positivity shown by aSyn pY39, pY133 and pY136 antibodies in close proximity to aSyn pS129-positive aggregates are shown by arrowheads. Note the non-specific diffuse positivity revealed by the two monoclonal nY39 antibodies 5E1-G8 and 5E1-C10 in the WT hippocampal neurons are also revealed in the aSyn KO neurons using these two antibodies (Supplementary Figure 5). aSyn = alpha-synuclein; ICC = immunocytochemistry; IHC – immunohistochemistry; KO = knockout; PFFs = pre-formed fibrils; PTM = post-translational modification; WT = wild-type

Supplementary Figure 1: Validation and epitope mapping of aSyn antibodies. WB validation of the novel monoclonal, in-house polyclonal and commercially available aSyn antibodies against the N-terminal, non-amyloid component (NAC) and the C-terminal regions of aSyn for epitope mapping, specificity and species reactivity using a selected library of aSyn recombinant proteins under denatured conditions. Protein loading control was run via re-blotting the membranes with complementary aSyn antibodies. All loaded proteins represent human alpha-synuclein (aSyn) forms except for human beta-synuclein (bSyn) and mouse aSyn full-length (m FL) proteins. Red arrows highlight the sensitivities of the antibodies to the presence of neighbouring aSyn PTMs. aSyn = alpha-synuclein; bSyn = beta-synuclein; FL = full-length; m = mouse; PTM = post-translational modification; WB = Western blot

Supplementary Figure 2: Validation of the aSyn PTM antibodies via DB, WB and SPR using human recombinant aSyn standards. In-house and commercial aSyn PTM antibodies were validated by **(A)** WB screening. Further **(B)** DB and **(C)** WB analyses on 6A3-E9 showed that this antibody is specific to human aSyn truncated at residue 120. **(D)** SPR sensograms showed the binding responses of immobilised antibody 6A3-E9 against varying concentrations of aSyn human 1-120 (top) or aSyn human full-length (bottom). aSyn = alpha-synuclein; DB = dot blot; PTM = post-translational modification; SPR = surface plasmon resonance; WB = Western blot; WT = wild-type

Supplementary Figure 3: Amino acid sequences of aSyn, of its mouse orthologue and its protein homologues. **(A)** The amino acid sequence of aSyn human and its mouse orthologue. The residue differences between the two proteins are highlighted in red. **(B)** The synuclein family comprises three homologous proteins – alpha (aSyn), beta (bSyn) and gamma synuclein (gSyn). Only alpha- and beta-synuclein were included in this study. The sequence differences are highlighted in red.

Supplementary Figure 4: Specificity validation of non-modified aSyn antibodies on aSyn KO hippocampal and cortical neurons by ICC. PBS- and PFF-treated aSyn KO **(A)** hippocampal and **(B)** cortical neurons were immunostained to validate the specificity of the antibodies with epitopes against the N-terminus, NAC region and C-terminus of aSyn. Blue arrows indicate bSyn positivity in PBS-treated neurons, green arrows indicate positivity to aSyn mouse WT fibrils in PFF-treated neurons, and red

arrows indicate non-specific background both in PBS- and PFF-treated neurons. aSyn = alpha-synuclein; bSyn = beta-synuclein; ICC= immunocytochemistry; KO = knockout; MAP2 = microtubule associated protein 2; PBS = phosphate buffered saline; PFF = pre-formed fibril; WT = wild-type

Supplementary Figure 5: Specificity validation of aSyn PTM antibodies on aSyn KO hippocampal and cortical neurons by ICC. PBS- and PFF-treated aSyn KO **(A)** hippocampal and **(B)** cortical neurons were immunostained to validate the specificity of the antibodies with epitopes against the PTMs of aSyn. Green arrows indicate positivity to aSyn mouse WT fibrils in PFF-treated neurons, and red arrows indicate non-specific background both in PBS- and PFF-treated neurons. aSyn = alpha-synuclein; bSyn = beta-synuclein; ICC = immunocytochemistry; KO = knockout; MAP2 = microtubule associated protein 2; PBS = phosphate buffered saline; PFF = pre-formed fibril; PTM = post-translational modification; WT = wild-type

Supplementary Figure 6: Specificity validation of aSyn antibodies on aSyn KO hippocampal and cortical neurons by WB. PBS- and PFF-treated aSyn KO hippocampal and cortical neurons were separated to soluble and insoluble fractions by sequential extraction, and stained using **(A)** non-modified and **(B)** aSyn PTM antibodies for specificity validation. Green arrows indicate bands specific to aSyn mouse WT fibrils, blue arrows indicate bSyn-specific bands, and red arrows indicate non-specific background. aSyn = alpha-synuclein; bSyn = beta-synuclein; KO = knockout; PBS = phosphate buffered saline; PFF = pre-formed fibril; PTM = post-translational modification; WB = Western blot; WT = wild-type

Supplementary Figure 7: Specificity validation of aSyn antibodies on aSyn KO mouse brain tissue by IF. The in-house and commercial antibodies against **(A)** non-modified aSyn and **(B)** aSyn PTMs were screened for their specificity using aSyn KO mouse amygdala sections. Red arrows indicate non-specific background. aSyn = alpha-synuclein; IF = immunofluorescence; KO = knockout; PTM = post-translational modification

Supplementary Figure 8: IF labelling of PD cingulate cortex using the aSyn N-terminal LASH-EGTNter 1-20 or LASH-BL 34-45, aSyn C-terminal BL 4B12 103-108 or AB 134-138, and aSyn pS129 BL 81A-biotin antibodies. aSyn = alpha-synuclein; IF = immunofluorescence; IHC = immunohistochemistry; PD = Parkinson's disease

Supplementary Figure 9: Specificity validation of the aSyn antibodies against C-terminal tyrosine phosphorylations on aSyn KO hippocampal and cortical neurons by ICC and WB. PBS- and PFF-treated aSyn KO **(A)** hippocampal and **(B)** cortical neurons were immunostained to validate the specificity of the Abcam antibodies with epitopes against aSyn pY125, pY133 and pY136. **(C)** PBS- and PFF-treated aSyn KO hippocampal and cortical neurons were separated to soluble and insoluble fractions by sequential extraction, and stained using Abcam pY125, pY133 and pY136 antibodies for specificity

validation. aSyn = alpha-synuclein; ICC = immunocytochemistry; KO = knockout; MAP2 = microtubule associated protein 2; PBS = phosphate buffered saline; PFF = pre-formed fibril; WB = Western blot

Supplementary Figure 10: Specificity validation of aSyn antibodies on post-mortem human tissues via IHC. The frontal cortices of PSP and CBD, and the hippocampi of AD, PiD and FTLD-TDP type C were stained using the selection of aSyn non-modified and PTM antibodies. No cross-reactivity was observed. Arrows indicate aSyn-positive structures detected on each tissue. AD = Alzheimer's disease; aSyn = alpha-synuclein; CBD = corticobasal degeneration; ctx = cortex; FTLD-TDP/C = frontotemporal lobar degeneration of TAR DNA-binding protein 43 type C; hipp = hippocampus; IHC = immunohistochemistry; PiD = Pick's disease; PSP = posterior supranuclear palsy

Table 1: Characterisation of non-modified aSyn antibodies using recombinant synuclein proteins and peptides. aSyn = alpha-synuclein; bSyn = beta-synuclein; DB = dot blot; f = fibril; hu = human; m = monomer; mus = mouse; o = oligomer; PTM = post-translational modification; WB = Western blot

Table 2: Specificity summary of aSyn antibodies on aSyn KO mouse neuronal culture and brain tissues. aSyn = alpha-synuclein; bSyn = beta-synuclein; ICC = immunocytochemistry; hu = human; IHC = immunohistochemistry; KO = knockout; mus = mouse; WB = Western blot

Table 3: A summary of the pathology detection patterns of aSyn non-modified and PTM antibodies on LBD substantia nigra. aSyn = alpha-synuclein; LB = Lewy body; LBD = Lewy body disease; LN = Lewy neurite; PTM = post-translational modification; - absent; + mild; ++ moderate; +++ frequent

Table 4: A summary of the mouse aSyn-reactive antibody detection patterns of exogenous PFFs in aSyn KO neurons, newly formed aggregates in PFF-seeded WT neurons and mouse brain tissues. *aSyn pS129 revealed by BL 81A mouse monoclonal and AB MJF-R13 rabbit monoclonal antibodies. aSyn = alpha-synuclein; ICC = immunocytochemistry; KO = knockout; PFF = pre-formed fibril; WB = Western blot; WT = wild-type

Supplementary Table 1: A list of all the programmes initialised to generate monoclonal antibodies against aSyn.

Supplementary Table 2: A list of all aSyn proteins and peptides included in this study. Mouse aSyn proteins are marked in blue.

Supplementary Table 3: A list of all the purified antibodies after finalisation of the monoclonal antibody generation programmes.

Supplementary Table 4: A list of all the primary and secondary antibodies used in this study.

Contributions of the authors

HAL conceived and conceptualised the study. HAL and MFA designed the experiments. STK ran the SPR experiment. JB provided the aSyn KO and PFF-seeded WT mouse brain tissues for IHC. SJ generated and characterised the aSyn oligomers. JLH selected the human cases. LP contributed to the optimisation of the IHC assays on human cases. JLH, YM and LP contributed to the analysis of the human data. MFA performed all other experiments involved in the study and wrote the first draft of the manuscript, which was reviewed by all the authors.

HAL: Hilal A. Lashuel

JB: Johannes Burtscher

JLH: Janice L. Holton

LP: Laura Parkkinen

MFA: Melek Firat Altay

SJ: Somanath Jagannath

STK: Senthil T. Kumar

YM: Yasuo Miki

Acknowledgments

This work was support by grants from the Swiss National Science Foundation (31ER30_186198), Michael J Fox Foundation (MJFF-020698) and EPFL. The Queen Square Brain Bank is supported by the Reta Lila Weston Institute of Neurological Studies, UCL Queen Square Institute of Neurology. We thank Jonathan Ricci and Driss Boudeffa for contributing to the Western blot and dot blot analysis experiments during the antibody generation stage. We thank Dr Sergey Nazarov for providing us with the aSyn fibril reconstruction images in Figure 1B. We thank all the individuals and their families for agreeing to donate to QSBB.

Conflict of interest disclosure

Hilal A. Lashuel is the co-founder and chief scientific officer of ND BioSciences, Epalinges, Switzerland, a company that develops diagnostics and treatments for neurodegenerative diseases (NDs) based on platforms that reproduce the complexity and diversity of proteins implicated in NDs and their pathologies. HAL has received funding from industry to support research on neurodegenerative diseases, including Merck Serono, UCB, and Abbvie. These companies had no specific role in the conceptualization, preparation of and decision to publish this manuscript.

REFERENCES

Agin-Liebes, J., Cortes, E., Vonsattel, J.-P., Marder, K., Alcalay, R.N., 2020. Movement disorders rounds: A case of missing pathology in a patient with LRRK2 Parkinson's disease. Parkinsonism & Related Disorders 74, 76–77. https://doi.org/10.1016/j.parkreldis.2019.11.006

Alafuzoff, I., Ince, P.G., Arzberger, T., Al-Sarraj, S., Bell, J., Bodi, I., Bogdanovic, N., Bugiani, O., Ferrer, I., Gelpi, E., Gentleman, S., Giaccone, G., Ironside, J.W., Kavantzas, N., King, A., Korkolopoulou, P., Kovács, G.G., Meyronet, D., Monoranu, C., Parchi, P., Parkkinen, L., Patsouris, E., Roggendorf, W., Rozemuller, A., Stadelmann-Nessler, C., Streichenberger, N., Thal, D.R., Kretzschmar, H., 2009. Staging/typing of Lewy body related α-synuclein pathology: a study of the BrainNet Europe Consortium. Acta Neuropathol 117, 635–652. https://doi.org/10.1007/s00401-009-0523-2

Almandoz-Gil, L., Lindström, V., Sigvardson, J., Kahle, P.J., Lannfelt, L., Ingelsson, M., Bergström, J., 2017. Mapping of Surface-Exposed Epitopes of In Vitro and In Vivo Aggregated Species of Alpha-Synuclein. Cell Mol Neurobiol 37, 1217–1226. https://doi.org/10.1007/s10571-016-0454-0

Anderson, J.P., Walker, D.E., Goldstein, J.M., de Laat, R., Banducci, K., Caccavello, R.J., Barbour, R., Huang, J., Kling, K., Lee, M., Diep, L., Keim, P.S., Shen, X., Chataway, T., Schlossmacher, M.G., Seubert, P., Schenk, D., Sinha, S., Gai, W.P., Chilcote, T.J., 2006. Phosphorylation of Ser-129 Is the Dominant Pathological Modification of α-Synuclein in Familial and Sporadic Lewy Body Disease. J. Biol. Chem. 281, 29739–29752. https://doi.org/10.1074/jbc.M600933200

Appel-Cresswell, S., Vilarino-Guell, C., Encarnacion, M., Sherman, H., Yu, I., Shah, B., Weir, D., Thompson, C., Szu-Tu, C., Trinh, J., Aasly, J.O., Rajput, A., Rajput, A.H., Jon Stoessl, A., Farrer, M.J., 2013. Alpha-synuclein p.H50Q, a novel pathogenic mutation for Parkinson's disease: α- Synuclein p.H50q, A Novel Mutation For Pd. Mov Disord. 28, 811–813. https://doi.org/10.1002/mds.25421

Arotcarena, M.-L., Dovero, S., Prigent, A., Bourdenx, M., Camus, S., Porras, G., Thiolat, M.-L., Tasselli, M., Aubert, P., Kruse, N., Mollenhauer, B., Trigo Damas, I., Estrada, C., Garcia-Carrillo, N., Vaikath, N.N., El-Agnaf, O.M.A., Herrero, M.T., Vila, M., Obeso, J.A., Derkinderen, P., Dehay, B., Bezard, E., 2020. Bidirectional gut-to-brain and brain-to-gut propagation of synucleinopathy in non-human primates. Brain 143, 1462–1475. https://doi.org/10.1093/brain/awaa096

Baba, M., Nakajo, S., Tu, P.H., Tomita, T., Nakaya, K., Lee, V.M., Trojanowski, J.Q., Iwatsubo, T., 1998. Aggregation of alpha-synuclein in Lewy bodies of sporadic Parkinson's disease and dementia with Lewy bodies. Am J Pathol 152, 879–884.

Bhattacharjee, P., Öhrfelt, A., Lashley, T., Blennow, K., Brinkmalm, A., Zetterberg, H., 2019. Mass Spectrometric Analysis of Lewy Body-Enriched α-Synuclein in Parkinson's Disease. J. Proteome Res. 18, 2109–2120. https://doi.org/10.1021/acs.jproteome.8b00982

Braak, E., Sandmann-Keil, D., Rüb, U., Gai, W.P., de Vos, R.A.I., Jansen Steur, E.N.H., Arai, K., Braak, H., 2001. α-Synuclein immunopositive Parkinson's disease-related inclusion bodies in lower brain stem nuclei. Acta Neuropathol 101, 195–201. https://doi.org/10.1007/s004010000247

Braak, H., Del Tredici, K., Bratzke, H., Hamm-Clement, J., Sandmann-Keil, D., Rüb, U., 2002. Staging of the intracerebral inclusion body pathology associated with idiopathic Parkinson's disease (preclinical and clinical stages). Journal of Neurology 249, 1–1. https://doi.org/10.1007/s00415-002-1301-4

Braak, H., Tredici, K.D., Rüb, U., de Vos, R.A.I., Jansen Steur, E.N.H., Braak, E., 2003. Staging of brain pathology related to sporadic Parkinson's disease. Neurobiology of Aging 24, 197–211. https://doi.org/10.1016/S0197-4580(02)00065-9

Burtscher, J., Copin, J.-C., Rodrigues, J., Kumar, S.T., Chiki, A., Guillot de Suduiraut, I., Sandi, C., Lashuel, H.A., 2019. Chronic corticosterone aggravates behavioral and neuronal symptomatology in a mouse model of alpha-synuclein pathology. Neurobiology of Aging 83, 11–20. https://doi.org/10.1016/j.neurobiolaging.2019.08.007

Campbell, B.C.V., McLean, C.A., Culvenor, J.G., Gai, W.P., Blumbergs, P.C., Jakala, P., Beyreuther, K., Masters, C.L., Li, Q.-X., 2001. The solubility of a-synuclein in multiple system atrophy differs from that of dementia with Lewy bodies and Parkinson's disease. Journal of Neurochemistry 10.

Chartier-Harlin, M.-C., Kachergus, J., Roumier, C., Mouroux, V., Douay, X., Lincoln, S., Levecque, C., Larvor, L., Andrieux, J., Hulihan, M., Waucquier, N., Defebvre, L., Amouyel, P., Farrer, M., Destée, A., 2004. α-synuclein locus duplication as a cause of familial Parkinson's disease. The Lancet 364, 1167–1169. https://doi.org/10.1016/S0140-6736(04)17103-1

Chen, L., Periquet, M., Wang, X., Negro, A., McLean, P.J., Hyman, B.T., Feany, M.B., 2009. Tyrosine and serine phosphorylation of α-synuclein have opposing effects on neurotoxicity and soluble oligomer formation. J. Clin. Invest. JCI39088. https://doi.org/10.1172/JCI39088

Covell, D.J., Robinson, J.L., Akhtar, R.S., Grossman, M., Weintraub, D., Bucklin, H.M., Pitkin, R.M., Riddle, D., Yousef, A., Trojanowski, J.Q., Lee, V.M.-Y., 2017. Novel conformation-selective alpha-synuclein antibodies raised against different *in vitro* fibril forms show distinct patterns of Lewy pathology in Parkinson's disease. Neuropathol Appl Neurobiol 43, 604–620. https://doi.org/10.1111/nan.12402

Croisier, E., Elfant, D., Deprez, M., Goldring, K., Dexter, D.T., Pearce, R.K.B., Graeber, M.B., Roncaroli, F., 2006. Comparative study of commercially available anti-alpha-synuclein antibodies. Neuropathol Appl Neurobiol 32, 351–356. https://doi.org/10.1111/j.1365-2990.2006.00722.x

Dehay, B., Bezard, E., 2019. Intrastriatal injection of alpha-synuclein fibrils induces Parkinson-like pathology in macaques. Brain 142, 3321–3322. https://doi.org/10.1093/brain/awz329

Delic, V., Chandra, S., Abdelmotilib, H., Maltbie, T., Wang, S., Kem, D., Scott, H.J., Underwood, R.N., Liu, Z., Volpicelli-Daley, L.A., West, A.B., 2018. Sensitivity and specificity of phospho-Ser129 α-synuclein monoclonal antibodies. Journal of Comparative Neurology 526, 1978–1990. https://doi.org/10.1002/cne.24468

Dhillon, J.S., Riffe, C., Moore, B.D., Ran, Y., Chakrabarty, P., Golde, T.E., Giasson, B.I., 2017. A novel panel of α-synuclein antibodies reveal distinctive staining profiles in synucleinopathies. PLoS ONE 12, e0184731. https://doi.org/10.1371/journal.pone.0184731

Dickson, D.W., Lin, W., Liu, W.-K., Yen, S.-H., 1999. Multiple System Atrophy: A Sporadic Synucleinopathy. Brain Pathology 9, 721–732. https://doi.org/10.1111/j.1750-3639.1999.tb00553.x

Duda, J.E., Giasson, B.I., Chen, Q., Gur, T.L., Hurtig, H.I., Stern, M.B., Gollomp, S.M., Ischiropoulos, H., Lee, V.M.-Y., Trojanowski, J.Q., 2000a. Widespread Nitration of Pathological Inclusions in Neurodegenerative Synucleinopathies. The American Journal of Pathology 157, 1439–1445. https://doi.org/10.1016/S0002-9440(10)64781-5

Duda, J.E., Giasson, B.I., Gur, T.L., Montine, T.J., Robertson, D., Biaggioni, I., Hurtig, H.I., Stern, M.B., Gollomp, S.M., Grossman, M., 2000b. Immunohistochemical and Biochemical Studies Demonstrate a Distinct Profile of ␣-Synuclein Permutations in Multiple System Atrophy. J Neuropathol Exp Neurol 59, 12.

Duda, J.E., Giasson, B.I., Mabon, M.E., Lee, V.M.-Y., Trojanowski, J.Q., 2002. Novel antibodies to synuclein show abundant striatal pathology in Lewy body diseases. Ann Neurol. 52, 205–210. https://doi.org/10.1002/ana.10279

Elfarrash, S., Jensen, N.M., Ferreira, N., Betzer, C., Thevathasan, J.V., Diekmann, R., Adel, M., Omar, N.M., Boraie, M.Z., Gad, S., Ries, J., Kirik, D., Nabavi, S., Jensen, P.H., 2019. Organotypic slice culture model demonstrates inter-neuronal spreading of alpha-synuclein aggregates. acta neuropathol commun 7, 213. https://doi.org/10.1186/s40478-019-0865-5

Fagerqvist, T., Lindström, V., Nordström, E., Lord, A., Tucker, S.M.E., Su, X., Sahlin, C., Kasrayan, A., Andersson, J., Welander, H., Näsström, T., Holmquist, M., Schell, H., Kahle, P.J., Kalimo, H., Möller, C., Gellerfors, P., Lannfelt, L., Bergström, J., Ingelsson, M., 2013. Monoclonal antibodies selective for α-synuclein oligomers/protofibrils recognize brain pathology in Lewy body disorders and α-synuclein transgenic mice with the disease-causing A30P mutation. J. Neurochem. 126, 131–144. https://doi.org/10.1111/jnc.12175

Fauvet, B., Mbefo, M.K., Fares, M.-B., Desobry, C., Michael, S., Ardah, M.T., Tsika, E., Coune, P., Prudent, M., Lion, N., Eliezer, D., Moore, D.J., Schneider, B., Aebischer, P., El-Agnaf, O.M., Masliah, E., Lashuel, H.A., 2012. α-Synuclein in Central Nervous System and from Erythrocytes, Mammalian Cells, and *Escherichia coli* Exists Predominantly as Disordered Monomer. J. Biol. Chem. 287, 15345–15364. https://doi.org/10.1074/jbc.M111.318949

Fayyad, M., Majbour, N.K., Vaikath, N.N., Erskine, D., El-Tarawneh, H., Sudhakaran, I.P., Abdesselem, H., El-Agnaf, O.M.A., 2020. Generation of monoclonal antibodies against phosphorylated α-Synuclein at serine 129: Research tools for synucleinopathies. Neuroscience Letters 725, 134899. https://doi.org/10.1016/j.neulet.2020.134899

Fujiwara, H., Hasegawa, M., Dohmae, N., Kawashima, A., Masliah, E., Goldberg, M.S., Shen, J., Takio, K., Iwatsubo, T., 2002. α-Synuclein is phosphorylated in synucleinopathy lesions. Nat Cell Biol 4, 160–164. https://doi.org/10.1038/ncb748

Funayama, M., Hasegawa, K., Ohta, E., Kawashima, N., Komiyama, M., Kowa, H., Tsuji, S., Obata, F., 2005. An LRRK2 mutation as a cause for the parkinsonism in the original PARK8 family. Ann Neurol. 57, 918–921. https://doi.org/10.1002/ana.20484

Gai, W.P., Power, J.H.T., Blumbergs, P.C., Culvenor, J.G., Jensen, P.H., 1999. Alpha-synuclein Immunoisolation of Glial Inclusions from Multiple System Atrophy Brain Tissue Reveals Multiprotein Components. J. Neurochem. 73, 8. https://doi.org/10.1046/j.1471-4159.1999.02093.x

Gaig, C., Marti, M.J., Ezquerra, M., Rey, M.J., Cardozo, A., Tolosa, E., 2007. G2019S LRRK2 mutation causing Parkinson's disease without Lewy bodies. Journal of Neurology, Neurosurgery & Psychiatry 78, 626–628. https://doi.org/10.1136/jnnp.2006.107904

Galvin, J.E., Giasson, B., Hurtig, H.I., Lee, V.M.-Y., Trojanowski, J.Q., 2000. Neurodegeneration with Brain Iron Accumulation, Type 1 Is Characterized by α-, β-, and γ-Synuclein Neuropathology. The American Journal of Pathology 157, 361–368. https://doi.org/10.1016/S0002-9440(10)64548-8

Ghanem, S.S., Majbour, N.K., Vaikath, N.N., Ardah, M.T., Erskine, D., Jensen, N.M., Fayyad, M., Sudhakaran, I.P., Vasili, E., Melachroinou, K., Abdi, I.Y., Poggiolini, I., Santos, P., Dorn, A., Carloni, P., Vekrellis, K., Attems, J., McKeith, I., Outeiro, T.F., Jensen, P.H., El-Agnaf, O.M.A., 2022. α-Synuclein phosphorylation at serine 129 occurs after initial protein deposition and inhibits seeded fibril formation and toxicity. Proc. Natl. Acad. Sci. U.S.A. 119, e2109617119. https://doi.org/10.1073/pnas.2109617119

Giasson, B.I., Covy, J.P., Bonini, N.M., Hurtig, H.I., Farrer, M.J., Trojanowski, J.Q., Van Deerlin, V.M., 2006. Biochemical and pathological characterization of Lrrk2. Ann Neurol. 59, 315–322. https://doi.org/10.1002/ana.20791

Giasson, B.I., Duda, J.E., Murray, I.V.J., Chen, C., Souza, J.M., Hurtig, H.I., Ischiropoulos, H., Trojanowski, J.Q., Lee, V.M.-Y., 2000a. Oxidative Damage Linked to Neurodegeneration by Selective alpha -Synuclein Nitration in Synucleinopathy Lesions. Science 290, 985–989. https://doi.org/10.1126/science.290.5493.985

Giasson, B.I., Jakes, R., Goedert, M., Duda, J.E., Leight, S., Trojanowski, J.Q., Lee, V.M.Y., 2000b. A Panel of Epitope-Specific Antibodies Detects Protein Domains Distributed Throughout Human ␣ -Synuclein in Lewy Bodies of Parkinson's Disease. Journal of Neuroscience Research 6.

Guerrero-Ferreira, R., Taylor, N.M., Arteni, A.-A., Kumari, P., Mona, D., Ringler, P., Britschgi, M., Lauer, M.E., Makky, A., Verasdonck, J., Riek, R., Melki, R., Meier, B.H., Böckmann, A., Bousset, L., Stahlberg, H., 2019. Two new polymorphic structures of human full-length alpha-synuclein fibrils solved by cryo-electron microscopy. Elife 8. https://doi.org/10.7554/eLife.48907

Hejjaoui, M., Butterfield, S., Fauvet, B., Vercruysse, F., Cui, J., Dikiy, I., Prudent, M., Olschewski, D., Zhang, Y., Eliezer, D., Lashuel, H.A., 2012. Elucidating the Role of C-Terminal Post-Translational Modifications Using Protein Semisynthesis Strategies: α-Synuclein Phosphorylation at Tyrosine 125. J. Am. Chem. Soc. 134, 5196–5210. https://doi.org/10.1021/ja210866j

Henderson, M.X., Covell, D.J., Chung, C.H.-Y., Pitkin, R.M., Sandler, R.M., Decker, S.C., Riddle, D.M., Zhang, B., Gathagan, R.J., James, M.J., Trojanowski, J.Q., Brunden, K.R., Lee, V.M.Y., Luk, K.C., 2020. Characterization of novel conformation-selective α-synuclein antibodies as potential immunotherapeutic agents for Parkinson's disease. Neurobiology of Disease 136, 104712. https://doi.org/10.1016/j.nbd.2019.104712

Henderson, M.X., Sengupta, M., Trojanowski, J.Q., Lee, V.M.Y., 2019. Alzheimer's disease tau is a prominent pathology in LRRK2 Parkinson's disease. acta neuropathol commun 7, 183. https://doi.org/10.1186/s40478-019-0836-x

Jellinger, K.A., 2009. Formation and development of Lewy pathology: a critical update. J Neurol 256, 270–279. https://doi.org/10.1007/s00415-009-5243-y

Kalia, L.V., Lang, A.E., Hazrati, L.-N., Fujioka, S., Wszolek, Z.K., Dickson, D.W., Ross, O.A., Van Deerlin, V.M., Trojanowski, J.Q., Hurtig, H.I., Alcalay, R.N., Marder, K.S., Clark, L.N., Gaig, C., Tolosa, E., Ruiz-Martínez, J., Marti-Masso, J.F., Ferrer, I., López de Munain, A., Goldman, S.M., Schüle, B., Langston, J.W., Aasly, J.O., Giordana, M.T., Bonifati, V., Puschmann, A., Canesi, M., Pezzoli, G., Maues De Paula, A., Hasegawa, K., Duyckaerts, C., Brice, A., Stoessl, A.J., Marras, C., 2015. Clinical Correlations With Lewy Body Pathology in *LRRK2* -Related Parkinson Disease. JAMA Neurol 72, 100. https://doi.org/10.1001/jamaneurol.2014.2704

Kapasi, A., Brosch, J.R., Nudelman, K.N., Agrawal, S., Foroud, T.M., Schneider, J.A., 2020. A novel SNCA E83Q mutation in a case of dementia with Lewy bodies and atypical frontotemporal lobar degeneration. Neuropathology neup.12687. https://doi.org/10.1111/neup.12687

Kellie, J.F., Higgs, R.E., Ryder, J.W., Major, A., Beach, T.G., Adler, C.H., Merchant, K., Knierman, M.D., 2015. Quantitative Measurement of Intact Alpha-Synuclein Proteoforms from Post-Mortem Control and Parkinson's Disease Brain Tissue by Intact Protein Mass Spectrometry. Sci Rep 4, 5797. https://doi.org/10.1038/srep05797

Kiely, A.P., Asi, Y.T., Kara, E., Limousin, P., Ling, H., Lewis, P., Proukakis, C., Quinn, N., Lees, A.J., Hardy, J., Revesz, T., Houlden, H., Holton, J.L., 2013. α-Synucleinopathy associated with G51D SNCA mutation: a link between Parkinson's disease and multiple system atrophy? Acta Neuropathol 125, 753–769. https://doi.org/10.1007/s00401-013-1096-7

Killinger, B.A., Madaj, Z., Sikora, J.W., Rey, N., Haas, A.J., Vepa, Y., Lindqvist, D., Chen, H., Thomas, P.M., Brundin, P., Brundin, L., Labrie, V., 2018. The vermiform appendix impacts the risk of developing Parkinson's disease. Science Translational Medicine 10, eaar5280. https://doi.org/10.1126/scitranslmed.aar5280

Kovacs, G.G., Wagner, U., Dumont, B., Pikkarainen, M., Osman, A.A., Streichenberger, N., Leisser, I., Verchère, J., Baron, T., Alafuzoff, I., Budka, H., Perret-Liaudet, A., Lachmann, I., 2012. An antibody with high reactivity for disease-associated α-synuclein reveals extensive brain pathology. Acta Neuropathol 124, 37–50. https://doi.org/10.1007/s00401-012-0964-x

Krueger, R., Kuhn, W., Müller, T., Woitalla, D., Graeber, M., Kösel, S., Przuntek, H., Epplen, J.T., Schols, L., Riess, O., 1998. Ala30Pro mutation in the gene encoding α-synuclein in Parkinson's disease. Nat Genet 18, 106–108. https://doi.org/10.1038/ng0298-106

Kumar, S.T., Donzelli, S., Chiki, A., Syed, M.M.K., Lashuel, H.A., 2020a. A simple, versatile and robust centrifugation-based filtration protocol for the isolation and quantification of α-synuclein monomers, oligomers and fibrils: Towards improving experimental reproducibility in α-synuclein research. J. Neurochem. 153, 103–119. https://doi.org/10.1111/jnc.14955

Kumar, S.T., Jagannath, S., Francois, C., Vanderstichele, H., Stoops, E., Lashuel, H.A., 2020b. How specific are the conformation-specific α-synuclein antibodies? Characterization and validation of 16 α-synuclein conformation-specific antibodies using well-characterized preparations of α-synuclein monomers, fibrils and oligomers with distinct structures and morphology. Neurobiology of Disease 146, 105086. https://doi.org/10.1016/j.nbd.2020.105086

Kumar, S.T., Mahul-Mellier, A.-L., Hegde, R.N., Moons, R., Magalhaes, P., Ibanez de Opakua, A., Riviere, G., Rostami, I., Donzelli, S., Zweckstetter, M., Sobott, F., Lashuel, H.A., 2021. A novel mutation (E83Q) unlocks the pathogenicity of human alpha-synuclein fibrils and recapitulates its pathological diversity. bioRxiv. https://doi.org/10.1101/2021.11.21.469421

Kuusisto, E., Parkkinen, L., Alafuzoff, I., 2003. Morphogenesis of Lewy Bodies: Dissimilar Incorporation of -Synuclein, Ubiquitin, and p62. J Neuropathol Exp Neurol 62, 13. https://doi.org/10.1093/jnen/62.12.1241

Lashuel, H.A., Mahul-Mellier, A.-L., Novello, S., Hegde, R.N., Jasiqi, Y., Altay, M.F., Donzelli, S., DeGuire, S.M., Burai, R., Magalhães, P., Chiki, A., Ricci, J., Boussouf, M., Sadek, A., Stoops, E., Iseli, C., Guex, N., 2022. Neighbouring modifications interfere with the detection of phosphorylated alpha-synuclein at Serine 129: Revisiting the specificity of pS129 antibodies. bioRxiv. https://doi.org/10.1101/2022.03.30.486322

Lesage, S., Anheim, M., Letournel, F., Bousset, L., Honoré, A., Rozas, N., Pieri, L., Madiona, K., Dürr, A., Melki, R., Verny, C., Brice, A., for the French Parkinson's Disease Genetics Study Group, 2013. G51D α-synuclein mutation causes a novel Parkinsonian-pyramidal syndrome: SNCA G51D in Parkinsonism. Ann Neurol. 73, 459–471. https://doi.org/10.1002/ana.23894

Leverenz, J.B., Umar, I., Wang, Q., Montine, T.J., McMillan, P.J., Tsuang, D.W., Jin, J., Pan, C., Shin, J., Zhu, D., Zhang, J., 2007. Proteomic Identification of Novel Proteins in Cortical Lewy Bodies. Brain Pathology 17, 139–145. https://doi.org/10.1111/j.1750-3639.2007.00048.x

Lewis, K.A., Su, Y., Jou, O., Ritchie, C., Foong, C., Hynan, L.S., White, C.L., Thomas, P.J., Hatanpaa, K.J., 2010. Abnormal Neurites Containing C-Terminally Truncated α-Synuclein Are Present in Alzheimer's Disease without Conventional Lewy Body Pathology. The American Journal of Pathology 177, 3037–3050. https://doi.org/10.2353/ajpath.2010.100552

Li, B., Ge, P., Murray, K.A., Sheth, P., Zhang, M., Nair, G., Sawaya, M.R., Shin, W.S., Boyer, D.R., Ye, S., Eisenberg, D.S., Zhou, Z.H., Jiang, L., 2018. Cryo-EM of full-length α-synuclein reveals fibril polymorphs with a common structural kernel. Nature Communications 9, 3609. https://doi.org/10.1038/s41467-018-05971-2

Luk, K.C., Kehm, V.M., Zhang, B., O'Brien, P., Trojanowski, J.Q., Lee, V.M.Y., 2012. Intracerebral inoculation of pathological α-synuclein initiates a rapidly progressive neurodegenerative α-synucleinopathy in mice. The Journal of Experimental Medicine 209, 975–986. https://doi.org/10.1084/jem.20112457

Luk, K.C., Song, C., O'Brien, P., Stieber, A., Branch, J.R., Brunden, K.R., Trojanowski, J.Q., Lee, V.M.-Y., 2009. Exogenous -synuclein fibrils seed the formation of Lewy body-like intracellular inclusions in cultured cells. Proceedings of the National Academy of Sciences 106, 20051–20056. https://doi.org/10.1073/pnas.0908005106

Mahul-Mellier, A.-L., Altay, M.F., Burtscher, J., Maharjan, N., Ait-Bouziad, N., Chiki, A., Vingill, S., Wade-Martins, R., Holton, J., Strand, C., Haikal, C., Li, J.-Y., Hamelin, R., Croisier, M., Knott, G., Mairet-Coello, G., Weerens, L., Michel, A., Downey, P., Citron, M., A. Lashuel, H., 2018. The making of a Lewy body: the role of α-synuclein post-fibrillization modifications in regulating the formation and the maturation of pathological inclusions. bioRxiv 500058. https://doi.org/10.1101/500058

Mahul-Mellier, A.-L., Burtscher, J., Maharjan, N., Weerens, L., Croisier, M., Kuttler, F., Leleu, M., Knott, G.W., Lashuel, H.A., 2020. The process of Lewy body formation, rather than simply α-synuclein fibrillization, is one of the major drivers of neurodegeneration. Proc Natl Acad Sci USA 117, 4971. https://doi.org/10.1073/pnas.1913904117

Mahul-Mellier, A.-L., Fauvet, B., Gysbers, A., Dikiy, I., Oueslati, A., Georgeon, S., Lamontanara, A.J., Bisquertt, A., Eliezer, D., Masliah, E., Halliday, G., Hantschel, O., Lashuel, H.A., 2014. c-Abl phosphorylates α-synuclein and regulates its degradation: implication for α-synuclein clearance and contribution to the pathogenesis of Parkinson's disease. Human Molecular Genetics 23, 2858–2879. https://doi.org/10.1093/hmg/ddt674

Mahul-Mellier, A.-L., Vercruysse, F., Maco, B., Ait-Bouziad, N., De Roo, M., Muller, D., Lashuel, H.A., 2015. Fibril growth and seeding capacity play key roles in α-synuclein-mediated apoptotic cell death. Cell Death Differ 22, 2107–2122. https://doi.org/10.1038/cdd.2015.79

Marti-Masso, J.-F., Ruiz-Martínez, J., Bolaño, M.J., Ruiz, I., Gorostidi, A., Moreno, F., Ferrer, I., de Munain, A.L., 2009. Neuropathology of Parkinson's disease with the R1441G mutation in *LRRK2*: Neuropathology of Parkinson's Disease. Mov. Disord. 24, 1998–2001. https://doi.org/10.1002/mds.22677

Masuda-Suzukake, M., Nonaka, T., Hosokawa, M., Oikawa, T., Arai, T., Akiyama, H., Mann, D.M.A., Hasegawa, M., 2013. Prion-like spreading of pathological α-synuclein in brain. Brain 136, 1128–1138. https://doi.org/10.1093/brain/awt037

Milber, J.M., Noorigian, J.V., Morley, J.F., Petrovitch, H., White, L., Ross, G.W., Duda, J.E., 2012. Lewy pathology is not the first sign of degeneration in vulnerable neurons in Parkinson disease. Neurology 79, 2307–2314. https://doi.org/10.1212/WNL.0b013e318278fe32

Moors, T.E., Maat, C.A., Niedieker, D., Mona, D., Petersen, D., Timmermans-Huisman, E., Kole, J., El-Mashtoly, S.F., Spycher, L., Zago, W., Barbour, R., Mundigl, O., Kaluza, K., Huber, S., Hug, M.N., Kremer, T., Ritter, M., Dziadek, S., Geurts, J.J.G., Gerwert, K., Britschgi, M., van de Berg, W.D.J., 2021. The subcellular arrangement of alpha-synuclein proteoforms in the Parkinson's disease brain as revealed by multicolor STED microscopy. Acta Neuropathol. https://doi.org/10.1007/s00401-021-02329-9

Moors, T.E., Maat, C.A., Niedieker, D., Mona, D., Petersen, D., Timmermans-Huisman, E., Kole, J., El-Mashtoly, S.F., Spycher, L., Zago, W., Barbour, R., Mundigl, O., Kaluza, K., Huber, S., Hug, M.N., Kremer, T., Ritter, M., Dziadek, S., Geurts, J.J.G., Gerwert, K., Britschgi, M., van de Berg, W.D.J., 2019. Subcellular orchestration of alpha-synuclein variants in Parkinson's disease brains revealed by 3D multicolor STED microscopy. bioRxiv 470476. https://doi.org/10.1101/470476

Ohrfelt, A., Zetterberg, H., Andersson, K., Persson, R., Secic, D., Brinkmalm, G., Wallin, A., Mulugeta, E., Francis, P.T., Vanmechelen, E., Aarsland, D., Ballard, C., Blennow, K., Westman-Brinkmalm, A., 2011. Identification of Novel α-Synuclein Isoforms in Human Brain Tissue by using an Online NanoLC-ESI-FTICR-MS Method. Neurochem Res 36, 2029–2042. https://doi.org/10.1007/s11064-011-0527-x

Parkkinen, L., Hartikainen, P., Alafuzoff, I., 2007. Abundant glial a-synuclein pathology in a case without overt clinical symptoms. Clinical Neuropathology 8.

Parkkinen, L., O'Sullivan, S.S., Collins, C., Petrie, A., Holton, J.L., Revesz, T., Lees, A.J., 2011. Disentangling the Relationship between Lewy Bodies and Nigral Neuronal Loss in Parkinson's Disease. Journal of Parkinson's Disease 1, 277–286. https://doi.org/10.3233/JPD-2011-11046

Parkkinen, L., Pirttilä, T., Alafuzoff, I., 2008. Applicability of current staging/categorization of α-synuclein pathology and their clinical relevance. Acta Neuropathol 115, 399–407. https://doi.org/10.1007/s00401-008-0346-6

Pasanen, P., Myllykangas, L., Siitonen, M., Raunio, A., Kaakkola, S., Lyytinen, J., Tienari, P.J., Pöyhönen, M., Paetau, A., 2014. A novel α-synuclein mutation A53E associated with atypical multiple system atrophy and Parkinson's disease-type pathology. Neurobiology of Aging 35, 2180.e1-2180.e5. https://doi.org/10.1016/j.neurobiolaging.2014.03.024

Peng, C., Gathagan, R.J., Covell, D.J., Medellin, C., Stieber, A., Robinson, J.L., Zhang, B., Pitkin, R.M., Olufemi, M.F., Luk, K.C., Trojanowski, J.Q., Lee, V.M.-Y., 2018. Cellular milieu imparts distinct

pathological α-synuclein strains in α-synucleinopathies. Nature 557, 558–563. https://doi.org/10.1038/s41586-018-0104-4
Polymeropoulos, M.H., Higgins, J.J., Golbe, L.I., Johnson, W.G., Ide, S.E., Di Iorio, G., Sanges, G., Stenroos, E.S., Pho, L.T., Schaffer, A.A., Lazzarini, A.M., Nussbaum, R.L., Duvoisin, R.C., 1996. Mapping of a Gene for Parkinson's Disease to Chromosome 4q21-q23. Science 274, 1197–1199. https://doi.org/10.1126/science.274.5290.1197
Polymeropoulos, M.H., Lavedan, C., Leroy, E., Ide, S.E., Dehejia, A., Dutra, A., Pike, B., Root, H., Rubenstein, J., Boyer, R., Stenroos, E.S., Chandrasekharappa, S., Athanassiadou, A., Papapetropoulos, T., Johnson, W.G., Lazzarini, A.M., Duvoisin, R.C., Di Iorio, G., Golbe, L.I., Nussbaum, R.L., 1997. Mutation in the -Synuclein Gene Identified in Families with Parkinson's Disease. Science 276, 2045–2047. https://doi.org/10.1126/science.276.5321.2045
Prasad, K., Beach, T.G., Hedreen, J., Richfield, E.K., 2012. Critical Role of Truncated α-Synuclein and Aggregates in Parkinson's Disease and Incidental Lewy Body Disease: Role of Truncated α-Synuclein. Brain Pathology 22, 811–825. https://doi.org/10.1111/j.1750-3639.2012.00597.x
Proukakis, C., Dudzik, C.G., Brier, T., MacKay, D.S., Cooper, J.M., Millhauser, G.L., Houlden, H., Schapira, A.H., 2013. A novel -synuclein missense mutation in Parkinson disease. Neurology 80, 1062–1064. https://doi.org/10.1212/WNL.0b013e31828727ba
Recasens, A., Dehay, B., Bové, J., Carballo-Carbajal, I., Dovero, S., Pérez-Villalba, A., Fernagut, P.-O., Blesa, J., Parent, A., Perier, C., Fariñas, I., Obeso, J.A., Bezard, E., Vila, M., 2014. Lewy body extracts from Parkinson disease brains trigger α-synuclein pathology and neurodegeneration in mice and monkeys: LB-Induced Pathology. Ann Neurol. 75, 351–362. https://doi.org/10.1002/ana.24066
Rey, N.L., Petit, G.H., Bousset, L., Melki, R., Brundin, P., 2013. Transfer of human α-synuclein from the olfactory bulb to interconnected brain regions in mice. Acta Neuropathol 126, 555–573. https://doi.org/10.1007/s00401-013-1160-3
Rey, N.L., Steiner, J.A., Maroof, N., Luk, K.C., Madaj, Z., Trojanowski, J.Q., Lee, V.M.-Y., Brundin, P., 2016. Widespread transneuronal propagation of α-synucleinopathy triggered in olfactory bulb mimics prodromal Parkinson's disease. The Journal of Experimental Medicine 213, 1759–1778. https://doi.org/10.1084/jem.20160368
Sano, K., Iwasaki, Y., Yamashita, Y., Irie, K., Hosokawa, M., Satoh, K., Mishima, K., 2021. Tyrosine 136 phosphorylation of α-synuclein aggregates in the Lewy body dementia brain: involvement of serine 129 phosphorylation by casein kinase 2. acta neuropathol commun 9, 182. https://doi.org/10.1186/s40478-021-01281-9
Schweighauser, M., Shi, Y., Tarutani, A., Kametani, F., Murzin, A.G., Ghetti, B., Matsubara, T., Tomita, T., Ando, T., Hasegawa, K., Murayama, S., Yoshida, M., Hasegawa, M., Scheres, S.H.W., Goedert, M., 2020. Structures of α-synuclein filaments from multiple system atrophy. Nature 1–6. https://doi.org/10.1038/s41586-020-2317-6
Shahmoradian, S.H., Lewis, A.J., Genoud, C., Hench, J., Moors, T.E., Navarro, P.P., Castaño-Díez, D., Schweighauser, G., Graff-Meyer, A., Goldie, K.N., Sütterlin, R., Huisman, E., Ingrassia, A., Gier, Y. de, Rozemuller, A.J.M., Wang, J., Paepe, A.D., Erny, J., Staempfli, A., Hoernschemeyer, J., Großerüschkamp, F., Niedieker, D., El-Mashtoly, S.F., Quadri, M., Van IJcken, W.F.J., Bonifati, V., Gerwert, K., Bohrmann, B., Frank, S., Britschgi, M., Stahlberg, H., Van de Berg, W.D.J., Lauer, M.E., 2019. Lewy pathology in Parkinson's disease consists of crowded organelles and lipid membranes. Nat Neurosci 22, 1099–1109. https://doi.org/10.1038/s41593-019-0423-2
Singleton, A.B., Farrer, M., Johnson, J., Singleton, A., Hague, S., Kachergus, J., Hulihan, M., Peuralinna, T., Dutra, A., Nussbaum, R., Lincoln, S., Crawley, A., Hanson, M., Maraganore, D., Adler, C., Cookson, M.R., Muenter, M., Baptista, M., Miller, D., Blancato, J., Hardy, J., Gwinn-Hardy, K., 2003. Alpha-synuclein Locus Triplication Causes Parkinson's Disease. Science 302, 841–841. https://doi.org/10.1126/science.1090278
Sonustun, B., Altay, M.F., Strand, C., Ebanks, K., Hondhamuni, G., Warner, T.T., Lashuel, H.A., Bandopadhyay, R., 2022. Pathological Relevance of Post-Translationally Modified Alpha-Synuclein (pSer87, pSer129, nTyr39) in Idiopathic Parkinson's Disease and Multiple System Atrophy. Cells 11, 906. https://doi.org/10.3390/cells11050906
Spillantini, M.G., Crowther, R.A., Jakes, R., Cairns, N.J., Lantos, P.L., Goedert, M., 1998a. Filamentous a-synuclein inclusions link multiple system atrophy with Parkinson's disease and dementia with Lewy bodies. Neuroscience Letters 4.
Spillantini, M.G., Crowther, R.A., Jakes, R., Hasegawa, M., Goedert, M., 1998b. Alpha-synuclein in filamentous inclusions of Lewy bodies from Parkinson's disease and dementia with Lewy bodies. Proceedings of the National Academy of Sciences 95, 6469–6473. https://doi.org/10.1073/pnas.95.11.6469

Spira, P.J., Sharpe, D.M., Halliday, G., Cavanagh, J., Nicholson, G.A., 2001. Clinical and pathological features of a parkinsonian syndrome in a family with an Ala53Thr ?-synuclein mutation. Ann Neurol. 49, 313–319. https://doi.org/10.1002/ana.67

Steiner, J.A., Quansah, E., Brundin, P., 2018. The concept of alpha-synuclein as a prion-like protein: ten years after. Cell Tissue Res 373, 161–173. https://doi.org/10.1007/s00441-018-2814-1

Steiner, P., Sarria, J.-C.F., Glauser, L., Magnin, S., Catsicas, S., Hirling, H., 2002. Modulation of receptor cycling by neuron-enriched endosomal protein of 21 kD. Journal of Cell Biology 157, 1197–1209. https://doi.org/10.1083/jcb.200202022

Strohaeker, T., Jung, B.C., Liou, S.-H., Fernandez, C.O., Riedel, D., Becker, S., Halliday, G.M., Bennati, M., Kim, W.S., Lee, S.-J., Zweckstetter, M., 2019. Structural heterogeneity of α-synuclein fibrils amplified from patient brain extracts. Nat Commun 10, 5535. https://doi.org/10.1038/s41467-019-13564-w

Takanashi, M., Funayama, M., Matsuura, E., Yoshino, H., Li, Y., Tsuyama, S., Takashima, H., Nishioka, K., Hattori, N., 2018. Isolated nigral degeneration without pathological protein aggregation in autopsied brains with LRRK2 p.R1441H homozygous and heterozygous mutations. acta neuropathol commun 6, 105. https://doi.org/10.1186/s40478-018-0617-y

Tarutani, A., Suzuki, G., Shimozawa, A., Nonaka, T., Akiyama, H., Hisanaga, S., Hasegawa, M., 2016. The Effect of Fragmented Pathogenic α-Synuclein Seeds on Prion-like Propagation. J. Biol. Chem. 291, 18675–18688. https://doi.org/10.1074/jbc.M116.734707

Tofaris, G.K., Razzaq, A., Ghetti, B., Lilley, K.S., Spillantini, M.G., 2003. Ubiquitination of α-Synuclein in Lewy Bodies Is a Pathological Event Not Associated with Impairment of Proteasome Function. J. Biol. Chem. 278, 44405–44411. https://doi.org/10.1074/jbc.M308041200

Tong, J., Wong, H., Guttman, M., Ang, L.C., Forno, L.S., Shimadzu, M., Rajput, A.H., Muenter, M.D., Kish, S.J., Hornykiewicz, O., Furukawa, Y., 2010. Brain α-synuclein accumulation in multiple system atrophy, Parkinson's disease and progressive supranuclear palsy: a comparative investigation. Brain 133, 172–188. https://doi.org/10.1093/brain/awp282

Vaikath, N.N., Majbour, N.K., Paleologou, K.E., Ardah, M.T., van Dam, E., van de Berg, W.D.J., Forrest, S.L., Parkkinen, L., Gai, W.-P., Hattori, N., Takanashi, M., Lee, S.-J., Mann, D.M.A., Imai, Y., Halliday, G.M., Li, J.-Yi., El-Agnaf, O.M.A., 2015. Generation and characterization of novel conformation-specific monoclonal antibodies for α-synuclein pathology. Neurobiology of Disease 79, 81–99. https://doi.org/10.1016/j.nbd.2015.04.009

Vilas, D., Gelpi, E., Aldecoa, I., Grau, O., Rodriguez-Diehl, R., Jaumà, S., Martí, M.J., Tolosa, E., 2019. Lack of central and peripheral nervous system synuclein pathology in R1441G *LRRK2* -associated Parkinson's disease. J Neurol Neurosurg Psychiatry 90, 832–833. https://doi.org/10.1136/jnnp-2018-318473

Volpicelli-Daley, L.A., Luk, K.C., Lee, V.M.-Y., 2014. Addition of exogenous α-synuclein preformed fibrils to primary neuronal cultures to seed recruitment of endogenous α-synuclein to Lewy body and Lewy neurite–like aggregates. Nat Protoc 9, 2135–2146. https://doi.org/10.1038/nprot.2014.143

Volpicelli-Daley, L.A., Luk, K.C., Patel, T.P., Tanik, S.A., Riddle, D.M., Stieber, A., Meaney, D.F., Trojanowski, J.Q., Lee, V.M.-Y., 2011. Exogenous α-Synuclein Fibrils Induce Lewy Body Pathology Leading to Synaptic Dysfunction and Neuron Death. Neuron 72, 57–71. https://doi.org/10.1016/j.neuron.2011.08.033

Wakabayashi, K., Hayashi, S., Yoshimoto, M., Kudo, H., Takahashi, H., 2000. NACP/α-synuclein-positive filamentous inclusions in astrocytes and oligodendrocytes of Parkinson's disease brains. Acta Neuropathol 99, 14–20. https://doi.org/10.1007/PL00007400

Wakabayashi, K., Tanji, K., Odagiri, S., Miki, Y., Mori, F., Takahashi, H., 2013. The Lewy Body in Parkinson's Disease and Related Neurodegenerative Disorders. Mol Neurobiol 47, 495–508. https://doi.org/10.1007/s12035-012-8280-y

Waxman, E.A., Duda, J.E., Giasson, B.I., 2008. Characterization of antibodies that selectively detect α-synuclein in pathological inclusions. Acta Neuropathol 116, 37–46. https://doi.org/10.1007/s00401-008-0375-1

Wszolek, Z.K., Pfeiffer, R.F., Tsuboi, Y., Uitti, R.J., McComb, R.D., Stoessl, A.J., Strongosky, A.J., Zimprich, A., Müller-Myhsok, B., Farrer, M.J., Gasser, T., Calne, D.B., Dickson, D.W., 2004. Autosomal dominant parkinsonism associated with variable synuclein and tau pathology. Neurology 62, 1619–1622. https://doi.org/10.1212/01.WNL.0000125015.06989.DB

Xia, Q., Liao, L., Cheng, D., Duong, D.M., Gearing, M., Lah, J.J., Levey, A.I., Peng, J., 2008. Proteomic identification of novel proteins associated with Lewy bodies. Front. Biosci. 13, 3850–3856. https://doi.org/10.2741/2973

Zarranz, J.J., Alegre, J., Gómez-Esteban, J.C., Lezcano, E., Ros, R., Ampuero, I., Vidal, L., Hoenicka, J., Rodriguez, O., Atarés, B., Llorens, V., Tortosa, E.G., del Ser, T., Muñoz, D.G., de Yebenes,

J.G., 2004. The new mutation, E46K, of α-synuclein causes parkinson and Lewy body dementia: New α-Synuclein Gene Mutation. Ann Neurol. 55, 164–173. https://doi.org/10.1002/ana.10795

FIGURE 1

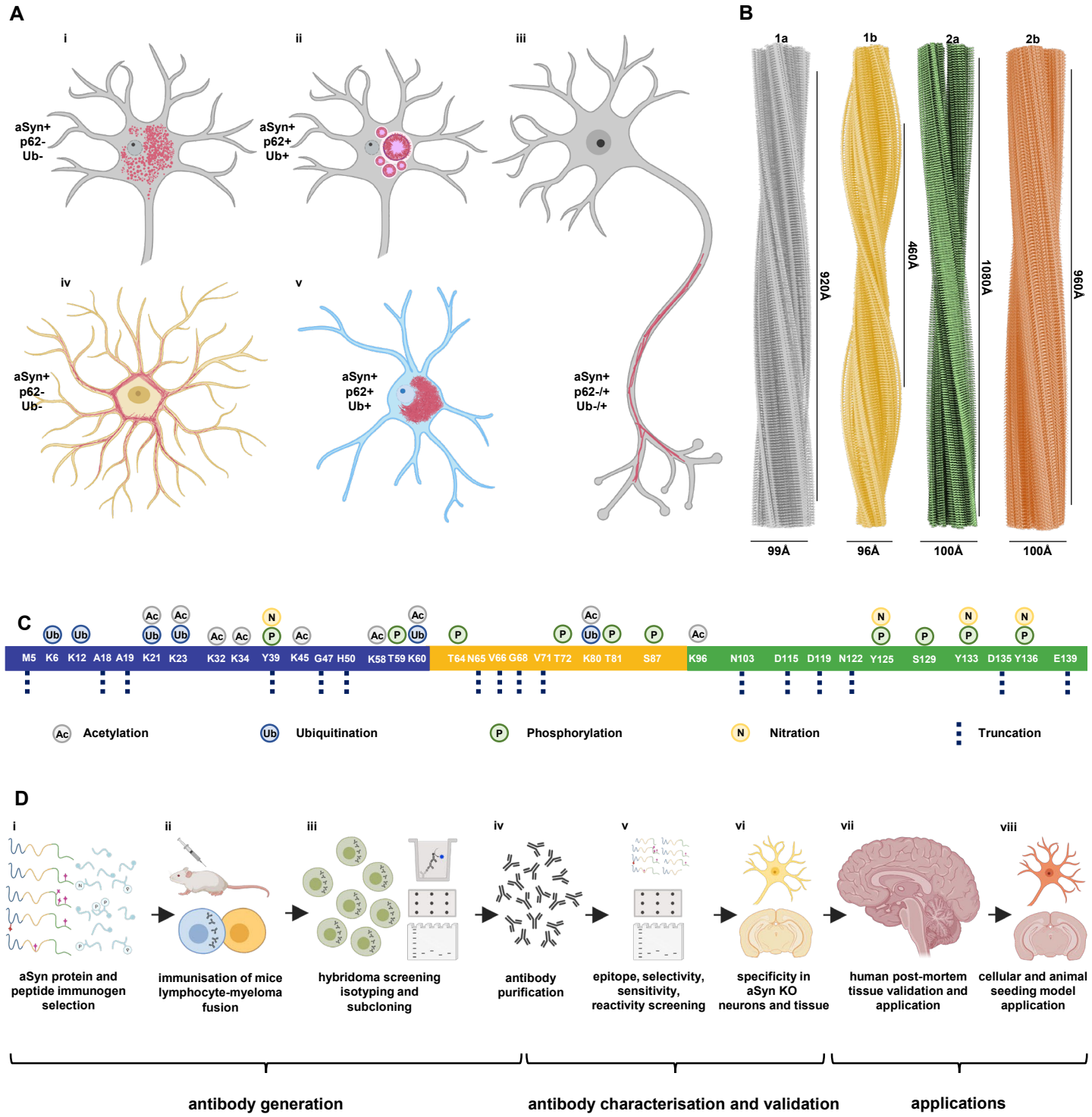
A
i
aSyn+
p62-
Ub-
ii
aSyn+
p62+
Ub+
iii
iv
aSyn+
p62-
Ub-
v
aSyn+
p62+
Ub+
aSyn+
p62-/+
Ub-/+
B
1a
1b
2a
2b
920Å
460Å
1080Å
960Å
99Å
96Å
100Å
100Å
C
M5 K6 K12 A18 A19 K21 K23 K32 K34 Y39 K45 G47 H50 K58 T59 K60 T64 N65 V66 G68 V71 T72 K80 T81 S87 K96 N103 D115 D119 N122 Y125 S129 Y133 D135 Y136 E139
Acetylation
Ubiquitination
Phosphorylation
Nitration
Truncation
D
i
aSyn protein and peptide immunogen selection
ii
immunisation of mice lymphocyte-myeloma fusion
iii
hybridoma screening isotyping and subcloning
iv
antibody purification
v
epitope, selectivity, sensitivity, reactivity screening
vi
specificity in aSyn KO neurons and tissue
vii
human post-mortem tissue validation and application
viii
cellular and animal seeding model application
antibody generation
antibody characterisation and validation
applications

FIGURE 2

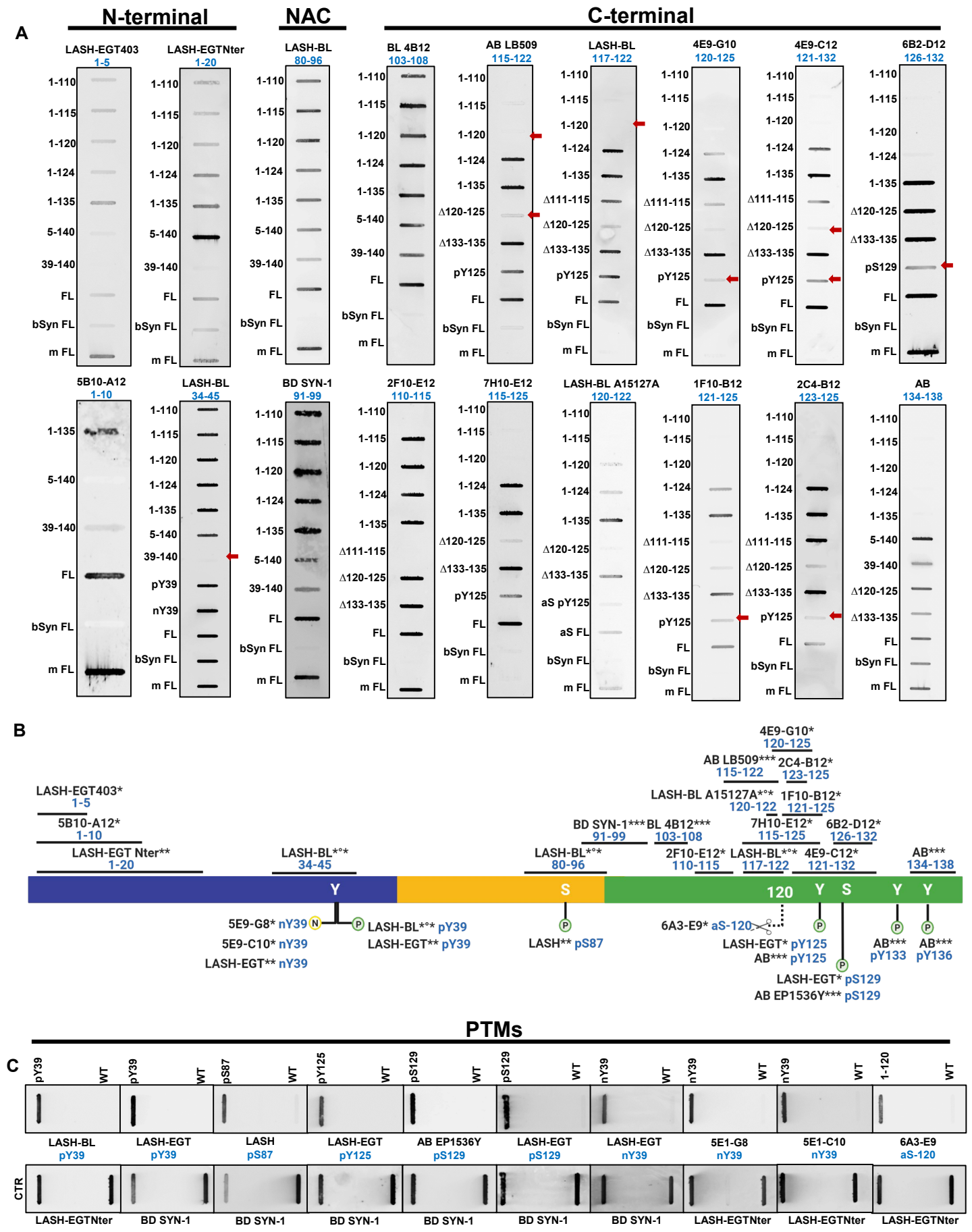
A
N-terminal
NAC
C-terminal
LASH-EGT403 1-5
LASH-EGTNter 1-20
LASH-BL 80-96
BL 4B12 103-108
AB LB509 115-122
LASH-BL 117-122
4E9-G10 120-125
4E9-C12 121-132
6B2-D12 126-132
5B10-A12 1-10
LASH-BL 34-45
BD SYN-1 91-99
2F10-E12 110-115
7H10-E12 115-125
LASH-BL A15127A 120-122
1F10-B12 121-125
2C4-B12 123-125
AB 134-138
1-110
1-115
1-120
1-124
1-135
5-140
39-140
FL
bSyn FL
m FL
pY39
nY39
Δ111-115
Δ120-125
Δ133-135
pY125
aS pY125
aS FL
pS129
B
LASH-EGT403* 1-5
5B10-A12* 1-10
LASH-EGT Nter** 1-20
LASH-BL*°* 34-45
BD SYN-1*** 91-99
BL 4B12*** 103-108
LASH-BL*°* 80-96
2F10-E12* 110-115
LASH-BL*°* 117-122
4E9-C12* 121-132
7H10-E12* 115-125
6B2-D12* 126-132
AB*** 134-138
AB LB509*** 115-122
2C4-B12* 123-125
4E9-G10* 120-125
LASH-BL A15127A*°* 120-122
1F10-B12* 121-125
Y
S
120
Y
S
Y
Y
5E9-G8* nY39
LASH-BL*°* pY39
5E9-C10* nY39
LASH-EGT** pY39
LASH-EGT** nY39
LASH** pS87
6A3-E9* aS-120
LASH-EGT* pY125
AB*** pY125
LASH-EGT* pS129
AB EP1536Y*** pS129
AB*** pY133
AB*** pY136
PTMs
C
pY39
WT
pS87
pY125
pS129
nY39
1-120
LASH-BL pY39
LASH-EGT pY39
LASH pS87
LASH-EGT pY125
AB EP1536Y pS129
LASH-EGT pS129
LASH-EGT nY39
5E1-G8 nY39
5E1-C10 nY39
6A3-E9 aS-120
CTR
LASH-EGTNter
BD SYN-1

FIGURE 3

A

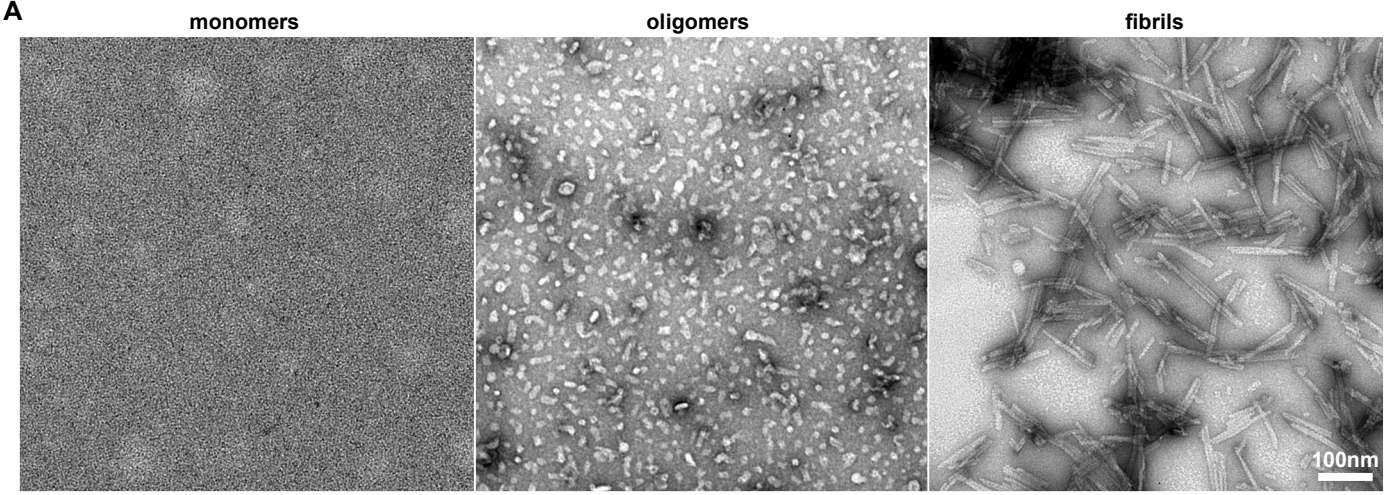
monomers
oligomers
fibrils
100nm

B

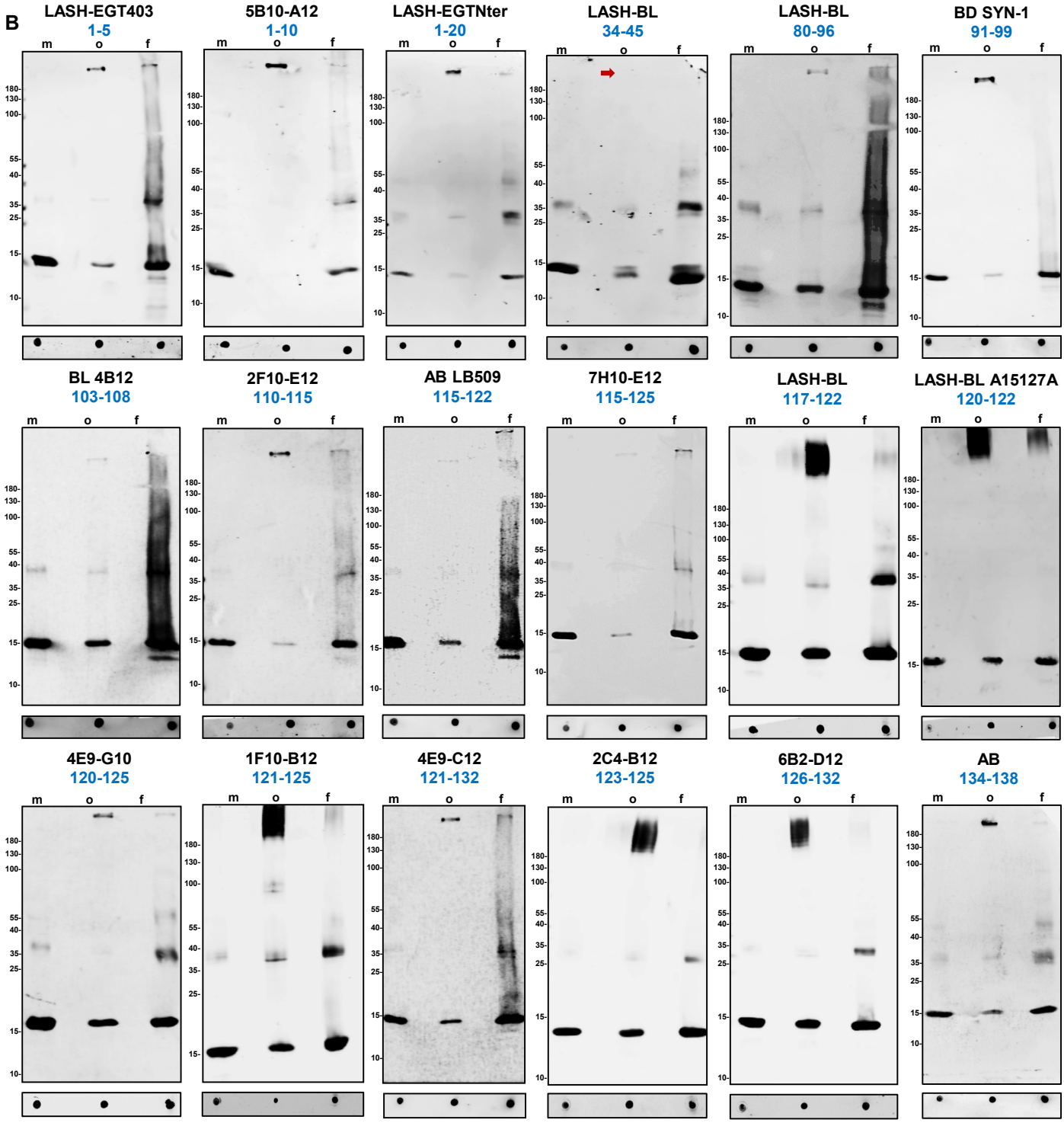
LASH-EGT403
1-5
5B10-A12
1-10
LASH-EGTNter
1-20
LASH-BL
34-45
LASH-BL
80-96
BD SYN-1
91-99
BL 4B12
103-108
2F10-E12
110-115
AB LB509
115-122
7H10-E12
115-125
LASH-BL
117-122
LASH-BL A15127A
120-122
4E9-G10
120-125
1F10-B12
121-125
4E9-C12
121-132
2C4-B12
123-125
6B2-D12
126-132
AB
134-138
m
o
f
180-
130-
100-
55-
40-
35-
25-
15-
10-

FIGURE 4

A

N-terminal | NAC | C-terminal

LASH-EGT403 1-5 | LASH-EGTNter 1-20 | LASH-BL 80-96 | BL 4B12 103-108 | AB LB509 115-122 | LASH-BL 117-122 | 4E9-G10 120-125

5B10-A12 1-10 | LASH-BL 34-45 | BD SYN-1 91-99 | 2F10-E12 110-115 | 7H10-E12 115-125 | LASH-BL A15127A 120-122 | 1F10-B12 121-125

20µm

C-terminal | PTMs

4E9-C12 121-132 | 6B2-D12 126-132 | LASH-BL pY39 | LASH pS87 | AB EP1536Y pS129 | LASH-EGT nY39 | 5E1-C10 nY39

2C4-B12 123-125 | AB 134-138 | LASH-EGT pY39 | LASH-EGT pY125 | LASH-EGT pS129 | 5E1-G8 nY39 | 6A3-E9 aS-120

20µm

B

LASH-BL 34-45 | AB 134-138 | BL 81A-b pS129 | MERGE/ DAPI

20µm

20µm

FIGURE 5

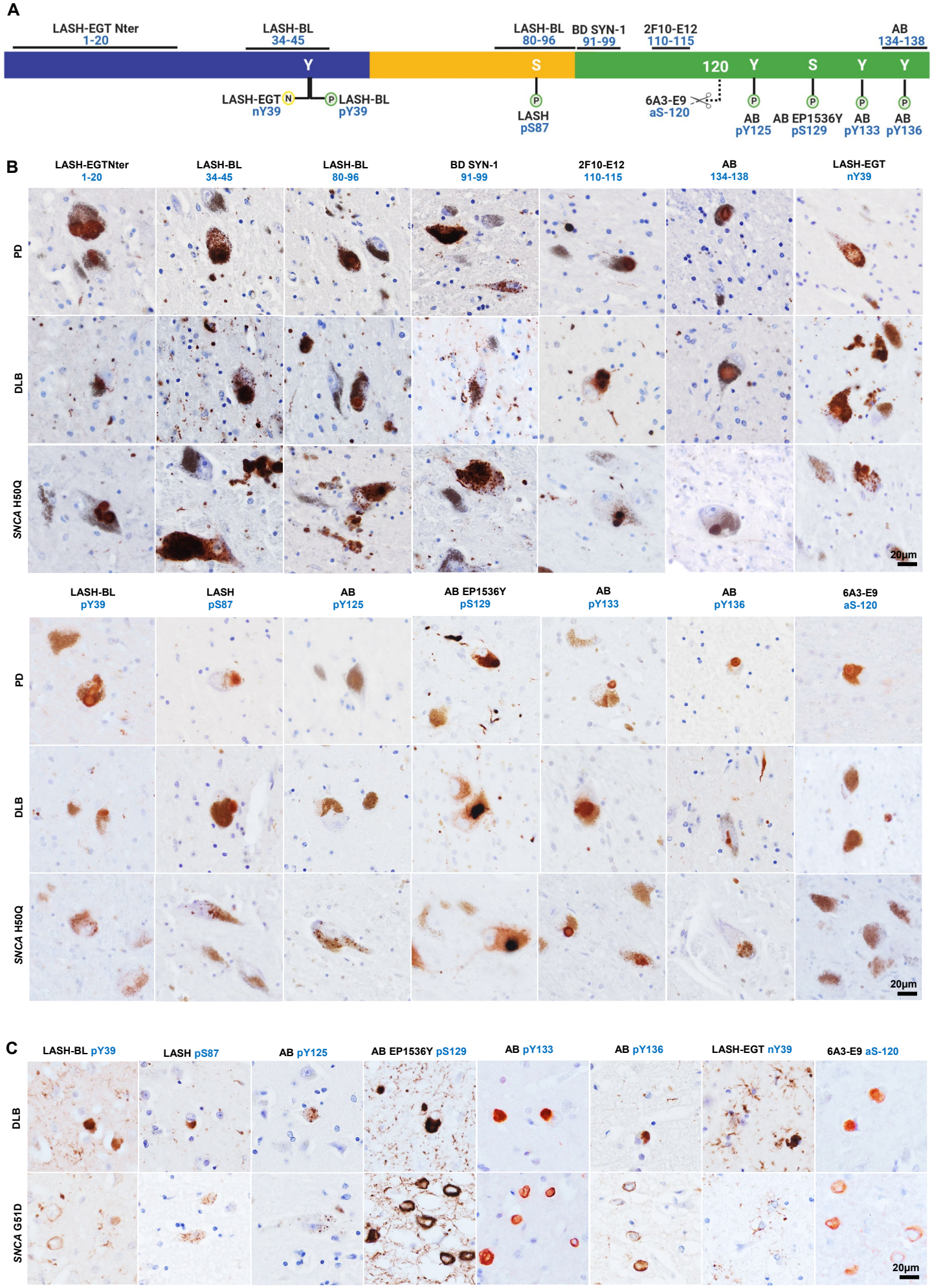
A
LASH-EGT Nter 1-20
LASH-BL 34-45
LASH-BL 80-96
BD SYN-1 91-99
2F10-E12 110-115
AB 134-138
Y
S
120
Y
S
Y
Y
LASH-EGT nY39
LASH-BL pY39
LASH pS87
6A3-E9 aS-120
AB pY125
AB EP1536Y pS129
AB pY133
AB pY136
B
LASH-EGTNter 1-20
LASH-BL 34-45
LASH-BL 80-96
BD SYN-1 91-99
2F10-E12 110-115
AB 134-138
LASH-EGT nY39
PD
DLB
SNCA H50Q
20µm
LASH-BL pY39
LASH pS87
AB pY125
AB EP1536Y pS129
AB pY133
AB pY136
6A3-E9 aS-120
PD
DLB
SNCA H50Q
20µm
C
LASH-BL pY39
LASH pS87
AB pY125
AB EP1536Y pS129
AB pY133
AB pY136
LASH-EGT nY39
6A3-E9 aS-120
DLB
SNCA G51D
20µm

FIGURE 6

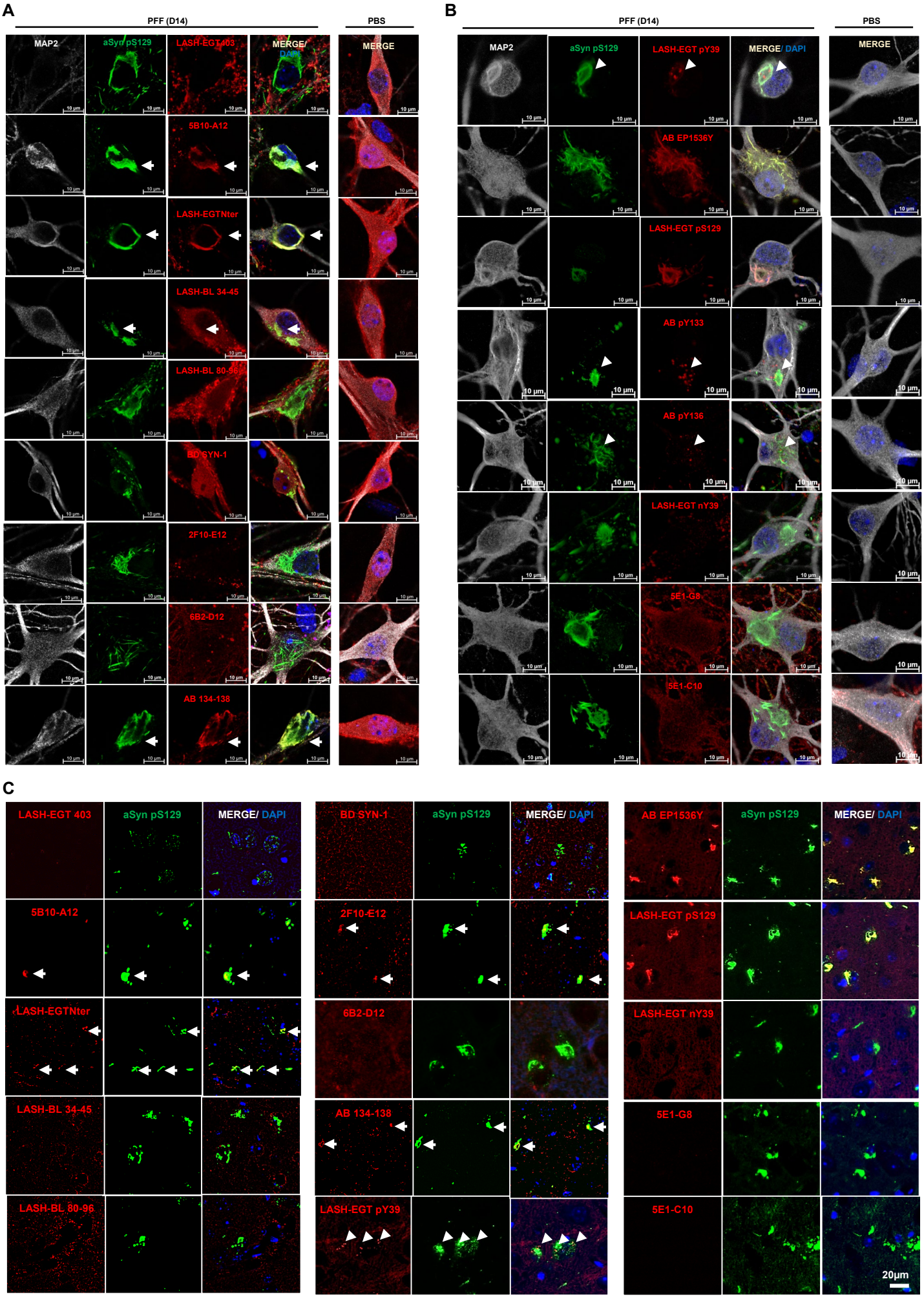
A
PFF (D14)
PBS
MAP2
aSyn pS129
LASH-EGT403
MERGE/ DAPI
MERGE
5B10-A12
LASH-EGTNter
LASH-BL 34-45
LASH-BL 80-96
BD SYN-1
2F10-E12
6B2-D12
AB 134-138
B
PFF (D14)
PBS
MAP2
aSyn pS129
LASH-EGT pY39
MERGE/ DAPI
MERGE
AB EP1536Y
LASH-EGT pS129
AB pY133
AB pY136
LASH-EGT nY39
5E1-G8
5E1-C10
10 µm
C
LASH-EGT 403
aSyn pS129
MERGE/ DAPI
5B10-A12
LASH-EGTNter
LASH-BL 34-45
LASH-BL 80-96
BD SYN-1
2F10-E12
6B2-D12
AB 134-138
LASH-EGT pY39
AB EP1536Y
LASH-EGT pS129
LASH-EGT nY39
5E1-G8
5E1-C10
20µm

TABLE 1

antibody	epitope	species reactivity	bSyn detection	neighbouring PTM sensitivity	conformational selectivity	
					WB	DB
LASH-EGT403	1-5	hu, mus	yes	-	m/ o/ f	m/ o/ f
5B10-A12	1-10	hu, mus	-	truncation at ~5	m/ o/ f	m/ o/ f
LASH-EGTNter	1-20	hu, mus	yes	-	m/ o/ f	m/ o/ f
LASH-BL 34-45	34-45	hu, mus	yes	truncation at ~39	m/ f	m/ o/ f
LASH-BL 80-96	80-96	hu, mus	-	-	m/ o/ f	m/ o/ f
BD SYN-1	91-99	hu, mus	-	pS87	m/ o/ f	m/ o/ f
BL 4B12	103-108	hu	-	-	m/ o/ f	m/ o/ f
2F10-E12	110-115	hu, mus	-	-	m/ o/ f	m/ o/ f
AB LB509	115-122	hu	-	truncation at ~119-122	m/ o/ f	m/ o/ f
7H10-E12	115-125	hu	-	truncation at ~119-125	m/ o/ f	m/ o/ f
LASH-BL 117-122	117-122	hu	-	truncation at ~119-122	m/ o/ f	m/ o/ f
LASH-BL A15127A	120-122	hu	-	pY125	m/ o/ f	m/ o/ f
4E9-G10	120-125	hu	-	pY125	m/ o/ f	m/ o/ f
1F10-B12	121-125	hu	-	pY125 (DB only)	m/ o/ f	m/ o/ f
4E9-C12	121-132	hu	-	truncation at ~125, pY125	m/ o/ f	m/ o/ f
2C4-B12	123-125	hu	-	pY125 (DB only)	m/ o/ f	m/ o/ f
6B2-D12	126-132	hu, mus	-	pS129 (DB only)	m/ o/ f	m/ o/ f
AB 134-138	134-138	hu, mus	yes	-	m/ o/ f	m/ o/ f

aSyn = alpha-synuclein; bSyn = beta-synuclein; DB = dot blot; f = fibril; hu = human; m = monomer; mus = mouse; o = oligomer; PTM = post-translational modification; WB = Western blot

TABLE 2

antibody	epitope	reactivity	specificity aSyn KO neurons - ICC	specificity aSyn KO neurons – WB		specificity aSyn KO tissue – IHC
				15kDa	35-180kDa	
LASH-EGT403	1-5	hu, mus	specific	specific	non-specific bands	specific
5B10-A12	1-10	hu, mus	specific	specific	non-specific bands	specific
LASH-EGTNter	1-20	hu, mus	specific (bSyn-positive)	specific	non-specific bands	specific
LASH-BL 34-45	34-45	hu, mus	specific (bSyn-positive)	specific	non-specific bands	specific
LASH-BL 80-96	80-96	hu, mus	non-specific in hipp aSyn KO only	specific	non-specific bands	specific
BD SYN-1	91-99	hu, mus	specific	specific	specific	specific
BL 4B12	103-108	hu	mild nuclear positivity	specific	non-specific bands	specific
2F10-E12	110-115	hu, mus	specific	specific	non-specific bands	specific
AB LB509	115-122	hu	specific	specific	non-specific bands	specific
7H10-E12	115-125	hu	non-specific	specific	specific	specific
LASH-BL 117-122	117-122	hu	non-specific	specific	specific	specific
LASH-BL A15127A	120-122	hu	non-specific	specific	non-specific bands	specific
4E9-G10	120-125	hu	specific	specific	non-specific bands	specific
1F10-B12	121-125	hu	non-specific	specific	specific	specific
4E9-C12	121-132	hu	specific	specific	specific	specific
2C4-B12	123-125	hu	non-specific	specific	specific	specific
6B2-D12	126-132	hu, mus	specific	specific	non-specific bands	specific
AB 134-138	134-138	hu, mus	specific (bSyn-positive)	specific (bSyn-positive)	non-specific bands	specific
LASH-BL pY39	pY39	hu	specific	specific	non-specific bands	specific
LASH-EGT pY39	pY39	hu, mus	specific	specific	non-specific bands	specific
LASH pS87	pS87	hu	mild nuclear positivity	specific	specific	punctate cytoplasmic
LASH-EGT pY125	pY125	hu	specific	specific	specific	punctate cytoplasmic
AB pY125	pY125	hu	specific	specific	specific	specific
AB EP1536Y	pS129	hu, mus	specific	specific	specific	specific
LASH-EGT pS129	pS129	hu, mus	specific	non-specific	non-specific bands	punctate cytoplasmic
AB pY133	pY133	hu, mus	specific	specific	specific	specific
AB pY136	pY136	hu, mus	specific	specific	specific	specific
LASH-EGT nY39	nY39	hu, mus	specific	specific	specific	specific
5E1-G8	nY39	hu, mus	non-specific	specific	non-specific bands	mild diffuse background
5E1-C10	nY39	hu, mus	non-specific	specific	non-specific bands	mild diffuse background
6A3-E9	aSyn-120	hu	specific	specific	specific	specific

aSyn = alpha-synuclein; bSyn = beta-synuclein; ICC = immunocytochemistry; hu = human; IHC = immunohistochemistry; KO = knockout; mus = mouse; WB = Western blot

TABLE 3

antibody	NEURONAL				GLIAL		EXTRACELLULAR
	LBs	diffuse cytoplasmic with an aggregate	punctate cytoplasmic	LNs & neuropil dots	astroglial	coiled body-like oligodendroglial	
LASH-EGTNter 1-20	++	++	-	++	-	+	+
LASH-BL 34-45	+++	+	+++	+++	+++	+	+
LASH-BL 80-96	++	+	++	++	++	+	+
BD SYN-1 91-99	++	+	++	++	++	+	+
2F10-E12 110-115	+++	++	-	+++	-	++	+
AB 134-138	++	++	-	++	-	-	+
LASH-BL pY39	+	-	-/+	+	+	+	+
LASH pS87	+	+	-/+	+	-	-	+
AB pY125	-	+	-/+	-	-	-	-
AB EP1536Y pS129	+++	++	-	+++	-	+	+
AB pY133	+	+	-	+	-	-	+
AB pY136	++	-	-	++	-	-	+
LASH-EGT nY39	+	+	++	+	++	-	++
6A3-E9 aSyn-120	-	+	-	-	-	-	++

aSyn = alpha-synuclein; LB = Lewy body; LN = Lewy neurite; - absent; + mild; ++ moderate; +++ frequent

Morphological visualisation of the pathological aSyn accumulations summarised in the table above:

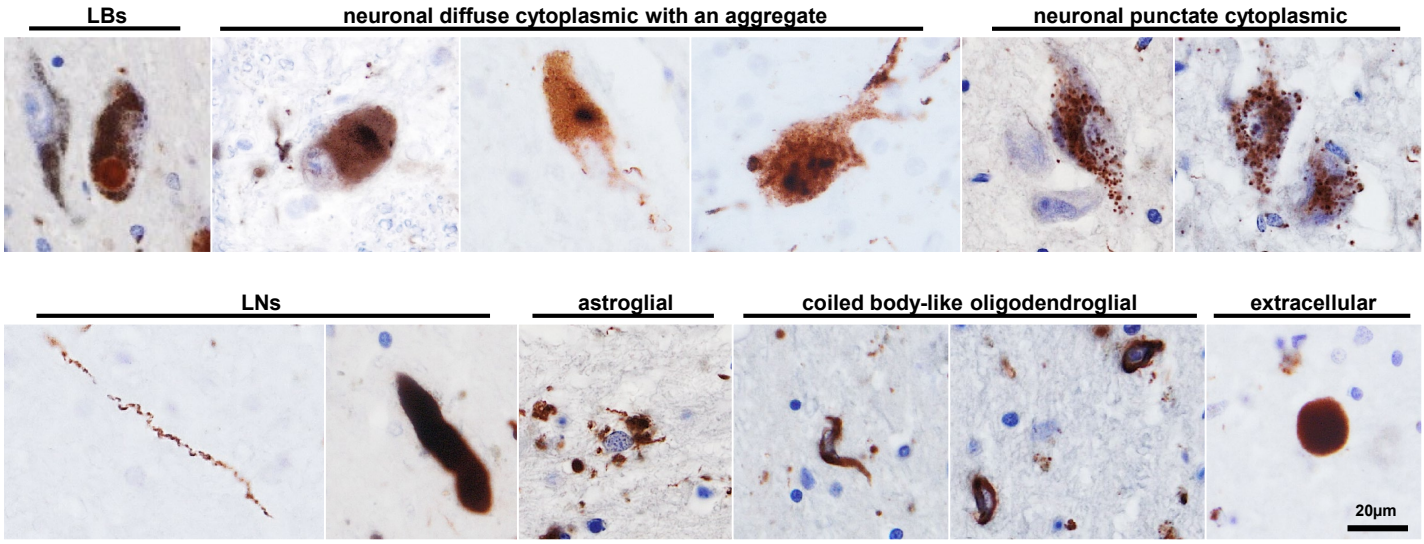

TABLE 4

antibody	epitope	aSyn KO neurons		PFF seeding model: WT primary neurons		PFF seeding model: WT mouse brain tissue	
		PFF detection ICC	PFF detection WB	positivity	aSyn pS129* overlap	positivity	aSyn pS129* overlap
LASH-EGT403	1-5	yes	yes	yes	no	no	no
5B10-A12	1-10	yes	yes	yes	yes	yes	yes
LASH-EGTNter	1-20	yes	yes	yes	yes	yes	yes
LASH-BL 34-45	34-45	yes	yes	yes	yes	yes	no
LASH-BL 80-96	80-96	yes	yes	yes	no	yes	no
BD SYN-1	91-99	yes	yes	yes	no	yes	no
2F10-E12	110-115	yes	yes	yes	no	yes	yes
6B2-D12	126-132	yes	no	yes	no	yes	no
AB 134-138	134-138	yes	yes	yes	yes	yes	yes
LASH-EGT pY39	pY39	no	no	yes	no	yes	no
AB EP1536Y	pS129	no	no	yes	yes	yes	yes
LASH-EGT pS129	pS129	no	no	yes	yes	yes	yes
AB pY133	pY133	no	no	yes	no	not tested	not tested
AB pY136	pY136	no	no	yes	no	not tested	not tested
LASH-EGT nY39	nY39	no	no	no	no	no	no
5E1-G8	nY39	yes (non-specific)	no	yes (non-specific)	no	no	no
5E1-C10	nY39	yes (non-specific)	no	yes (non-specific)	no	no	no

*aSyn pS129 revealed by BL 81A mouse monoclonal and AB MJF-R13 rabbit monoclonal antibodies. aSyn = alpha-synuclein; ICC = immunocytochemistry; KO = knockout; PFF = pre-formed fibril; WB = Western blot; WT = wild-type

SUPPLEMENTARY FIGURE 1

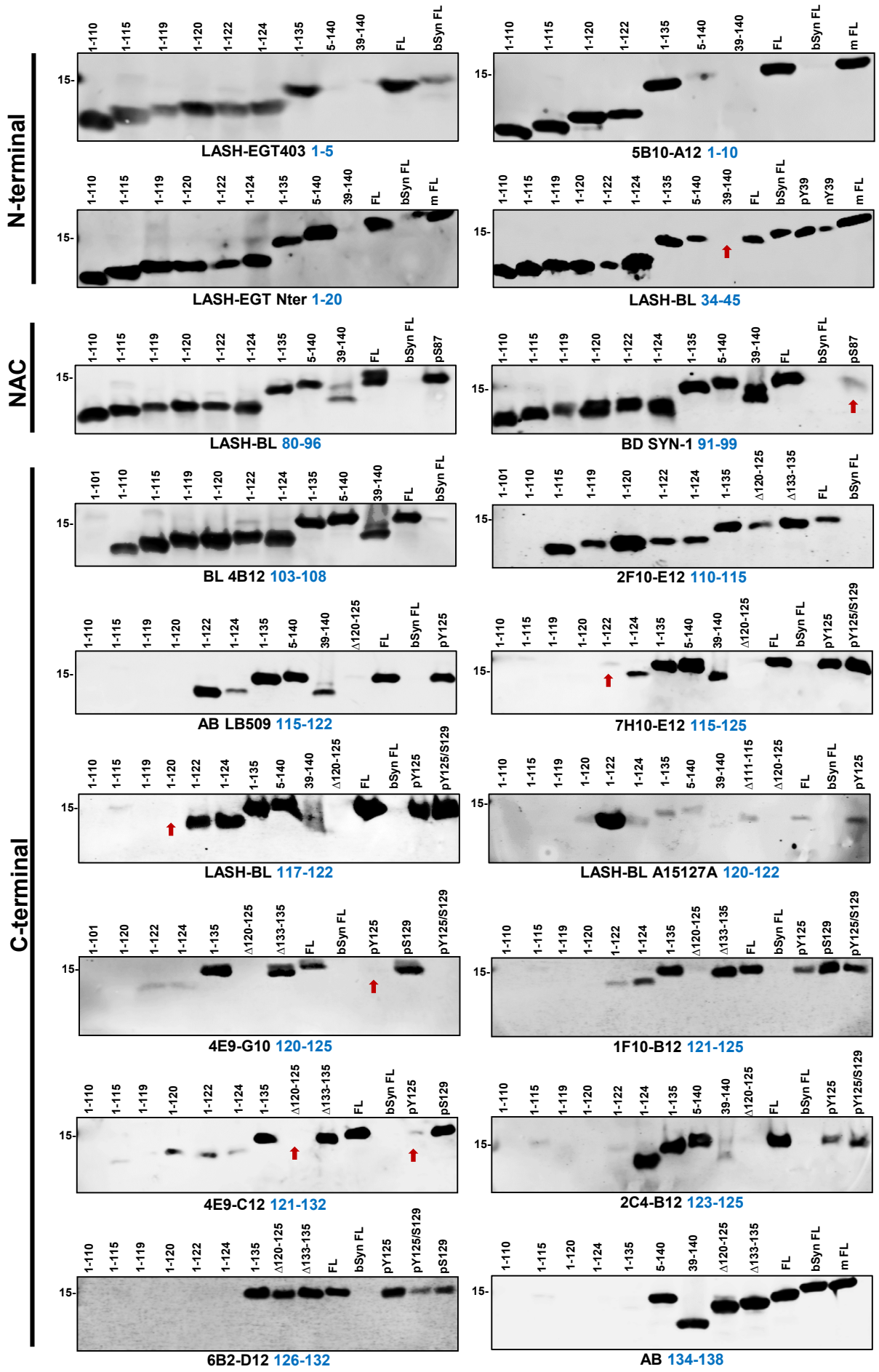

SUPPLEMENTARY FIGURE 2

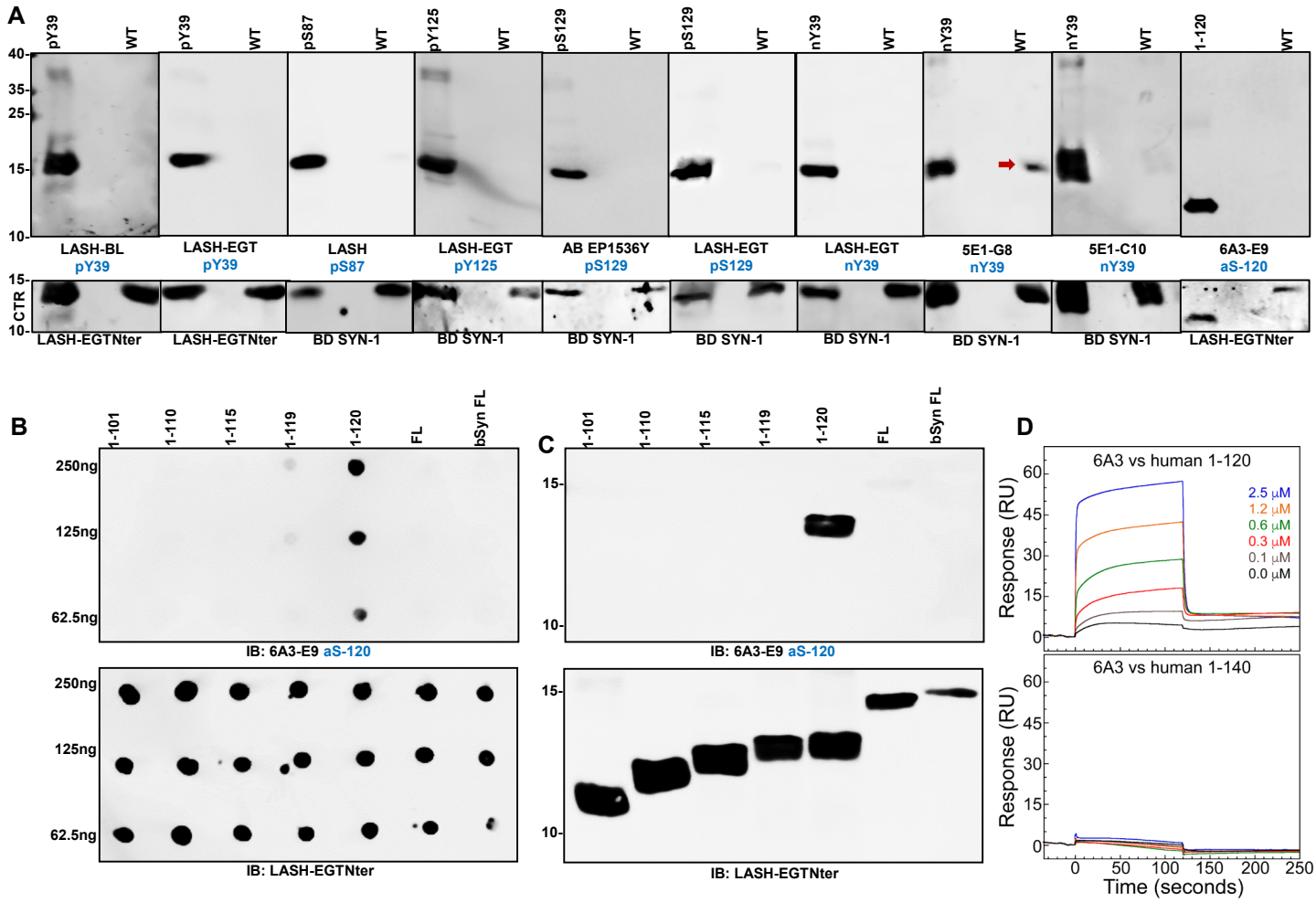

SUPPLEMENTARY FIGURE 3

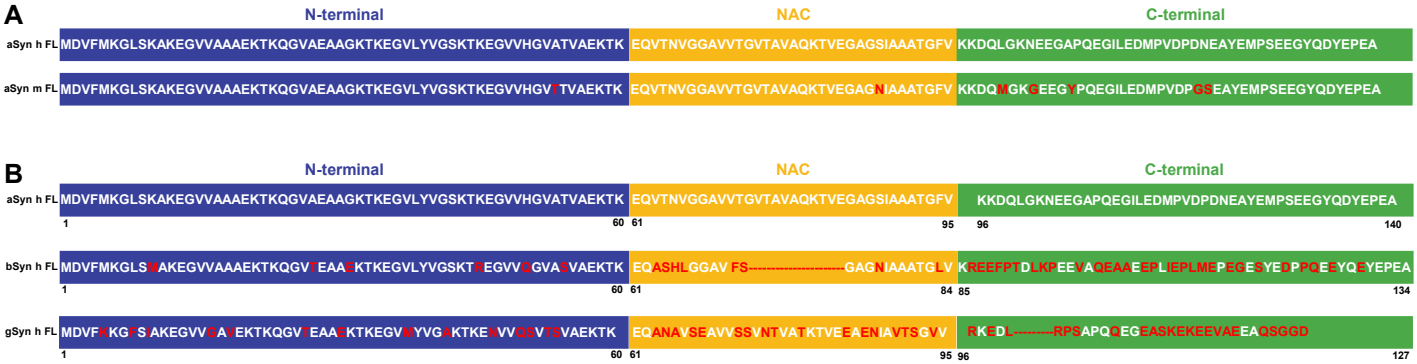

SUPPLEMENTARY FIGURE 4

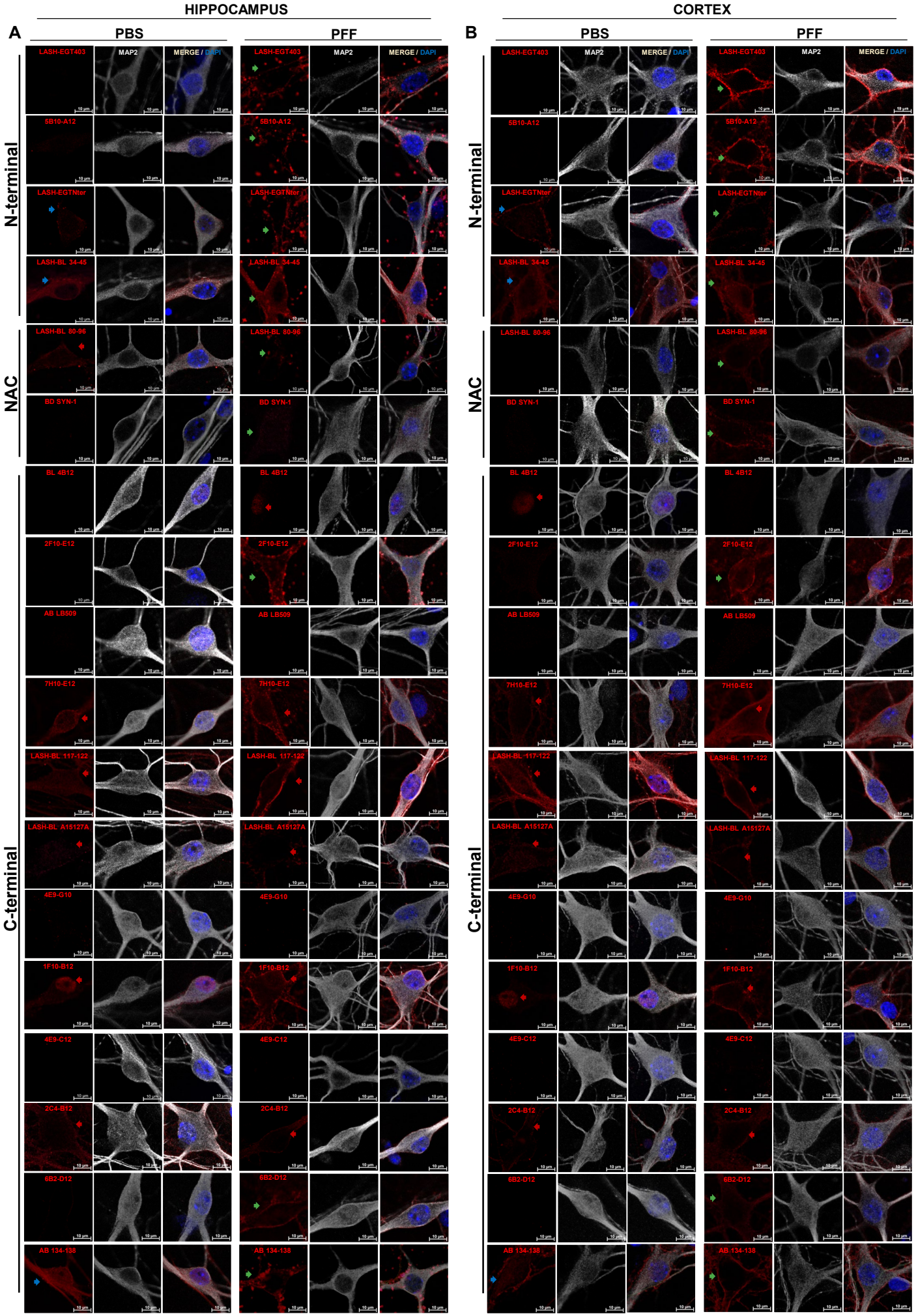

SUPPLEMENTARY FIGURE 5

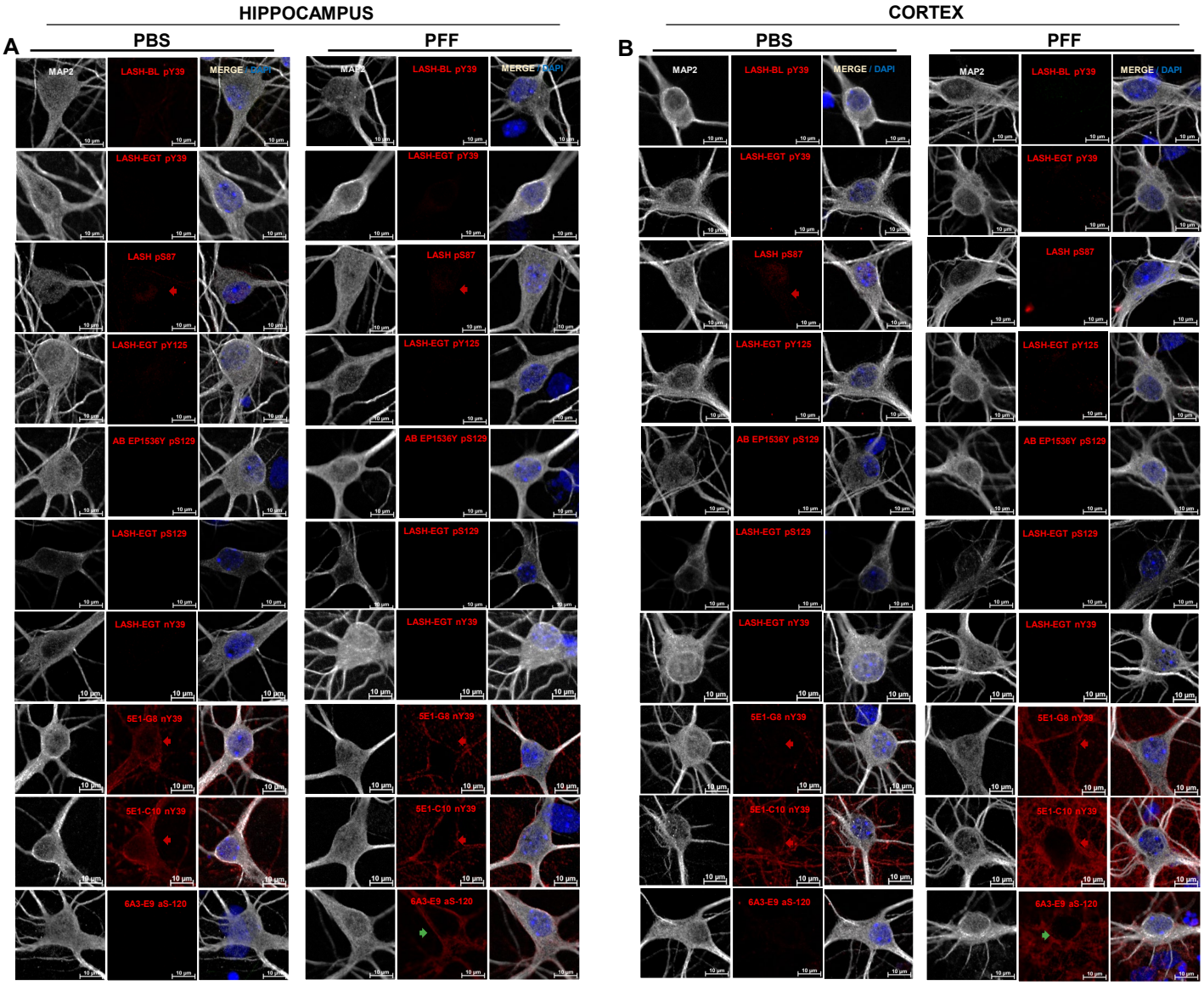

SUPPLEMENTARY FIGURE 6

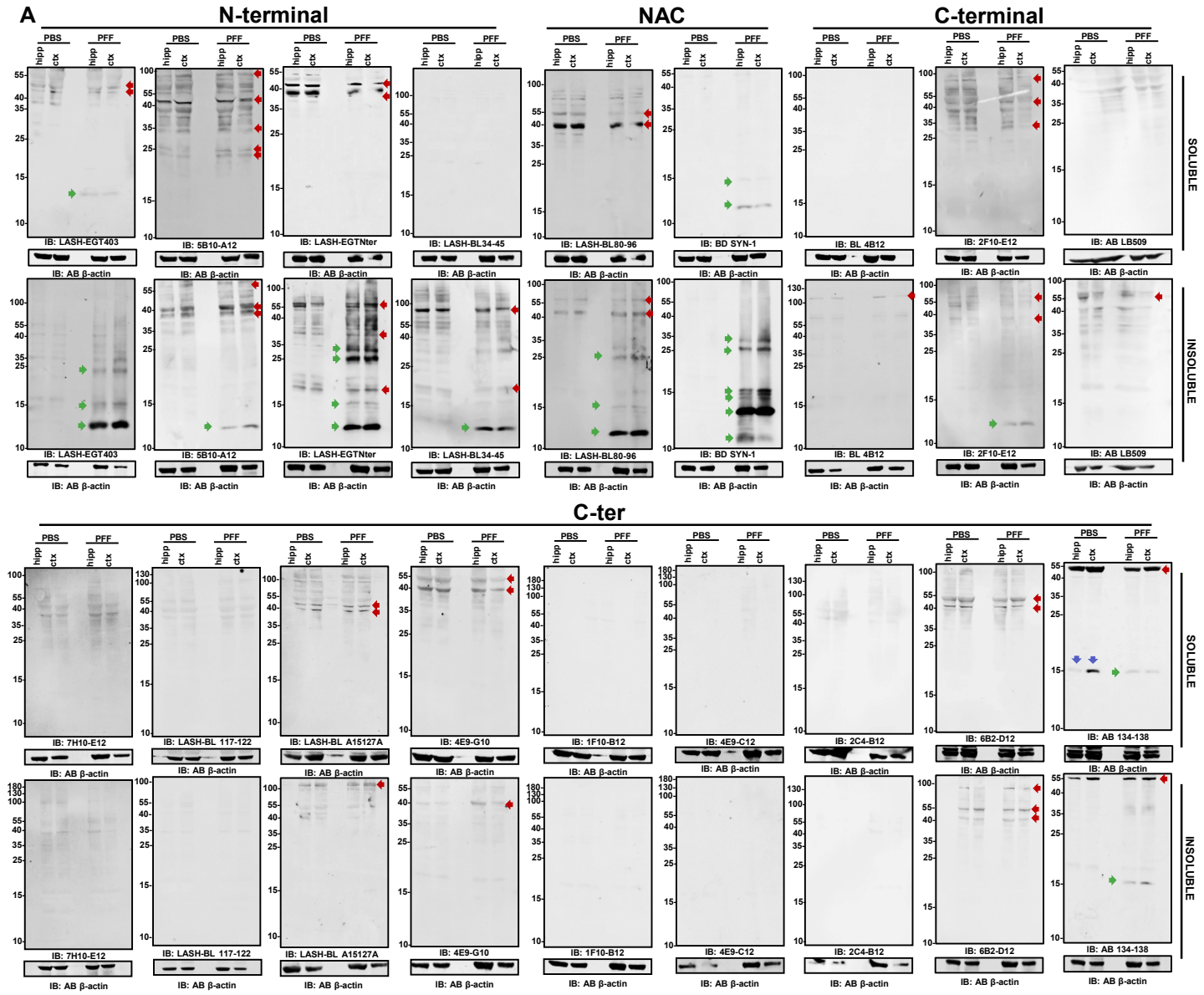

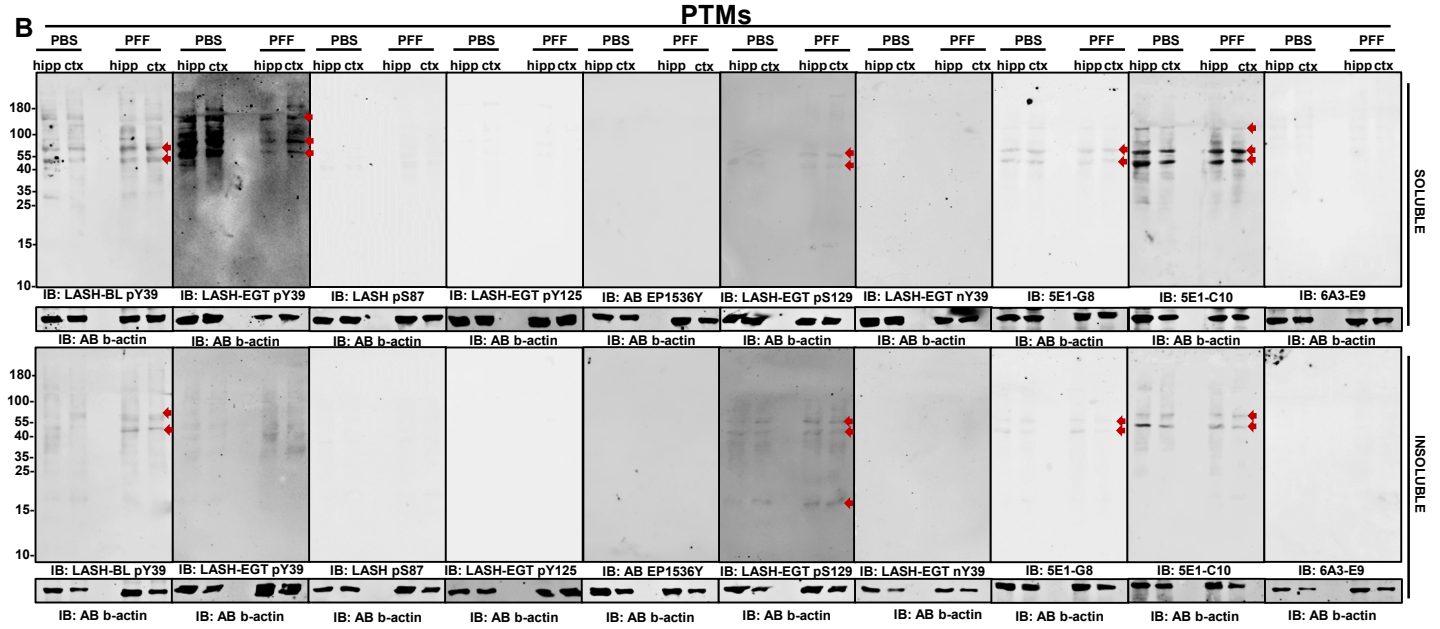

SUPPLEMENTARY FIGURE 7

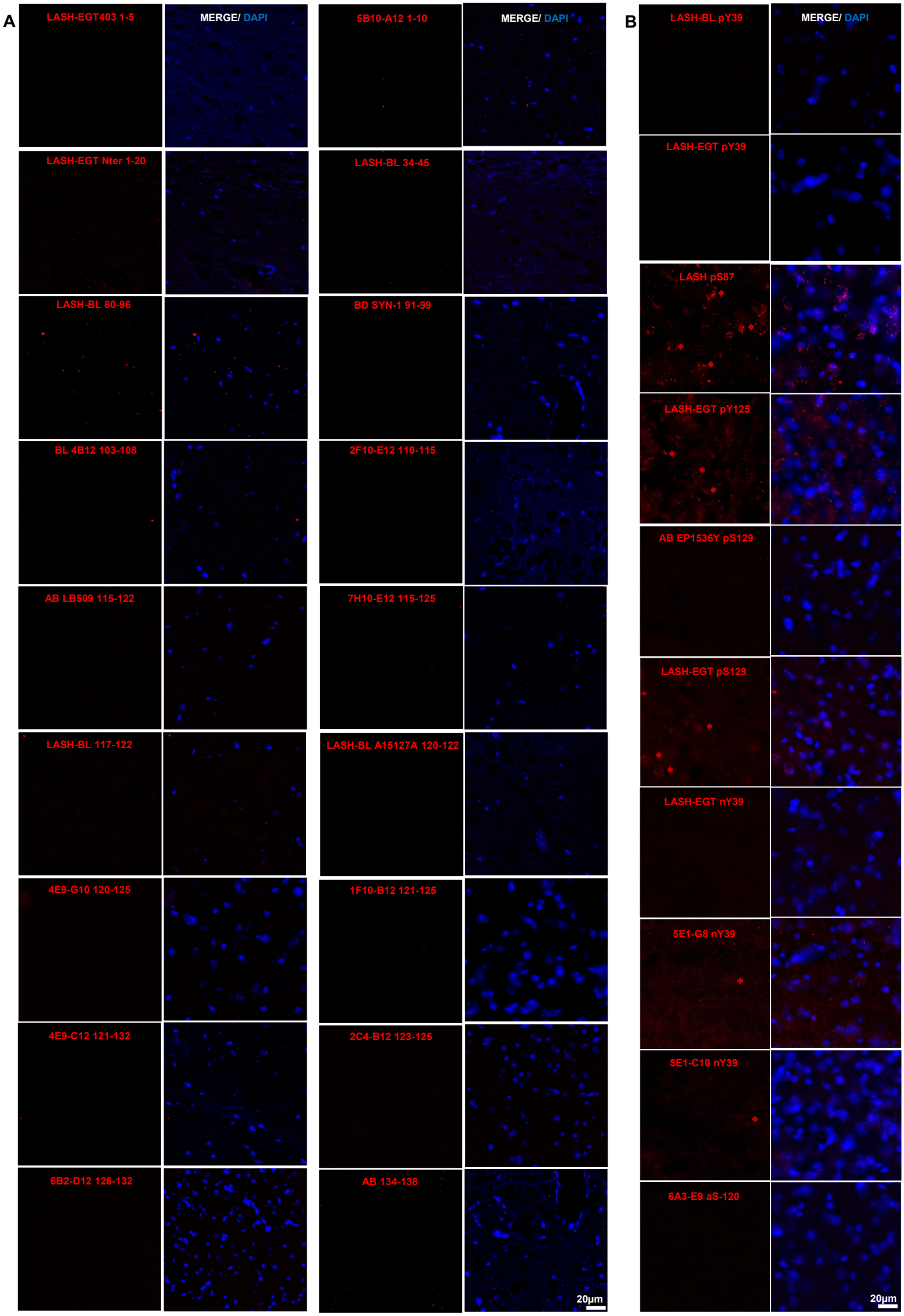

SUPPLEMENTARY FIGURE 8

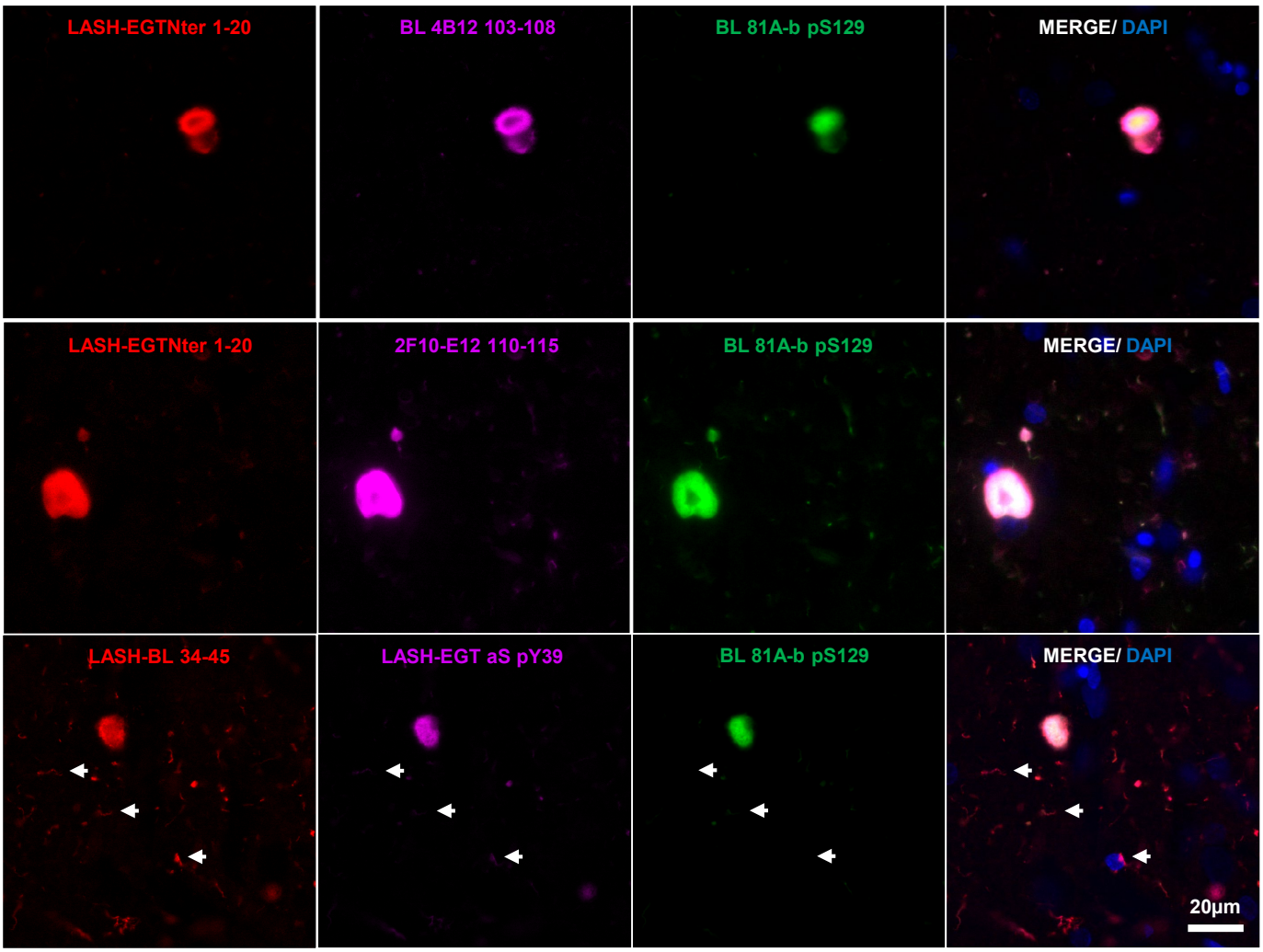

SUPPLEMENTARY FIGURE 9

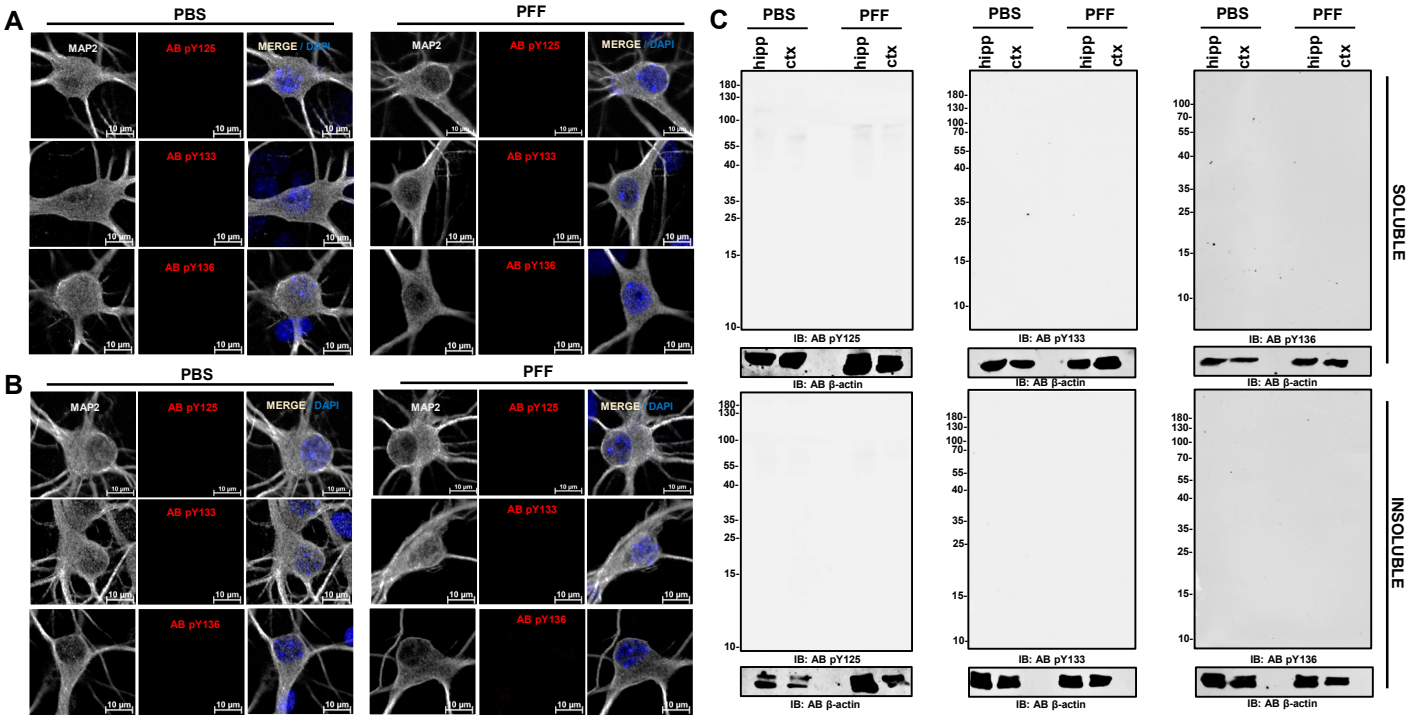

SUPPLEMENTARY FIGURE 10

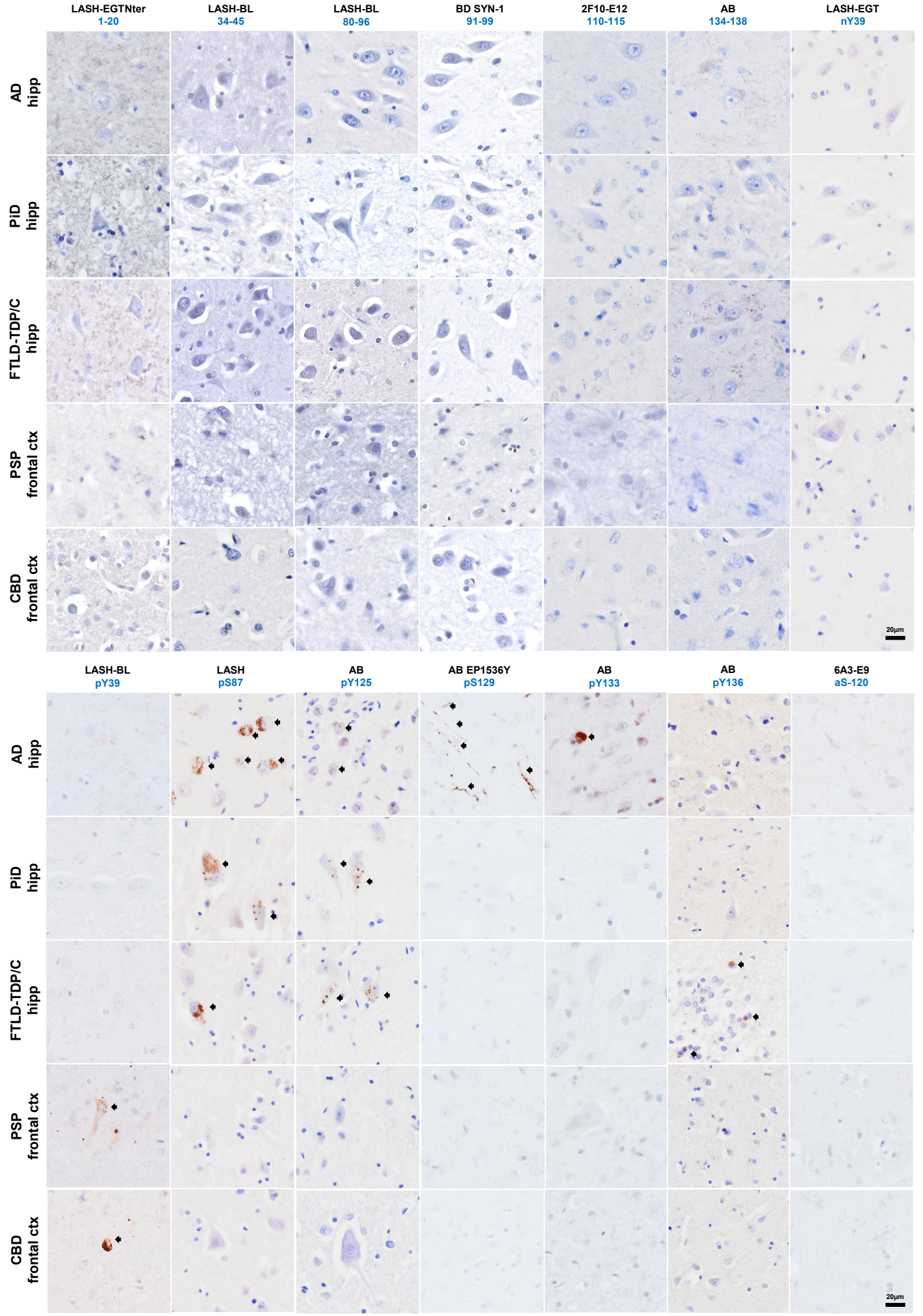

SUPPLEMENTARY TABLE 1

programme	immunogen	protein or peptide origin	carrier	antigen sequence
LASH-EGT403	UniProtKB - P37840 (SYUA_HUMAN) **1-20**	Eurogentec	KLH	MDVFMKGLSK AKEGVVAAAE
LASH-EGT404	UniProtKB - P37840 (SYUA_HUMAN) **1-140**	Eurogentec	n/a	recombinant aSyn human FL (1-140)
LASH-EGT405	UniProtKB - P37840 (SYUA_HUMAN) **113-127**	Eurogentec	KLH	LEDMPVDP DNEAYEM
LASH-EGT406	UniProtKB - P37840 (SYUA_HUMAN) **108-120**	Eurogentec	KLH	PQE GILEDMPVDP
LASH-EGT407	UniProtKB - P37840 (SYUA_HUMAN) **124-135 pS129**	Eurogentec	KLH	AYEMP(pS)E EGYQD
LASH-EGT408	UniProtKB - P37840 (SYUA_HUMAN) **108-140**	Lashuel Laboratory	n/a	PQE GILEDMPVDP DNEAYEMPSE EGYQDYEPEA
LASH-EGT409	UniProtKB - P37840 (SYUA_HUMAN) **120-135 pY125/pS129**	Eurogentec	KLH	P DNEA(pY)EM P(pS)E EGYQD
LASH-EGT410	UniProtKB - P37840 (SYUA_HUMAN) **1-119**	Lashuel Laboratory	n/a	recombinant aSyn human 1-119
LASH-EGT416	UniProtKB - P37840 (SYUA_HUMAN) **34-45 nY39**	Eurogentec	KLH	KEGVL(nY)VGSKTK

aSyn = alpha-synuclein; FL = full-length

SUPPLEMENTARY TABLE 2

protein/ peptide	Mw/ Da	protein/ peptide	Mw/ Da	protein/ peptide	Mw/ Da	protein/ peptide	Mw/ Da
aSyn 1-11	1,227	aSyn h 1-133	13,627	aSyn h FL	14,460	aSyn h pS129	14,540
aSyn h 1-101	10,062	aSyn h 1-135	13,871	bSyn h FL	14,288	aSyn h pY125/pY133/pY136	14,745
aSyn h 1-110	11,045	aSyn h 5-140	13,968	aSyn h Y39F	14,444	aSyn m 1-120	12,222
aSyn h 1-114	11,457	aSyn h 39-140	10,600	aSyn h Y133/136F nY39	14,490	aSyn m Δ120-125	13,881
aSyn h 1-115	11,572	aSyn h 65-140	7,872	aSyn h nY39	14,522	aSyn m Δ133-135	14,079
aSyn h 1-119	12,015	aSyn h 71-140	7,374	aSyn h nY125	14,522	aSyn m 20-140	12,551
aSyn h 1-120	12,112	aSyn h Δ111-115	13,933	aSyn h pY39	14,540	aSyn m FL	14,485
aSyn h 1-122	12,341	aSyn h Δ111-115/133-135	13,526	aSyn h pS87	14,540	aSyn m E114A	14,427
aSyn h 1-123	12,470	aSyn h Δ120-125	13,770	aSyn h pY125	14,540	aSyn m D115A	14,441
aSyn h 1-124	12,541	aSyn h Δ133-135	14,054	aSyn h pY125/S129	14,620	aSyn m pS129	14,580

aSyn = alpha-synuclein; bSyn = beta-synuclein; Da = dalton; FL = full-length; h = human; m = mouse; Mw = molecular weight

SUPPLEMENTARY TABLE 3

antibody full name	antibody short name	epitope	species/ clonality	isotype	reactivity	concentration	amount
LASH-EGT403 6D10-F10	LASH-EGT403	1-5	mouse monoclonal	IgG1 K	human, mouse	1.1mg/mL	56.2mg
LASH-EGT410 5B10-A12	5B10-A12	1-10	mouse monoclonal	IgG1 K	human, mouse	1.4mg/mL	56.2mg
LASH-EGT406 2F10-E12	2F10-E12	110-115	mouse monoclonal	IgG1 K	human, mouse	1.8mg/mL	79.7mg
LASH-EGT405 7H10-E12	7H10-E12	115-125	mouse monoclonal	IgG1 K	human	1.6mg/mL	38.4mg
LASH-EGT408 4E9-C12	4E9-C12	121-132	mouse monoclonal	IgG1 K	human	1.2mg/mL	35.5mg
LASH-EGT405 2C4-B12	2C4-B12	123-125	mouse monoclonal	IgG1 K	human	1.0mg/mL	28.7mg
LASH-EGT408 4E9-G10	4E9-G10	120-125	mouse monoclonal	IgG1 K	human	0.9mg/mL	26.5mg
LASH-EGT410 6B2-D12	6B2-D12	126-132	mouse monoclonal	IgG1 K	human, mouse	1.2mg/mL	37.2mg
LASH-EGT410 1F10-B12	1F10-B12	121-125	mouse monoclonal	IgG1 K	human	1.2mg/mL	36.7mg
LASH-EGT406 6A3-E9	6A3-E9	aS-120	mouse monoclonal	IgG1 K	human	1.0mg/mL	23.0mg
LASH-EGT416 5E1-G8	5E1-G8	nY39	mouse monoclonal	IgG1 K	human, mouse	1.3mg/mL	52.2mg
LASH-EGT416 5E1-C10	5E1-C10	nY39	mouse monoclonal	IgG1 K	human, mouse	1.3mg/mL	53.1mg

SUPPLEMENTARY TABLE 4

primary antibodies

antibody name	epitope	species/ clonality	reactivity	concentration (mg/mL)	company	catalogue #
LASH-EGT403	aSyn 1-5	mus mc	h, m	1.12	-	-
5B10-A12	aSyn 1-10	mus mc	h, m	1.40	-	-
LASH-EGTNter	aSyn 1-20	rab pc	h, m	1.34	-	-
LASH-BL 34-45	aSyn 34-45	mus mc	h, m	1.00	Biolegend	849102
LASH-BL 80-96	aSyn 80-96	mus mc	h, m	1.00	Biolegend	848302
BD SYN-1	aSyn 91-99	mus mc	h, m	0.25	BD Transduction	BD610787
BL 4B12	aSyn 103-108	mus mc	h	1.00	Biolegend	807801
2F10-E12	aSyn 110-115	mus mc	h, m	1.81	-	-
AB LB509	aSyn 115-122	mus mc	h	1.00	Abcam	ab27766
7H10-E12	aSyn 115-125	mus mc	h	1.60	-	-
LASH-BL 117-122	aSyn 117-122	mus mc	h	1.53	Biolegend	848601
LASH-BL A15127A	aSyn 120-122	mus mc	h	5.19	Biolegend	848401
4E9-G10	aSyn 120-125	mus mc	h	0.89	-	-
1F10-B12	aSyn 121-125	mus mc	h	1.23	-	-
4E9-C12	aSyn 121-132	mus mc	h	1.18	-	-
2C4-B12	aSyn 123-125	mus mc	h	0.96	-	-
6B2-D12	aSyn 126-132	mus mc	h, m	1.24	-	-
AB 134-138	aSyn 134-138	rab pc	h, m	1.00	Abcam	ab131508
LASH-BL pY39	aSyn pY39	mus mc	h	1.00	Biolegend	849201
LASH-EGT pY39	aSyn pY39	rab pc	h, m	0.50	-	-
LASH pS87	aSyn pS87	rab pc	h	0.40	-	-
LASH-EGT pY125	aSyn pY125	rab pc	h	0.20	-	-
AB pY125	aSyn pY125	rab pc	h	0.50	Abcam	ab10789
AB EP1536Y	aSyn pS129	rab mc	h, m	2.68	Abcam	ab51253
LASH-EGT pS129	aSyn pS129	rab pc	h, m	0.10	-	-
BL 81A	aSyn pS129	mus mc	h, m	1.00	Biolegend	825701
BL 81A biotin	aSyn pS129	mus mc	h, m	0.50	Biolegend	824704
AB MJF-R13	aSyn pS129	rab mc	h, m	4.20	Abcam	ab168381
AB pY133	aSyn pY133	rab pc	h, m	1.50	Abcam	ab194910
AB pY136	aSyn pY136	rab pc	h, m	1.00	Abcam	ab131491
LASH-EGT nY39	aSyn nY39	rab pc	h, m	0.53	-	-
5E1-G8	aSyn nY39	mus mc	h, m	1.31	-	-
5E1-C10	aSyn nY39	mus mc	h, m	1.27	-	-
6A3-E9	aSyn-120	mus mc	h	0.96	-	-
AB β-actin AC-15	β-actin	mus mc	h, m	1.00	Abcam	ab6276
AB anti-MAP2	MAP2	ch pc	m, r	na	Abcam	ab5392

secondary antibodies

antibody name	concentration (mg/mL)	company	catalogue #
DAPI 461	2.00	ThermoFisher	D1306
goat anti-mouse Alexa Fluor 488	2.00	ThermoFisher	A-11029
donkey anti-rabbit Alexa Fluor 488	2.00	ThermoFisher	A-21206
goat anti-chicken Alexa Fluor 568	2.00	ThermoFisher	A-11041
donkey anti-rabbit Alexa Fluor 568	2.00	ThermoFisher	A-10042
donkey anti-mouse Alexa Fluor 647	2.00	ThermoFisher	A-31571
donkey anti-rabbit Alexa Fluor 647	2.00	ThermoFisher	A-31573
IRDye 680RD goat anti-mouse	-	Li-Cor	926-68070
IRDye 800CW goat anti-rabbit	-	Li-Cor	926-32211

aSyn = alpha-synuclein; ch = chicken; h = human; mc = monoclonal; mus or m = mouse; pc = polyclonal rab or r = rabbit